Brain Pericyte Calcium Signaling during Vasomotion and Neurovascular Coupling in Murine Models.

By

Jessica Meza Resillas

A Thesis submitted to the Faculty of Graduate Studies of
The University of Manitoba
in partial fulfillment of the requirements for the degree of

MASTER OF SCIENCE

College of Pharmacy
Rady Faculty of Health Sciences
University of Manitoba
Winnipeg

Abstract

Pericytes, which are mural cells located on the external surface of blood vessels in the brain, play a role in various processes such as vasomotion and neurovascular coupling (NVC), which control the flow of blood to the brain. These cells possess contractile abilities, but recent research has identified different types of pericytes with varying morphology and protein expression, leading to a debate regarding their functional roles in regulating cerebral blood flow (CBF).

The objective of this study is to examine the impact of different pericyte types on vasomotion and NVC by investigating specific calcium channels that could generate intracellular calcium events and influence their capacity to constrict or dilate. By utilizing in vivo two-photon microscopy, we assessed the calcium signaling of distinct pericyte populations—ensheathing pericytes (EP) and capillary pericytes (CP)—in transgenic mice expressing genetically encoded calcium indicators (RCaMP1.07 and GCaMP6s). Concurrently, we measured the hemodynamic properties of nearby blood vessels. We also studied the effects of calcium channel blockers, namely nimodipine and Pyr3, on pericyte calcium signals and vessel hemodynamics.

Our findings revealed differential impacts of specific calcium pathways in brain pericytes on local hemodynamic behavior. Nimodipine and Pyr3 reduced calcium activity in both pericyte types, and this reduction was different in distinct pericyte sub-cellular compartments (somata vs. processes). Nimodipine increased the diameter of vessels covered by EP, reduced their CBF and diminished the response to NVC. Likewise, nimodipine reduced CBF and NVC response of blood vessels covered by CP. Interestingly, Pyr3 caused vasodilation in both EP and CP, and it solely decreased the response to NVC in EP.

Our data provide fresh insights into the mechanisms of calcium signaling in brain pericytes, shedding light on the role of these cells in regulating CBF. This knowledge holds potential for advancing our understanding of cerebrovascular and neurodegenerative diseases, where the full understanding of their development is yet to be determined.

Acknowledgements.

I wish to express my deep appreciation to **Dr. Jillian Stobart**, my esteemed supervisor, for providing me with the opportunity to advance my scientific knowledge and skills. Her trust in my ability to contribute to the remarkable findings of her research team has been an invaluable asset. I would also like to extend my gratitude **to Dr. Hope Anderson** and **Dr. Marc Del Bigio**, members of my evaluation committee, for their invaluable time, guidance, and constructive feedback. Their multidisciplinary input has significantly enhanced the relevance and quality of this project.

I want to express my gratitude to **Finnegan O'Hara** for dedicating his time, making valuable contributions to this research, and helping in resolving the challenging bioinformatic aspect of this project.

I thank my wonderful friends and colleagues, **Noushin Ahmadpour**, **Meher Kantroo**, and **Shahin Shabanipour**, whose advice, guidance, and invaluable friendship have been instrumental to me throughout this journey.

Furthermore, I would like to express my gratitude to my fiancée, **Ryan Hnatiuk**, for his unconditional love and support. He has always been there for me, listening to my seminar practices, reading my proposals, papers, and providing me with his valuable opinion.

I wish to express my sincere gratitude to my mother, **Lucy Resillas**, my father **Rubén Meza**, my siblings **Karina** and **Aldo**, my grandparents, **Rufina, Consuelo, Marcelino,** and **Miguel**, for supporting me from the physical world and the heaven, for never leaving me alone, for loving me and cheer me up, and encourage me to pursuit my dreams.

Lastly, I would like to thank the mice that I worked with for this project. Their exceptional behavior and resilience throughout the project were remarkable, and I am grateful for their contribution to this project.

Dedication.

This thesis and hard work are dedicated to:

The memory of my loving grandmothers Consuelo Chávez Escamilla and Rufina Castro Argueta.

I will always honour them by being a person of good, with my actions and achievements.

My parents, Maria de la Luz Resillas Castro and Rubén Meza Chavez

For always making their best effort to give me the best education and opportunities, they have my eternal gratitude.

The memory of Koby

For being my dog friend during the long nights of study for 17 years.

Patients with neurodegenerative diseases.

For these findings to be helpful to you someday, for being strong and inspire the scientists' hard work.

Table of Contents.

List of Tables

List of Figures.

List of Abbreviations

αSMA, alpha smooth muscle actin;

ALS, amyotrophic lateral sclerosis;

Ang1-Tie2, angiopoietin-1/Tie2;

ATP, adenosine triphosphate;

BOLD, blood oxygen level-dependent imaging;

CASIDIL, cerebral autosomal dominant arteriopathy with sub-cortical infarcts and leukoencephalopathy;

CAA, cerebral amyloid angiopathy;

CBF, cerebral blood flow;

CHIPS, Cellular and Hemodynamic Two-photon Image Analysis;

CP, capillary pericytes;

CVR, cerebral vascular resistance;

DAG, diacylglycerol;

EP, ensheathing pericytes;

fMRI, functional magnetic resonance imaging;

GECI, genetically encoded calcium indicators;

GPCR, G protein-coupled receptor;

HIV, human immunodeficiency virus;

IOI, intrinsic optical imaging;

IP3, inositol trisphosphate;

MLCK, myosin light-chain kinase;

MLC, myosin light-chain;

MLCP, myosin light-chain phosphatase;

NVC, neurovascular coupling;

NVU, neurovascular unit;

OPCs, oligodendrocyte progenitor cells **;**

PDGFRβ, platelet-derived growth factor receptor beta;

PDGF-BB, platelet-derived growth factor BB;

PLC, phospholipase C;

RBC, red blood cells;

SMC, smooth muscle cells;

S1P, sphingosine-1-phosphate;

S1PR, sphingosine-1-phosphate receptor;

TRPC, transient receptor potential canonical;

TGFβR2, transforming growth factor, beta receptor II;

VGCC, voltage gated calcium channels;

VEGF, vascular endothelial growth factor;

VGIC, voltage gated ion channels.

1. Chapter I.

Introduction.

The human brain stands as the most metabolically demanding organ[1]. The delivery of oxygen and essential nutrients through blood circulation assumes a critical role in meeting its metabolic demands[2]. This intricate process is influenced by a group of cells collectively known as the neurovascular unit (NVU). Under resting conditions, the NVU actively regulates the delivery of blood flow into the brain. Furthermore, when a specific region of the brain becomes activated, the NVU dynamically participates in the redirection of cerebral blood flow (CBF) to match the region's specific metabolic requirements[3]. The NVU (defined in the early 2000's)[4] is composed by astrocytes, oligodendrocytes precursors cells (OPCs), neurons, smooth muscle cells (SMC), pericytes and endothelial cells[5]. Together, these cells work in concert to ensure proper CBF delivery which encompasses various processes, such as vasomotion, neurovascular coupling and cerebral autoregulation.

This thesis project focuses specifically on brain pericytes, which are mural cells situated on the basement membrane of capillaries. They are believed to participate in several functions that can influence cerebral blood flow (CBF) and the cellular environment around blood vessels[6]. Pericytes were first described by Eberth[7] and Rouget[8] in 1870s and later named by Zimmerman in 1923[9,10]. Although more than a century has passed since pericytes were described, many of their mechanisms and functions remain unclear. Thanks to the development of new cell surface markers, labeling techniques, genetics, and microscopy refinements, many discoveries about pericytes have been achieved in the last 20 years[10,11].

The aim of Chapter I of this thesis is to discuss the main characteristics, functions, and mechanisms of brain pericytes. Additionally, it delves into the recent advancements in organizing brain vasculature within the field for a better understanding of the pericyte's location. Moreover, this chapter explores the alterations in cerebral blood flow (CBF) during significant physiological processes, such as vasomotion and neurovascular coupling (NVC), emphasizing their importance in cerebral autoregulation.

Cerebral autoregulation is a mechanism employed by brain blood vessels to rapidly adapt their diameter in response to variations in perfusion pressure, ensuring consistent brain blood perfusion and optimal brain function[12,13]. While not the focus of this thesis, it is relevant for my later discussion.

1.1 Brain vascular organization

The brain blood vessels are arranged in a series of branching pathways that extend throughout the brain tissue. These pathways originate from large arteries like the middle cerebral artery. These arteries then branch out and travel along the surface of the brain in the subarachnoid space and pia matter. As they do so, they gradually decrease in diameter and transform into arterioles. The penetrating arterioles enter the cerebral cortex and continue to divide and become thinner as they go deeper, giving rise to precapillary arterioles, more recently labeled as blood vessels of the arteriole transition zone[14,15]. In the subsequent branching within deeper brain structures, the blood vessel diameter continues to decrease, creating a delicate network of capillaries. Towards the end of this capillary network, there is a change into post-capillary venules, marking the arteriovenous differentiation. Finally, the postcapillary venules begin to widen, forming the vein system that carries deoxygenated blood back to the heart (Figure I.A)[16].

In cerebrovascular anatomy, brain vessels have been recently classified according to the sequence of vessel bifurcations and their structural components. In contrast with blood vessels from other organs, brain blood vessels are conformed by specialized layers of components that confer to them unique barrier properties and interactions with cells in the neurovascular unit. The outermost layer of the brain blood vessels is called tunica external or tunica adventitia. This external layer is composed of collagen fibres and fibroblasts, and it is in close contact with cells like astrocytic end-feet, perivascular nerves and pericytes. Following the tunica external, a middle layer called tunica media is encountered, it is composed mainly of SMC along with collagen fibers and elastin. The last layer is situated in close contact with the blood vessel lumen, it is called the tunica intima. The tunica intima

comprises a single layer of endothelial cells and a well-developed internal elastic lamina, which separates it from the tunica media[17–20].

Even though these layers are present throughout all the brain vasculature, their components can vary according to the branching pattern of the brain blood vessels, conferring their different roles in the vascular system. For instance, large arteries such as the internal carotid artery can have in their tunica media up to 20 layers of SMC, in contrast, pial arteries possess around two to three layers of SMC. In addition, the blood vessels that penetrate into the brain (penetrating arterioles) have just one layer of SMC [17], and since they are the blood vessels where the branching pattern in the brain starts, they have been given the branching order "cero" (Figure. I.B).

The next bifurcations (from 1st to 4th branching order) give rise to the arteriole transition zone. In this vascular segment, a gradual transition from SMC to pericytes takes place (Figure. I.B) [21]. This transition is differentiated by changes in cell morphology and protein content. For example, SMC are spindle-shaped and have single elongated nuclei[22] and pericytes are spatially isolated cells with a bulging nuclei and ovoid somata[6]. Moreover, this transition is underscored by modifications in the cytosolic layers, wherein pericytes and endothelial cells find themselves enveloped by a basal lamina. This lamina is endowed with constituents like collagen, proteoglycans, and fibronectin, alongside other extracellular matrix proteins. Importantly, this basal lamina shares a continuous interface with the astrocytic end-feet, further highlighting the intricate interplay of these cellular elements within the cerebrovascular framework[17,18].

Lastly, the brain capillary bed is situated within the context of the 5th branching order or beyond[23]. The architectural composition of the blood vessels in this domain bears resemblance to that observed in the arteriole transition zone. Notably, within this particular sector of the cerebral vasculature, a decrease in the expression of alpha-smooth muscle actin (αSMA) among pericytes is evident [24] (Figure I.A). This diminution serves as a prominent discriminant, distinguishing the mural cell populations across distinct segments of the cerebral vascular network [24,25].

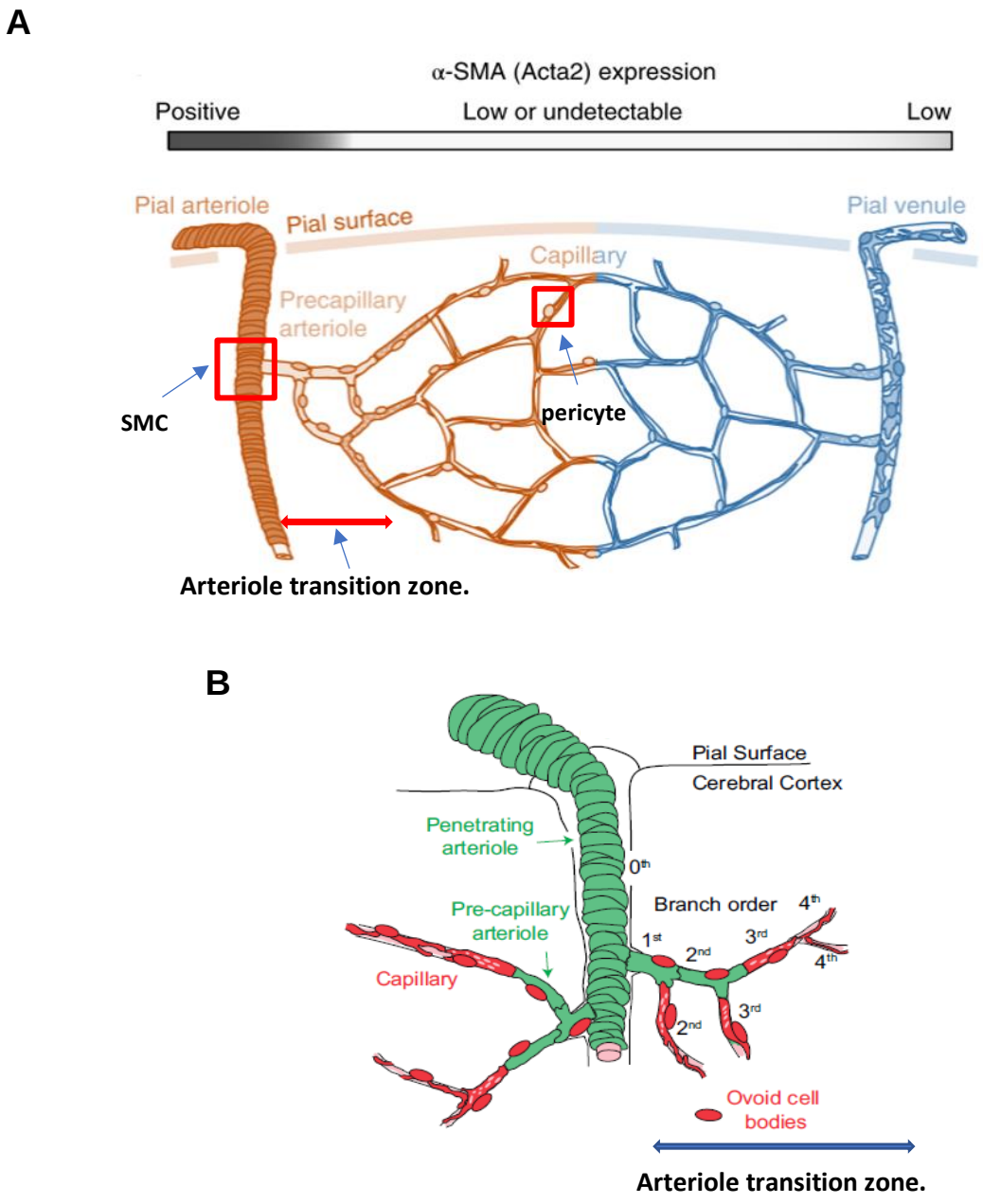

Figure I. **A** Brain vasculature blood vessels bifurcation and arteriovenous differentiation in capillaries (arteriovenous differentiation is depicted by the orange-blue transition of colors); Change in mural cell morphology (SMC and pericytes) and in the expression of αSMA trough the brain vasculature. **B** Categorization of the cerebrovascular tree according to the branch order of the blood vessels. Images adapted from Hartamnn et al 2021[26]and Grant et al 2019[23]. The color green represents smooth muscle, color red represents pericytes and color pink indicates endothelia.

It is noteworthy that according to the organization of brain vasculature, there are differences in the blood vessel's functional roles, which could impact the cerebral vascular resistance

and blood vessels' responsiveness to stimuli during NVC. These alterations may also be associated with the specific type of mural cells that envelop them. Subsequent sections will provide detailed explanations of cerebral vascular resistance, vasomotion, and NVC.

1.2 Cerebral vascular resistance.

Cerebral vascular resistance (CVR) refers to the resistance that brain blood vessels impose on the flow of blood. It is influenced by various factors, including the diameter and length of the blood vessel, as well as blood viscosity[27]. When the diameter of a blood vessel decreases, the CVR increases, whereas an increase in diameter leads to a reduction in CVR[28]. Similarly, elevated levels of components in the blood, such as a high hematocrit, increase its viscosity. This increased viscosity causes red blood cells to accumulate and collide with the vessel wall, thereby elevating the CVR[29]. The relationship between these parameters in determining CVR is described by the Hagen-Poiseuille equation, expressed as follows:

$$R = 8Ln/(\pi * r^4)$$

Where,

R= Resistance of blood flow

L= length of the blood vessel

n= viscosity of blood

r= radius of the blood vessel.

According to the equation, CVR is inversely proportional to the fourth power of the radius. Therefore, even a slight change in diameter can have significant consequences for CVR.

While Poiseuille's law provides insights into the relationship between factors influencing vascular resistance, its applicability is primarily limited to a single rigid pipe scenario with laminar flow. In the brain, however, the nature of vascular resistance becomes more intricate due to processes like vasomotion[13,30] (For detailed information of vasomotion please refer to section 1.3.1). Moreover, there are heterogeneous temporal responses occurring in different

brain compartments. For instance, while arterioles may generate high CVR, the capillary bed may exhibit lower CVR due to the extensive branching of capillaries from a single artery[13]. Furthermore, each brain compartment undergoes distinct hemodynamic changes that could result in CVR outputs of varying magnitudes.

Important mechanisms such as NVC and cerebral autoregulation significantly impact CVR[27,31]. NVC involves the redirection of blood flow and subsequent changes in blood vessel diameter in response to metabolic demands in specific brain regions, consequently affecting CVR (For detailed information about NVC please refer to section 1.3.2). Similarly, cerebral autoregulation plays a role in altering CVR during fluctuations in perfusion pressure[12,13].

Although certain studies have indicated that large arteries and small arterioles, such as the internal carotid and pial vessels, may contribute to approximately 50% of cerebral vascular resistance (CVR)[32,33], there is still a need for further research to better understand the regulatory mechanisms of CVR in both healthy and diseased conditions.

1.3 Cerebral blood flow in vasomotion and neurovascular coupling.

1.3.1 Vasomotion.

Vasomotion refers to the rhythmic variation in the constriction and dilation of blood vessels. As a result, this phenomenon induces blood flow motion, facilitating its delivery within an organ[34]. Vasomotion is considered a complex process due to the spontaneous oscillations through all the blood vessels. It varies in frequency, intensity, and location; therefore, the mechanisms originating vasomotion haven't been fully understood[30]. Nevertheless, it has been clarified that vasomotion is a local phenomenon intrinsic to blood vessels, and it can be generated without the requirement of external inputs. Some studies have shown that vasomotion can occur in *in vitro* experiments, suggesting that it is an inherent process to the vascular wall[35]. However, vasomotion seen in *in vivo* studies show that oscillations are more complex, and have considerable influence from the outer environment, such as synaptic and

endothelial cell interactions[34,36], changes in the blood pressure[37] and systemic factors such as heart rate or breathing[38].

Because of the above, vasomotion has been described to be heterogeneous in some cases. A study that measured rat mesenteric and femoral arteries *in vitro* described vasomotion to be an irregular and "chaotic" process[37]. In contrast, studies conducted in brain blood vessels have shown vasomotion to be a synchronized process with neuronal activity, and it has been shown that the disruption of this synchronization could be involved in disease conditions[39,40].

The mechanisms underlying the contraction/dilation system of synchronized vasomotion in brain blood vessels have been mainly related with calcium oscillations of mural cells[30,34,41]. In arteries, vasomotion is caused by local changes in smooth muscle constriction and dilation, and thus, it requires the coordinated activity of SMC that contain αSMA, a protein that is mainly involved in the contraction process[30,42]. Intracellular and extracellular events can lead to this process[41].

In the intracellular events, the signal that initiates SMC activity is the release of calcium from the endoplasmic reticulum; this induces the contraction mechanism and activates ion channels present in the cell membrane that, in turn, start electrical communication via gap junctions causing contraction in neighboring SMC and further oscillations in the vessel tone. In the extracellular events, cell membrane of SMC can be depolarized by external ions that allow the entry of calcium and follow the same mechanism of contraction and communication mentioned above (More information about the contraction mechanism of SMC can be found in section 1.5.1)[30,41]. Likewise, this increase in calcium subsequently causes the opening of potassium channels, resulting in hyperpolarization, closing of calcium channels and further vasodilation. This above mechanism has been suggested to be the one participating in the repeated cycles of vasomotion[40].

Synchronized and constant vasomotion has been related with processes that maintain the proper functioning and healthy status of the brain, such as tissue oxygenation [30,43], perivascular clearance of substances from the brain[44] and functional hyperemia during neurovascular coupling[45].

1.3.2 Neurovascular coupling.

Neurovascular coupling (NVC) can be defined as the dynamic temporal and regional adjustment of cerebral blood flow in response to neuronal activity and metabolic signals [46]. NVC is crucial for adequate supply of blood to support information processing and generate a response of activated areas of the brain [47,48].

In this process, the cells of the neurovascular unit (NVU) work together. Initially, signals are initiated in regions of the brain that require a high amount of energy, involving both glial cells and neurons. Neurons and astrocytes respond to an increase in neurotransmitters, like glutamate, sending vasoactive signals such as the production of nitric oxide[49,50]. Then, pericytes, SMC, and endothelial cells interpret these signals, resulting in modifications to the blood vessels, causing dilation of the arterioles and arteries upstream. These changes ultimately lead to an increase in CBF directed towards supplying the necessary oxygen and nutrients to meet the metabolic demands[46,51,52].

Studying NVC presents challenges due to the preference for non-invasive imaging techniques and the avoidance of sedatives and anesthetics to prevent alterations in brain activity[53]. Currently, assessment techniques for NVC include blood oxygen level-dependent (BOLD) imaging, functional magnetic resonance imaging (fMRI), intrinsic optical imaging (IOI), among others[52]. However, despite the advancements in these techniques, there are still unresolved questions regarding the precise location of synaptic activation, initiation of blood vessel dilation, signaling timing and distribution of blood flow[47].

In addition, it has been demonstrated that dysfunction in NVC can have significant implications for cognitive function, neuronal plasticity, and overall functionality, potentially leading to reduced capabilities [54]. For instance, diminished neurovascular coupling has been observed in conditions including stroke[55] and Alzheimer's disease[56].

NVC and vasomotion represent pivotal physiological processes in which mural cells, notably pericytes, assume a paramount role. Subsequent to this, the forthcoming sections will provide

an in-depth exploration of cerebral pericytes, furnishing intricate insights into their characteristics and functions within these critical physiological frameworks.

1.4 Brain pericytes.

1.4.1 Brain pericyte classification.

Brain pericytes are encountered on the precapillary arterioles, capillaries and postcapillary venules in the brain[9]. They are characterized for having a protruding soma (bump-on-a-log shape) and thin processes that extend along the vessels[6,11,23]. Depending on the location of pericytes in the brain vasculature, they have different morphology, protein expression, and potential function, giving rise to a subclassification of pericytes: ensheathing, capillary and stellate pericytes[6,57] (Figure II).

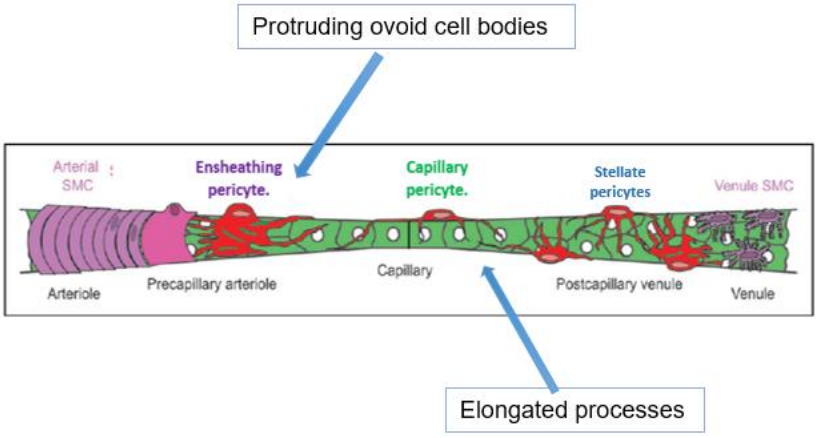

Figure II. Pericyte subtypes (represented in red color), ensheathing, capillary and stellate pericytes. They are characterized for having a protruding soma (bump-on-a-log shape) and thin processes that extend along the vessel. Image adapted from Hartmann et al 2015[57]. The color purple represents smooth muscle and color green represents the endothelia.

Ensheathing pericytes (EP) are found on the precapillary arterioles (now referred to as the arteriole-capillary transition zone), generally on branch order from 1 to 4. They possess a highly visible protruding ovoid soma and circumferential processes that enwrap the vessels (Figure III.A)[54]. **Capillary pericytes (CP)** are located on the capillary walls, more than 4 branch orders from the penetrating arteriole. They have elongated cell bodies (longer than

ensheathing pericytes) and slender processes that extend like thin strands along the capillary (Figure III. B)[58]. **Stellate pericytes (SP)** are found in the postcapillary venules, they have a stellate shape (resembling a star, as in shape), and they possess slender and shorter processes[59] (Figure III.C).

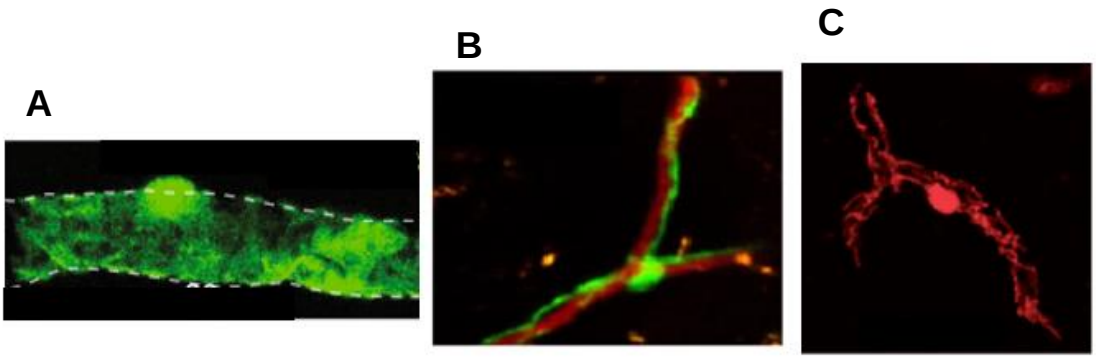

Figure III. **A** Ensheathing pericyte (color green) with a highly protruding ovoid soma and processes that enwrap the vessel; **B** Capillary pericyte (color green) with a more elongated soma and thin processes that go along the vessel. Brain vasculature is represented in color red; **C** Stellate pericyte (color red) with a stellate shape and processes that form a mesh work. Image adapted from Hartmann et al 2021[26].

For the classification and identification of pericytes, protein expression is a determinant factor. Table I summarizes the common and different protein markers for each pericyte subtype compared to SMC.

Table I. Pericyte subtypes and SMC common and different markers. X= expression; L= low expression; NA= no expression

Mural Cell	Smooth Muscle Cells	Ensheathing pericyte	Capillary pericyte	Stellate pericyte.
PDGFRβ[60–63]	X	X	X	X
NG2[47,60,64]	X	X	X	X
CD13[60,65]	X	X	X	X
Vimentin[51,66,67]	X	X	X	X
RGS5[68]	X	X	X	X

Desmin[60]	X	L	L	L
CD146[60,69]	X	L	L	L
αSMA[60,68,70]	X	X	L/NA	L/NA
CNN1[7172]	X	L	NA	NA
Transgelin[60]	X	L	NA	NA
ABCC9[71,72]	NA	NA	X	X

Pericytes subtypes and SMC share many common markers, but there are some proteins that distinguish the cell type. For example, Desmin, CD146, CNN1 and transgelin are highly expressed in SMC, but they have low or no expression in pericyte subtypes[10]. In contrast, αSMA is highly expressed in SMC and ensheathing pericytes, but it shows low or no expression in capillary and stellate pericytes [73,74]. Finally, ABCC9 is a protein that has been recently identified with high expression in capillary and stellate pericytes, but it is not encountered in SMC or ensheathing pericytes[10,72].

Due to the similarities between mural cells, the identification, classification, and naming of pericyte subtypes have been heterogeneous among the field (summarized in Table II)[9,23,26,60,75–77]. The primary problem lies in the fact that various types of pericytes share the same name or that certain studies have treated all pericytes as a single group, disregarding their specific locations within the brain vasculature [25,67,75,78].This has generated much confusion about the functional roles of pericytes within the neurovascular unit and their signaling mechanisms. Therefore, researchers in the field are pushing for a unanimous nomenclature and consistency in the characterization of pericytes that is based on several aspects, such as protein marker expression, cellular morphology, and position of the mural cell within the vascular network. For this thesis, the designations of pericyte types mentioned earlier (ensheathing, capillary, and stellate) were chosen in accordance with published

research that has explicitly classified subtypes of pericytes. This selection was made to prevent any potential confusion.[23,26,57,70,75].

The field of pericyte research is continually progressing in terms of developing tools that aid in pericyte classification, such as genetic modification techniques and advanced imaging methods. For example, a recent study demonstrated that the fluoro-Nissl dye NeuroTrace 500/525 is selectively taken up by capillary and stellate pericytes, while not being internalized by ensheathing pericytes[70]. This finding suggests that this dye could serve as a valuable tool for characterizing pericytes in future investigations. Techniques like *ex vivo* staining, *in vivo* measurements, and tracking the vessel hierarchy will enhance the identification of distinct pericyte types, which is crucial for studying their specific functions and metabolic mechanisms in the CNS.

Table II. Alternative names and classifications of pericyte subtypes found in the literature.

Type of pericyte	**Ensheathing**[26]	**Capillary**[26]	**Stellate**[26]
Alternative name	Transitional pericyte[75]	Thin strand pericyte[23,57,60]	Mesh pericyte[23,57]
	Pre-capillary pericyte[9]	Helical pericyte[57]	Post-capillary pericyte.[9]
	SMC cell pericyte hybrid.[57]	Mid-Capillary pericyte[75]	
	SMC [77]		

1.4.2 Brain pericyte function.

Different functions have been assigned to pericytes, such as regulating blood flow[79] and preserving the integrity of the blood-brain barrier (BBB)[80]. Additionally, pericytes play a role

in various processes, including guiding immune cells and facilitating their entry [81], stabilizing blood vessels [82], promoting tissue repair [83], contributing to pathological scarring [84], removing neurotoxic substances through phagocytosis [85], supporting angiogenesis [86], and responding to neuroinflammation and microglial activity [87]. It is worth mentioning that these functions may vary among different subtypes of pericytes.

Emerging hypotheses suggest that different pericyte morphology, protein expression and location in the brain vasculature dictate the function role of these cells. α-SMA is a protein involved in the constriction/dilation process of the smooth muscle and is widely known for being an essential part of contractile machinery of SMC[88–91], along with desmin[92]. As previously shown in Table I, desmin is expressed in SMC, and its filaments are mainly located at the dense bodies of SMC[92]. It is believed that desmin filaments are important in the maintenance of the structural integrity of the contractile apparatus by linking the contractile myofibrils to the sarcolemma and cellular organelles. Furthermore, desmin expression also varies according to the brain vasculature segment, being mainly expressed in arteries, and in a lower level in the arteriole transition zone[93]. Conversely, α-SMA is highly expressed in mural cells of the arteriole transition zone. The marked expression of α-SMA in mural cells of the arterioles and blood vessels of the transition zone has conferred on them the capacity to modulate CBF through constriction and dilation. Included in this group are EP that cover the blood vessels of the arteriole transition zone[60,94,95]. These cells are in the proximal branches coming off arterioles and have complex processes enwrapping the blood vessels that help to their contractile capacity[10,11,59,96]. In addition, EP highly contribute to NVC, responding to external signals from NVU and communicating with neighboring cells like SMC and endothelial cells[10,48,97]. It has been shown that following certain stimuli, blood vessels covered by EP exhibit dilation even before the penetrating arteriole in a scale of microseconds[25,98], indicating that ensheathing pericytes play a significant role in regulating CBF.

Conversely, CP are believed to participate in the maintenance of the BBB by controlling the expression of endothelial BBB tight and adherens junction proteins[99]. Also, they are related with small molecule transport[100], detection of neuronal activity[10] and response to vasoactive

signals with the elevation of calcium[59]. The contractile capacity of CP is a subject of debate, as they express very little or no αSMA; some authors deny their capacity to constrict capillaries [45,101,102]. However, others in the field suggest that the presence of αSMA should not be a rule for conferring contractile capacity, and that capillary pericytes can participate in a slow capillary contraction using different mechanisms, and this could regulate red blood cells (RBC) passage and CVR [11,25,26,59]. This functional role for CP remains under debate. Lastly, SP may participate in the immune cell entry regulation to the brain parenchyma influencing the opening of inter endothelial junctions[6]. They also have a contractile capacity[59], but the conditions under which they contribute to CBF have not been investigated.

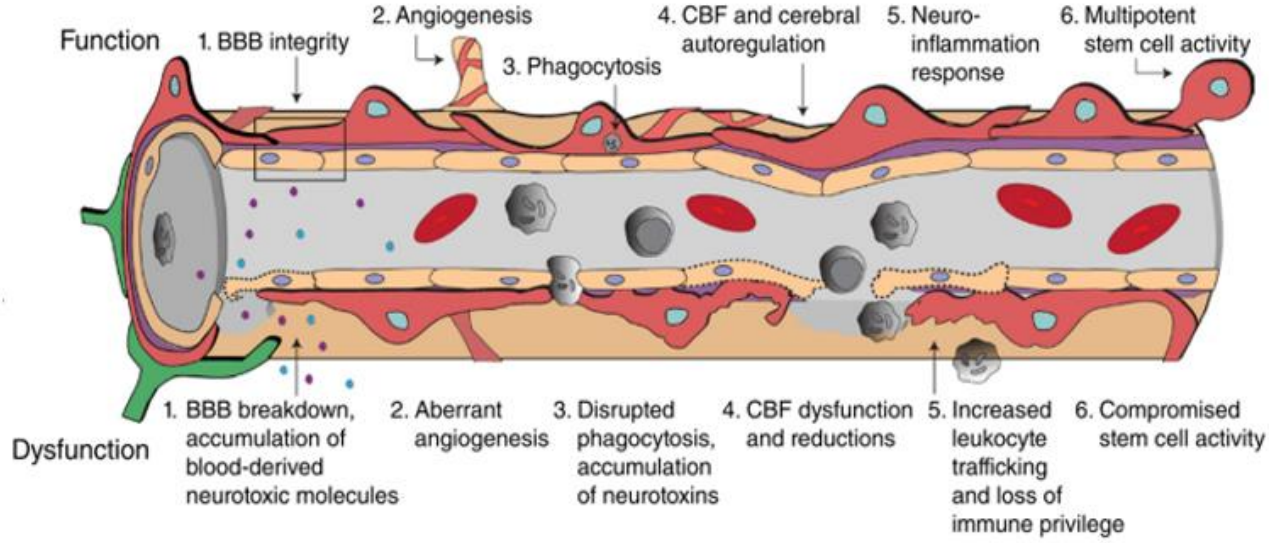

Figure IV. . Depiction of functions and dysfunctions of pericytes (no pericyte subtype specified). Color soft red represents pericytes; color orange with a blue circle inside represents endothelial cells; color tan represents the basal lamina; color gray represents the blood vessel lumen with erythrocytes in color strong red and leukocytes in color strong gray, color green represents astrocytes end-feet. Image Adapted from Sweeney et al 2016[51].

1.4.3 Brain pericytes in disease.

The varied functions of pericytes make them crucial for maintaining a healthy cellular environment. Any malfunction or impairment of pericytes can disrupt this balance and contribute to the development of various diseases (Figure IV). Several conditions including

microangiopathy associated with diabetes mellitus [103], HIV-related dementia[104], epilepsy [105], cerebral autosomal-dominant arteriopathy with subcortical infarcts and leukoencephalopathy (CASIDIL) [106] , and brain cancer [107] , have been linked to the degeneration of pericytes and subsequent cerebrovascular dysfunction. Several loss-of-function studies have examined the effects of pericyte depletion on brain health in an effort to understand pericyte degeneration in disease. Depletion of pericytes leads to a breakdown of the BBB in mouse brain, inducing inflammatory responses in endothelial cells and immune cell infiltration[82,108]. Furthermore, the loss of pericytes has been related to a decrease in CBF in response to NVC[10,75].

In ischemic conditions, irregularities in pericyte contractile function can cause a prolonged constriction of blood vessels, leading to a decrease in CBF and subsequent pericyte death by a loss of energy supply[25]. It has been shown that even after arterial recanalization in ischemic conditions, pericyte constriction can develop a non-reflow phenomenon[10,23]. Additionally, pericyte detachment and migration to the site of the ischemic lesion can cause further leakage of the BBB and leukocyte infiltration[25].

Pericyte dysfunction is believed to contribute to blood flow changes in the aged brain[109] and chronic hypoperfusion[110], possibly causing white matter functional deficits and neuronal loss, and to be critical for aggravating cognitive decline diseases such as dementia and Alzheimer Disease (AD)[10,111,112]. A recent study showed that capillaries in AD human brains are constricted by pericytes, decreasing blood flow. This study also shows that pericyte loss can worsen Aβ protein deposition in transgenic AD mice[113].

It is important to note that the majority of these disease studies have failed to consider different classifications of pericytes and the impact that this would have on functional alterations and underlying disease pathology, particularly if the pericyte subtype dictates the role of these cells in brain physiology. Furthermore, knowledge of pericyte sub-types and their roles in regulating the hemodynamics of normal health tissue will be critical for understanding pathological changes in pericytes in disease.

1.4.4 Brain pericyte and endothelial cell interactions.

Endothelial cells of the CNS are highly specialized, unlike endothelial cells from other organs, they play a paramount role in the protection of the blood vessels[114].They closely interact with pericytes to ensure BBB integrity and share many signaling pathways that modulate different functions[115]. Multiple signaling pathways are well described in the literature and they play an essential role in angiogenesis, vascular stability, and BBB formation during development[10]. These pathways include: 1) PDGF-BB/PDGFRβ, where platelet-derived growth factor BB (PDGF-BB) is secreted by endothelial cells, and it interacts with PDGFRβ that is expressed by pericytes. This signaling pathway is important for endothelial-mesenchymal communication, pericyte survival, migration, proliferation, differentiation and blood vessel stabilization and development[62,63,116,117]. Disruption in PDGF-BB/PDGFRβ signaling leads to pericyte and endothelial cell apoptosis, causing vascular abnormalities[51]. 2) Transforming growth factor beta receptor II (TGFβR2), where TGFβ–TGFβR2 signaling regulates blood vessel stability. TGF-β endothelial cell secretion regulates differentiation of pericytes and promotes pericyte contractile protein expression[118]. It also facilitates correct pericyte attachment in coordination with Notch signaling[119]. Furthermore, TGF-β pericyte secretion helps endothelial maturation through SMAD transcription factors signaling[10,86]. Aberrant TGFβ–TGFβR2 signaling leads to the development of brain hemorrhages[51]. 3) Angiopoietin 1/endothelium-specific receptor tyrosine kinase Tie-2 interaction (Ang1-Tie2) pathway, where Ang1 is secreted by pericytes and binds to Tie2 expressed by endothelial cells, which is essential for endothelial cell survival and angiogenesis[120]. Disruption of this signaling pathway can produce angiogenic deficits[121]. 4) vascular endothelial growth factor (VEGF), where VEGF is expressed by both pericyte and endothelial cells. It promotes endothelial cell sprouting, stabilization, and survival, as well as it induces pericyte proliferation and migration[82]. VEGF up-regulation by pericytes can cause disruption of BBB[82,122]. Lastly, the Sphingosine-1-phosphate /Sphingosine-1-phosphate receptor 1 (S1P/S1PR) pathway, where SP1 is secreted by endothelial cells and its receptor S1PR is expressed in pericytes. The signaling between them is essential for pericyte coverage and stabilization of endothelial cell adhesion through N-cadherin and maintains the BBB[10120].

The above mechanisms are just a few examples that show the dependence and synergism between endothelial cells and pericytes. Many other interactions can be found in the literature[10,51,97,121,123]. Several recent studies suggest that endothelial cells are critical for NVC in brain and retina and potentially send vasodilating or vasoconstricting messages to mural cells to regulate blood flow[54,97,124]. This communication is likely spread by gap junctions between pericytes and endothelial cells, and thus, this communication is highly important for the regulation of CBF[125].

1.5 Brain pericyte calcium signaling.

Calcium is a ubiquitous ion involved in important cell metabolic processes, i.e., molecule transport, neurotransmitter release, gene transcription among others[126]. Several studies have shown that EP calcium signaling has a paramount role in the contraction/dilation response of blood vessels following a similar mechanism as SMC[15,101,115,127,128]. CP calcium signaling has been associated with neurovascular unit communication[97,129,130], but little is known about the signaling mechanisms driving this process. Additionally, in the past years pericyte calcium signaling has been generalized among the different pericyte subtypes and compared with SMC[131], but recent publications have stated that EP and CP have different calcium signaling kinetics, and they respond differently to drugs that alter calcium signaling pathways[132,133].

Similar to many other brain cells, pericytes have fluctuations in intracellular calcium that are mediated by a number of different mechanisms. These calcium signals are believed to contribute to the functional roles of pericytes, such as αSMA-mediated contraction to regulate blood flow and pericyte-endothelial interactions that facilitate vascular stability and the BBB[11]. Therefore, it is important to understand the calcium signaling mechanisms in pericytes in order to better determine their functional roles in brain physiology.

Pericytes express a number of G-protein coupled receptors (GPCR) that elevate intracellular calcium, like glutamate, noradrenaline, endothelin-1, and purinergic ATP recepors[96]. In addition, pericytes express a wealth of different ion channels (for sodium, potassium,

chloride, and calcium) and have a resting membrane potential that ranges from -32 to -70 mV[134]. Membrane depolarization and hyperpolarization can influence the activity of voltage gated ion channels (VGIC) [51,96], such as voltage gated calcium channels (VGCC). Additionally, other calcium channels and transporters, such as transient receptor potential canonical channels (TRPC), sodium-calcium exchangers, and recently the storage operated calcium entry (SOCE) Orai1 channels have been reported to be expressed by pericytes[15,72,132,135].

1.5.1 L-type VGCC.

L-type VGCC are transmembrane proteins that selectively conduct calcium ions in response to cell membrane depolarization. They have a unique sensitivity to dihydropyridines like nifedipine, amlodipine, nimodipine among others, which has facilitated the study of its molecular mechanisms[136].

Voltage clamp experiments and calcium imaging have shown that pericyte cell membranes contain L-type VGCC [77,137] that are assumed to couple depolarization and calcium influx to contraction in the same manner as smooth muscle[136,138]. The contraction mechanism is initiated by signals coming from NVU cells i.e synaptic activity of neurons or astrocytes, which causes depolarization of the mural cell membrane, subsequent opening of the L-type VGCC, and Ca^{2+} influx to cytosolic space. The presence of Ca^{2+} forms a Ca^{2+}-calmodulin complex, that in turn activates myosin light chain kinase (MLCK) and phosphorylates the myosin light chain (MLC). Phosphorylated myosin can interact with actin generating force contraction. Furthermore, in the sarcoplasmic reticulum there are Ca^{2+} sensitive ryanodine receptors that are activated when Ca^{2+} is released. The activation of ryanodine receptors causes the release of more Ca^{2+} from the endoplasmic reticulum into the cytosol, and this intracellular calcium follows the same mechanism mentioned above to cause further contraction[11] (Figure V). It should be noted that calcium-independent contraction has been described in SMC. Myosin light chain phosphatase (MLCP) is mainly involved, and this enzyme dephosphorylates MLC to prevent further interaction with actin. Thus, no

constriction is generated. When MLCP is inhibited by the activity of Rho kinase or CPI-17, phosphorylation of MLC remains and leads to contraction[11]. However, it is important to remember that not all pericyte subtypes may express the same calcium channel subunits and contractility machinery and this may confer different calcium signaling properties in these cells.

1.5.2. TRPC3 channel.

Transient Receptor Potential (TRP) proteins are a superfamily of 27 cation channels, divided into 6 subfamilies based on gene sequence similarity: TRPC (Canonical), TRPM (Melastatin), TRPML (Mucolipins), TRPV (Vanilloid), TRPP (Policystin) and TRPA (Ankyrin-rich protein). All of them have diverse gating properties[139].

The TRPC subfamily consists of seven members, each designated by a specific number (TRPC1-7). These members have been implicated in various processes within the CNS, including neurite outgrowth, axon guidance, neurodegeneration, endothelium-mediated vasodilation, and SMC contraction[140]. Expression of TRPC3 channels has been demonstrated in SMC from brain vascular bed, and they are associated with the contractile response in cerebral arteries[141]. Recent transcriptome studies have identified TRPC3 expression in pericytes, with considerable RNA levels in capillary pericytes compared to other mural cells [72,142]. There is no literature yet that describes the molecular mechanism of these channels but signaling pathways of TRPC3 have been described in other cells like cardiomyocytes[143] and lymphocytes[144]. It is believed that TRCP3 channels are activated by the stimulation of GPCRs that leads to the activation of phospholipase-C (PLC). PLC activates TRPC3 channels allowing Ca^{2+} influx. PLC activation also produces diacylglycerol (DAG) and inositol triphosphate (IP3). IP3 binds to IP3 receptor in the sarcoplasmic reticulum generating calcium release and further increases cytosolic calcium. The calcium increase generated by this follows the same mechanisms of calcium-calmodulin complex for further contraction[139] (Figure V). Therefore, TRPC3 channels are important regulators of calcium (Ca^{2+}) signaling, and both can act either depolarizing the cell membrane or activating the release of intracellular Ca^{2+} [136,145].

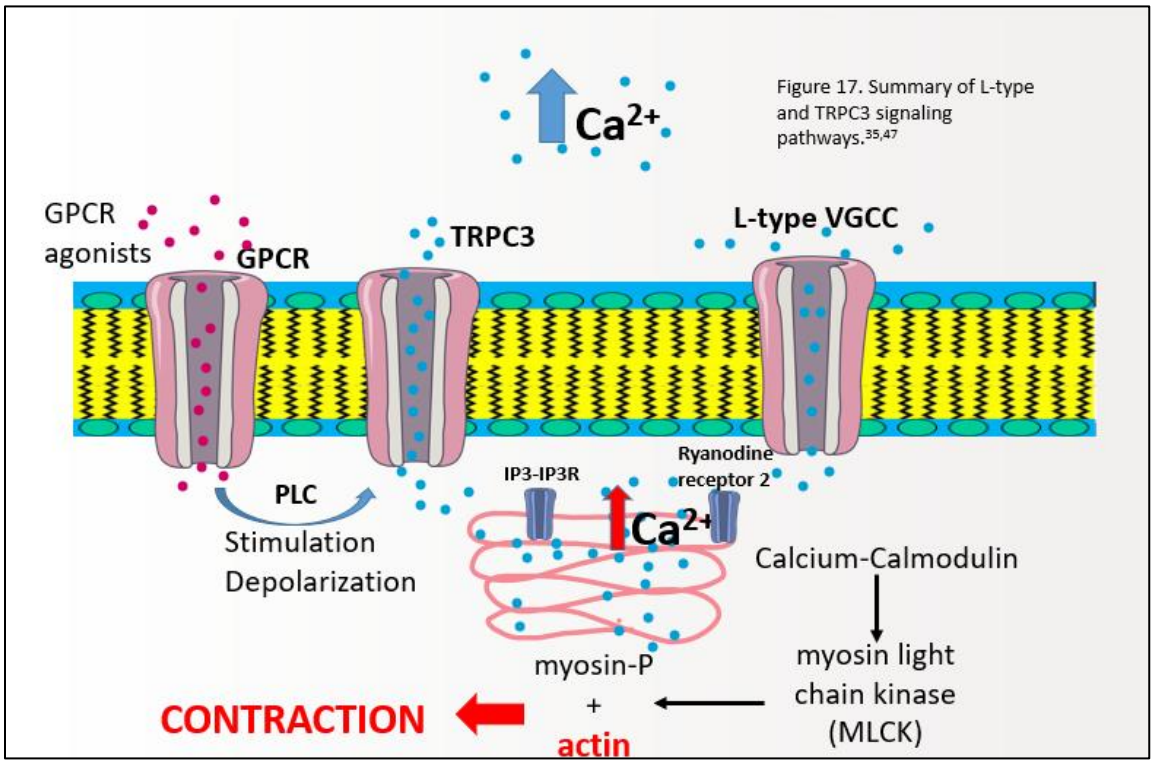

Figure V. Summary of L-type VGCC and TRPC3 signaling pathways.

1.6 Can capillary pericytes contract by mechanisms similar to SMC?

Currently, there is controversy in the contraction and dilation response in capillary pericytes, and in their association with CBF regulation. While some studies mention that blood vessels of the transition zone control the direction of blood flow[77,96], other study mentions that capillaries are the ones that dilate first and have the earliest response in blood flow changes[26,146]. Furthermore, it is known that capillaries are the zone where the exchange of blood and tissue takes place, prompting the formation of the hypothesis that capillaries play a more significant role than arterioles in the regulation of blood flow [11].

Because CP express very little or no αSMA recent studies have proposed that a slow Ca^{2+} independent contraction mechanism caused by the polymerization of G-actin and F-actin may take place[26,147], likewise, another study indicated that capillary pericyte contraction

could be mediated by the inhibition by Rho kinase[147], but this mechanisms needs further investigation.

However, recent findings have shown that CP possess Myh11, which is a contractile protein that may use calcium dependent mechanisms to contract[148]. Moreover, it has been suggested that CP contains different types of actin filaments, leading to the possibility that their calcium contractile machinery is not strictly ruled by αSMA[149].

Chapter II. Study Rationale, Hypothesis and Objectives

2.1 Study Rationale.

Brain pericytes are mural cells that play an important role in maintenance of optimal CNS function. In the last 20 years, advances in pericyte identification, classification and functional mechanisms have been described, but due to similarities between pericytes subtypes and SMC, there have been several disparities among studies. Much remains to be determined about how blood entering the neurovascular unit is distributed. Recent classification of pericyte sub-types suggests that ensheathing pericytes are possibly more important than capillary pericytes for regulating resting blood flow and NVC. However, the specific mechanisms underlying the role of pericytes in specific points of the brain vasculature remain to be established[47,26,54].

Recent *in vivo* two-photon calcium imaging data suggests that Ca^{2+} signals in different sub-types of pericytes exhibit heterogeneity, leading to the hypothesis that Ca^{2+} is regulated by distinct mechanisms in these populations. Both EP and CP express L-type VGCC and TRPC3 channels, but the contribution of these channels to pericyte Ca^{2+} signaling and nearby hemodynamics has not been determined. Therefore, a clearer understanding of pericyte Ca^{2+} signaling will advance our knowledge of the function role of these cells in the regulation of CFB.

2.2 Research project objectives and hypothesis

- **Objective 1. Characterize the mechanisms underlying Ca^{2+} signaling in different pericyte types.** *Hypothesis:* Synchronous and asynchronous Ca^{2+} signals in different pericyte types (ensheathing or capillary pericytes) are mediated by distinct calcium ion channels.

- **Objective 2. Determine the role of pericyte Ca^{2+} events in basal blood flow and neurovascular coupling.** *Hypothesis:* Calcium signals in ensheathing pericytes, but not capillary pericytes, are necessary for vasomotion, and NVC decreases these signals to induce dilation.

This project will be the first to provide novel mechanistic insight into capillary and ensheathing pericyte Ca^{2+} signaling via L-type VGCC and TRPC3 channels and their functional relevance in brain blood flow control and intercellular communication within the neurovascular unit. This will greatly enhance our limited knowledge of these cells, while opening new avenues of research into diseases such as vascular dementia and stroke, since pericyte dysfunction may play a role in these pathologies.

Chapter III. Materials and Methods

3.1 Animals and chronic cranial window implantation.

All procedures outlined below were approved by the Animal Care Committee at the University of Manitoba in accordance with the Canadian Council on Animal Care. To detect fluctuations in pericyte calcium we used genetically encoded calcium indicators (GECIs) which are fluorescent proteins that become brighter when calcium binds to their calmodulin binding domain[150]. The GECI genes are expressed in specific pericyte cell populations in two novel transgenic mouse lines: **Acta2-RCaMP1.07** (Tg(RP23-370F21-RCaMP1.07)B3-3Mik/J) and **PDGFRβ-CreERT2:GCaMP6s$^{fl/fl}$** (B6.Cg-Tg(Pdgfrb-cre/ERT2)6096Rha/J with B6;129S6-Gt(ROSA)26Sortm96(CAG-GCaMP6s)Hze/J). The Acta2-RCaMP1.07 mice line was used to visualize calcium events of ensheathing pericytes (EP) since they express red Ca^{2+} indicator RCaMP1.07 in mural cells with α-SMA expression. The PDGFRβ-CreERT2:GCaMP6sfl/fl mice line was used to visualize capillary pericytes (CP) under the expression of the Ca^{2+} indicator GCaMP6s in mural cells that express PDGFRβ after tamoxifen injection. Mice from 3 to 12 months old and both sexes were used.

To access the pericytes in the brains of live mice for two-photon imaging, a chronic cranial window was implanted as described by Stobart et al[151]. The surgery was done in two parts. Briefly, the mouse was anesthetized with isoflurane (4% induction, 2% maintenance) and a head post was surgically fixed at the back of the head with dental cement. In the second step 48-72 hours later, the mouse was anesthetized with a mix of medetomidine, midazolam, and fentanyl (5, 0.5, 0.05 mg/kg) and a 3x3mm piece of skull was removed and replaced with sapphire glass on the somatosensory area of the mice brain. The glass was permanently cemented (using dental cement) in place to seal the brain. Mice were allowed to recover from the surgery for at least three weeks before the imaging period. Likewise, the PDGFRβ-CreERT2:GCaMP6s$^{fl/fl}$ mice received tamoxifen gavage (5mg/day for 5 consecutive days) at least 2-3 weeks before imaging.

3.2 Intrinsic optical imaging (IOI) and selection of imaging area.

IOI was done to map and select highly activated areas of the mouse somatosensory cortex with whisker stimulation using the natural light-absorptive properties of hemoglobin to detect areas with increased blood flow[152]. In isoflurane anesthetized animals (4% induction, 1.5% maintenance), an Ace acA2040-55um camera was used to focus and visualize the chronic cranial window area under 630nm red light produced from LEDs. Next, specific whiskers (i.e., row A to E from dorsal to ventral and arc identified by numbers 1, 2 and so on from caudal to rostral) [153] were inserted into a glass capillary connected to a piezo actuator that vibrated at a frequency of 90 Hz. During whisker stimulation, pictures of the brain surface were captured to detect the absorption of light by increased oxygenated hemoglobin in the activated area. Complete cranial window images were repeatedly captured during this process for 10-20 trials of stimulation. Subsequently, the images were averaged and processed to encompass the most highly activated region by selecting the darkest area. The resulting image was used to select pericytes participating in neurovascular coupling and as a reference point to identify the blood vessel patterns within the circled area and enable consistent localization of the same pattern during subsequent imaging sessions.

3.3 Mouse preparation before two photon imaging sessions.

Mice were anesthetized with ketamine (20mg/kg) and xylazine (10mg/kg) applied via intraperitoneal (i.p.) injection. Subsequently, 30 µL of a solution of fluorescent dextran in saline (2.5% w/v) was injected intravenously using a catheter as previously described[154] to ensure the injection of the dextran and to reduce the waste of reagents caused by failed injections. Fluorescent dextran are biologically inert substances which have been employed for studying vascular permeability and the integrity of the blood-brain barrier[155]. In this study, two distinct variants of fluorescent dextran, fluorescein dextran and Texas red dextran, were utilized to achieve clear differentiation of the fluorescence emitted by the GECI and to visualize the brain's blood vessels. It is worth noting that the fluorescein dextran used had a molecular weight of 70,000, which aids in reducing their rapid elimination by the kidneys.

During non-baseline data collection, calcium channel blockers, nimodipine (1mg/kg) and Pyr3 (20mg/kg), were administered via intraperitoneal (i.p.) injection, diluted in the vehicle polyethylene glycol 400 (PEG 400), 20 minutes prior to pericyte imaging. Each drug was evaluated separately in distinct sessions. Additionally, PEG 400 (20 mg/kg) was also administered similarly to the calcium channel blockers and evaluated independently.

Consecutively, anesthetized mice were placed under a two-photon microscope using a platform to fix the head post to avoid movements. Likewise, a heating pad was placed under the mice to keep the body temperature. The cranial window surface was cleaned with a damp Bisco applicator and subsequently covered with ultrasound gel. Eye lubricant was applied on mice eyes to keep them moist. In addition, bipolar electrodes were percutaneously inserted into the superficial head of the masseter covering the whisker area from rostral to caudal to perform electrical whisker pad stimulation during the two-photon imaging sessions.

3.4 Two-photon imaging sessions.

All the procedures to conduct the two photon imaging sessions of brain pericytes in these mice models were previously described in depth and published in the journal of visualized experiments (JoVE) [156]. *Below is a brief outline of the procedure, but please refer to article for detailed information of the protocol.*

3.4.1 Brain pericyte selection with depth stacks.

A pulsed infrared two-photon laser (940 or 990nm) excited the GECI and fluorescent dextran for visualization of pericytes and the brain vasculature. Specifically, light of 940 nm wavelength was used to visualize brain pericytes from PDGFRβ-CreERT2:GCaMP6sfl/fl mice line and light of 990 nm wavelength was used to visualize pericytes from Acta2-RCaMP1.07 mice line.

To locate pericytes within the brain vasculature during the first imaging session, we performed a depth z-stack of the previously mapped highly activated whisker areas (Section 3.2 Materials and Methods). Starting from the penetrating arteriole, images of 512x512-pizel

resolution were taken every 2 µm and until reaching around the 200 µm depth. The laser power of the two-photon microscope was set to automatically increase in an exponential gradient to allow the visualization of deep structures. Subsequently, the depth stacks were open with the ImageJ software and brain pericytes were selected based on their morphology and blood vessel branch order, saving their position as a region of interest (ROI) for future visualization and re-localization in the repeated imaging sessions. In addition, individual images of pericytes were taken to stablish a field of view (FOV) and the coordinates in X, Y, and Z position were saved to increase accuracy of the repeated imaging sessions. Moreover, we also gathered information of the blood vessels covered by pericytes, categorizing the blood vessels of the arteriole transition zone with their respective branch order, and giving a unique vessel number to all the monitored blood vessels for future reference and analysis.

3.4.2 Brain pericyte calcium movies.

Using the depth stack information, previously selected pericytes were located. Movies of 128x128-pixel resolution and one minute long were taken during baseline imaging sessions and with the application of the calcium channel blockers and the vehicle PEG400. The movies were first taken at rest, and immediately after, a second movie with electrical whisker pad stimulation was taken without moving the FOV. STG4008 stimulus generator with MC_Stimulus II software was used to produce electrical stimulation that was performed after 5 seconds of baseline at an intensity of 500µA at 4Hz for 5 seconds.

Information of the laser power used in each session was saved to reproduce the same imaging conditions. All the pharmacology conditions were evaluated in separated different sessions and the mice were let to rest at least 2 days before a new imaging session or drug application.

3.4.3 Blood vessels hemodynamic kymographs.

After calcium movies, and using the same FOV, we used the line scan feature of the two-photon microscope software to obtain information of the hemodynamic properties of the blood vessels (already labeled with fluorescent dextran) such as diameter (µm), velocity (mm/second) and RBC flux (cells/second). First, we drew a line perpendicular to the blood

vessel of interest to record diameter information, followed by a parallel line within the vessel lumen to record velocity and flux. Subsequently, we took line scans for 30 seconds to obtain the hemodynamic measurements during this period. Line scan measurements were collected twice per FOV, one at rest and the second one during whisker stimulation. It is important to mention that we followed the same line scan drawing pattern to record hemodynamic properties in each repeated session to keep consistency of the measurements. As a result, we obtained kymographs (graphical representation of a spatial position over a period of time) which were further process in programming platforms described in the next section.

3.5 Image Processing.

3.5.1 Calcium movies.

The initial processing of the two-photon calcium movies involved using Image J. First, an average fluorescence projection of the movie was generated to identify regions exhibiting strong fluorescence. This projection aided in enhancing the visibility of pericyte morphology, specifically the soma and processes. Next, within Image J, lines were overlaid onto the pericyte structures using polygon selection. These lines were shaped to match the soma and processes, respectively, resulting in the creation of ROIs. Each ROI was assigned a unique letter and number corresponding to the structure it represented. Subsequently, the ROIs from each movie were saved alongside the movie file to enable their analysis in MATLAB.

For the analysis of the data acquired during the two-photon imaging sessions, we utilized the Cellular and Hemodynamic Two-photon Image Analysis (CHIPS) toolbox algorithms for MATLAB developed by Ellefsen et al. 2014[157] and Barret et al. 2018[158]. First, to ensure precise identification of fluorescence activity for defining calcium signaling features, CHIPS incorporated algorithms for spectral unmixing of the data. This process reduced the interference from fluorescein dextran bleeding through to the red fluorescence channel (RCaMP) and enhanced the detection of calcium signals. Next, CHIPS employed the saved ImageJ ROIs to delineate the specific area of calcium events for analysis using two different methods. These methods aimed to extract information regarding calcium signaling characteristics, including calcium amplitude and frequency. In the first method, the data

underwent a smoothing process using both long-pass and band-pass filters. This resulted in a normalized calcium trace from the ImageJ ROI, representing the fluctuations in fluorescence (dF/F) over time. The obtained traces contained valuable data for estimating calcium signaling amplitudes, which were saved as a .csv file for subsequent analysis in statistical platforms. In the second method, CHIPS automatically detected pixel activity and fluorescence changes in three dimensions (x, y, and time) within the pre-selected ROIs. In this instance, predefined fluorescence thresholds (3-5 times the standard deviation of the baseline) were employed to identify calcium events. When the fluorescence activity surpassed these thresholds, pixels were considered "active" and neighboring active pixels were grouped together to generate calcium events. CHIPS automatically assigned a unique name to each calcium event and saved this information in a .csv file that could be opened in statistical platforms for subsequent analysis. The frequency of calcium events occurring during the duration of the recorded movie was determined as calcium frequency (signals/minute) from this active pixel analysis.

3.5.2 Line Scans.

To collect diameter data, we utilized CHIPS diameter analysis algorithms in MATLAB to process the kymographs. This algorithm determined the diameter by calculating the full width at half maximum of the fluorescence within the kymographs. Likewise, CHIPS also included features to obtain information of blood vessel's wall oscillations (if present), according to the diameter fluorescence fluctuations, such as amplitude (vasomotor index; ΔD/D) and frequency (oscillations/minute).

For the velocity and RBC flux data, we employed CHIPS radon velocity analysis algorithms to examine the kymographs. In this step, we drew a box within the kymograph borders to focus on the fluorescence corresponding to the blood plasma and RBC activity. The RBC appeared as black streaks, and by inputting the angle of these streaks into a radon transformation, the velocity and flux were calculated. The results generated by CHIPS processing were .csv files that contained the raw hemodynamic information from the kymographs, which were saved with a unique ID according to the blood vessel of origin.

Since CHIPS erroneously detected constant fluorescence (i.e., stalled blood vessel) as extremely high numeric values (thousands of units) in the hemodynamic measurements, which significantly distorted the data distribution, we applied a post-processing code to clean the hemodynamic data by removing errant values. When analyzing blood vessels of arterioles in the transition zone, we established a threshold of 50 μm for diameter, 15 mm/second for velocity, and 200 cells/second for flux. For brain capillaries, the threshold values were set at 50 μm for diameter, 10 mm/second for velocity, and 100 cells/second for flux. Any data points exceeding these thresholds were replaced with the average of the two nearest data points to maintain data periodicity. It is worth noting that these thresholds were determined based on the average behavior of our data and aligned with reported values of similar hemodynamic properties of brain blood vessels in the literature. Subsequently, the cleaned data was interpolated to a frame period of 0.05, which was chosen as the most consistent frame period across the evaluated traces. Additionally, the data was smoothed to have 10 data points per second. The worked hemodynamic data were saved in .csv files to be imported into statistical platforms for further analysis.

3.6 Acute *in-vivo* pharmacology experiments.

Mice with cranial windows were imaged in baseline conditions following the same procedures of sections 3.2, 3.3 and 3.4 of this chapter, to obtain information about pericytes location. Next, anesthetized mice (2% isoflurane) underwent a cranial window removal surgery, in which the sapphire glass was carefully removed by drilling away the dental cement and trying to limit damage of the blood vessels. After the window removal, a solution of 10 μM of nimodipine dissolved in PEG400 (10 μL) and cortex buffer (990 μL), or PEG400 in cortex buffer (sham solution) was topically applied with a sponge to the surface of the exposed area and left there for 20 minutes. During this time intravenous injection of the corresponding fluorescent dextran according to the mice line was applied as in section 3.3 of this chapter. After the 20 minutes of nimodipine or sham solution application, a 2% agarose gel was applied to the brain surface and a new glass window was placed on top and covered it with ultrasound gel to facilitate two-photon imaging. Finally, ketamine (20mg/kg) and

xylazine (10mg/kg) were administered intraperitoneally and isoflurane anesthesia was removed.

Two-photon imaging of the mice and image processing were done using the same methodology as in sections 3.4 and 3.5 of this chapter. Mice from acute experiments were euthanized with a pentobarbital overdose (>150 mg/kg) after the two-photon imaging was concluded.

3.7 Blood pressure measurements.

Blood pressure measurements were taken using the CODA Monitor non-invasive blood pressure system. This system determines blood pressure based on the tail blood volume of the mice by using volume pressure recording (VPR). The obtained data goes through a differential pressure transducer to process the information and give measurements like systolic and diastolic blood pressure, mean blood pressure, and heart rate[159,160].

We measured blood pressure of the mice during two-photon imaging sessions of repeated *in-vivo* pharmacology and acute *in-vivo* pharmacology experiments. The mice, following steps 3.3 and 3.6, were placed on a heating pad with temperature control monitored by a rectal thermometer. The tail was inserted into the occlusion cuff and VPR systems after conducting preliminary tests to identify any air leaks. If any leaks were detected, the CODA system would not proceed with the measurements. Blood pressure readings were taken at 15-second intervals over 5-minute periods. Each imaging session involved approximately 10 measurement periods. The measurements were manually recorded and saved in .csv format for subsequent analysis using statistical software.

3.8 Statistical Analysis.

We used the R programming platform to analyze the data sets obtained from all our experiments. In the Repeated *in-vivo* pharmacology study, the results for calcium, hemodynamics and blood pressure measurements were averaged according to the detected signals from each pericyte and blood vessel per each trial taken. The Normal distribution of

the data was assessed visually with the Quantile-Quantile (Q-Q) plots, histograms, and box plots, and statistically with Shapiro-Wilk Test. When the data was not normally distributed, the conversion to log normal was used and the normal distribution was tested after the conversion with the above methodology. Detection of outlier data was done using the Rosner's test with a minimum value of 2 and a maximum value of 15 outliers for detection, the detected outliers were discarded from the data set. Linear Mix Models (LMM) were used to evaluate repeated measurements using the pharmacology condition as a fixed effect. Animal ID, number of pericyte spots or number of blood vessels were used as random effects. The likelihood-ratio of the LMM and their omnibus significance was performed with Anova test evaluating the LMM with and without the fixed effect. To evaluate the difference between pharmacology conditions pairwise comparisons with Holm-sequential Bonferroni correction were used.

In the Acute in vivo pharmacology study, the distribution of results for calcium, hemodynamics, and blood pressure measurements, as well as outlier detection were assessed as mentioned above. To test the significant difference independent samples t-test was used if the data were normally distributed, and the Mann-Whitney U test as a nonparametric test when the data set did not comply with normality.

3.9 Materials and Equipment used.

Table III. Materials and Equipment used.

Material/ Equipment	**Company**	**Catalog Number**	**Comments**
Acta2-RCaMP1.07 mice	The Jackson Laboratory	28345	Common Name: CHROMus line acta2-RCaMP1.07
Applicators (Regular)	Bisco	X-80250P	
Agarose	Sigma Aldrich		
ace acA2040-55um camera	Basler	107210	
BioFormats package for MATLAB	NA	NA	Available in: https://docs.openmicroscopy.org/bioformats/

CHIPS MATLAB toolbox	NA	NA	Barrett MJP, Ferrari KD, Stobart JL, Holub M, Weber B. CHIPS: an Extensible Toolbox for Cellular and Hemodynamic Two-Photon Image Analysis. Neuroinformatics. 2018;16(1):145-147. doi:10.1007/s12021-017-9344-y. Available in: https://github.com/EIN-lab/CHIPS
Clear Ultrasound Gel, Medium viscosity	HealthCare Plus	UGC250	
Dextran, fluorescein, 70,000 MW, anionic	Thermo Fisher Scientific	D1823	
Dextran, Texas Red, 70,000 MW, neutral	Thermo Fisher Scientific	D1830	
Dental cement	Bisco dental	NA	
Eye Lube Plus	Optixcare	NA	
FIJI	Image J	NA	Available in: https://imagej.net/Fiji/Downloads
GCaMP6s$^{fl/fl}$ mice	The Jackson Laboratory	28866	Common Name: Ai96(RCL-GCaMP6s) (C57BL/6J) or Ai96 (C57BL/6J)
Head Post	NA	NA	This product is custom made
Head Post fixing platform	University of Zurich	NA	
Isoflurane	University of Manitoba	NA	
Ketamine (Narketan 100 mg/mL)	Vetoquinol	440893	
MATLAB R2020b	Mathworks	NA	Available in: https://www.mathworks.com/downloads/
MC_Stimulus II	Multichannel systems	NA	Please refer: https://www.multichannelsystems.com/sites/multichannelsystems.com/files/documents/manuals/MCS_STG4004%2BSTG4008_Manual.pdf
30 G Needle 0.3mmx25mm	BD PrecisionGlide	305128	
Nimodipine	Sigma Aldrich	66085-59-4	

Objective XLUMPLFLN20XW	Olympus	NA	Please refer: https://www.olympus-lifescience.com/en/objectives/lumplfln-w/
PDGFRβ-CreERT2 mice	The Jackson Laboratory	30201	Common Name: PDGFRβ-P2A-CreER^{T2}
Polyethylene Tubing, PE10 I.D. 28mm (0.11") O.D. 61mm (.024")	BD Intramedic	427401	
Pyr3	TOCRIS	3751	
Prairie View	Bruker Fluorescence Microscopy	NA	Please refer: https://www.bruker.com/en/products-and-solutions/fluorescence-microscopy/multiphoton-microscopes/ultima-in-vitro.html
Polychrome IV	Till photonics	NA	
Saphire glass	NA	NA	This product is custom made
STG4008 stimulus generator	Multichannel systems	NA	Please refer: https://www.multichannelsystems.com/sites/multichannelsystems.com/files/documents/manuals/MCS_STG4004%2BSTG4008_Manual.pdf
Tamoxifen	Sigma Aldrich	10540-29-1	
Ultima In Vitro Multiphoton Microscope	Bruker Fluorescence Microscopy	NA	Please refer: https://www.bruker.com/en/products-and-solutions/fluorescence-microscopy/multiphoton-microscopes/ultima-in-vitro.html
Under Tank Heater	Reptitherm U.T.H	E169064	
Xylazine (Rompun 20 mg/mL)	Bayer HealthCare	2169592	

Chapter IV. Results.

4.1 Visualization and identification of brain pericyte subpopulations.

To visualize and make a sharp identification of the different pericyte populations, we utilized Acta2-RCaMP1.07 mice that express the red genetically encoded calcium indicator (GECI), RCaMP1.07, in alpha smooth muscle actin (α-SMA) expressing cells, and PDGFRβ-CreERT2:GCaMP6s$^{fl/fl}$ mice which express the green GECI GCaMP6s in cells with platelet-derived growth factor receptor beta (PDGFRβ) after a Cre-Lox recombination process derived from tamoxifen administration (Fig. 1A). In order to access brain pericytes, we performed a craniotomy over the somatosensory cortex to implant a chronic cranial window (as previously described)[161] for visualization of calcium fluctuations and fluorescence with two-photon microscopy (Section 3.1 Materials and methods). The recovery period of the mice was three weeks and tamoxifen injections for PDGFRβ-CreERT2:GCaMP6s$^{fl/fl}$ mice line were done during this time (Fig. 1A).

In the Acta2-RCaMP1.07 mice, we observed RCaMP1.07 fluorescence in α-SMA positive cells on arteries and arterioles (Fig. 1B upper image, pointed with white arrows). We could also see a clear definition of EP morphology such as the previously defined by others "bump-on-a-log" shape, with an ovoid cell soma and enwrapping processes around the blood vessels of the transition zone[162,163] (Fig. 1B lower image). It is important to mention that the RCaMP fluorescence gradually decreased at further blood vessel bifurcations towards the capillary zone. This matches with the reported decrease of α-SMA in higher branching order of downstream vessels[164,165]. To visualize capillary pericytes, we used PDGFRβ-CreERT2:GCaMP6s$^{fl/fl}$ mice and we observed GCaMP fluorescence (Fig. 1C upper image, pointed with white arrows) defining clear capillary pericyte morphology like an elongated ovoid soma and thin processes that travel along the brain capillaries (Fig. 1C lower image). This multimodal transgenic mice line approach allowed us to delimit ensheathing pericytes in the transition zone (1st to 4th branching order) thanks to the decrease of fluorescence with the decrease of αSMA in the Acta2-RCaMP1.07 mice line and to separately identify and compare structural morphology and localization of capillary pericytes in the capillary zone

(5th to higher branching order) with PDGFRβ-CreERT2:GCaMP6s$^{fl/fl}$ mice (Fig. 1D). This is crucial for establishing calcium signaling properties and the influence of pericyte populations on blood vessels hemodynamics, since the misunderstanding of pericyte types has created confusion in their functional roles and capacity to regulate CBF[101,131].

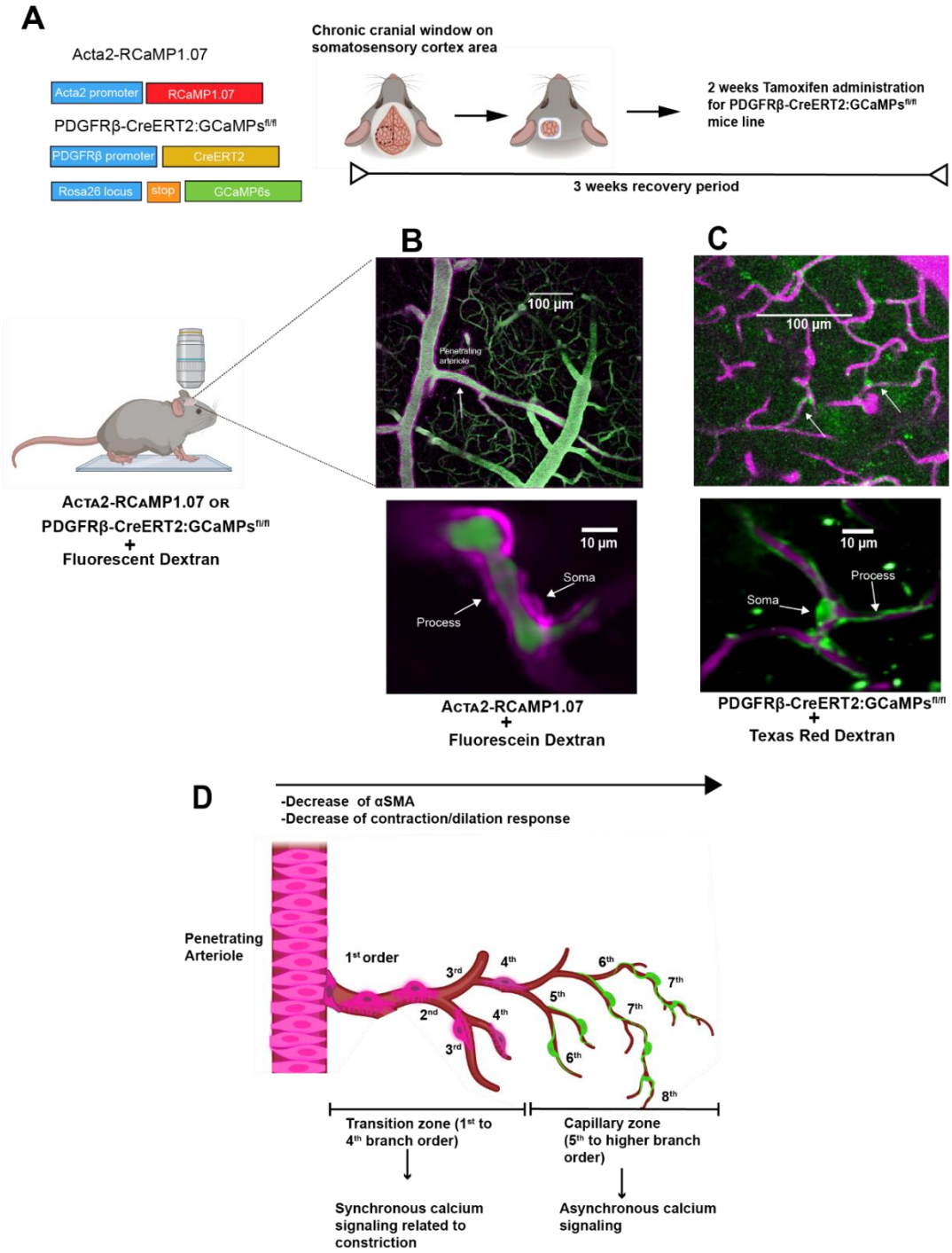

Figure 1. Visualization and identification of brain pericyte subpopulations. A) Mice models and surgical scheme. **B)** Visualization of cells expressing αSMA (upper image, white arrows) and EP morphology (lower image) in Acta2-RCaMP1.07 mice line. Blood vasculature was labeled using fluorescein dextran. **C)** Visualization of cells expressing PDGFRβ (upper image) and CP morphology (lower image) in PDGFRβ-CreERT2:GCaMPs$^{fl/fl}$ mice line. Blood vasculature was labeled using Texas red dextran. **D)** Diagram of brain vasculature transition and capillary zone covered by distinct types of pericytes. Description of brain pericyte calcium signaling characteristics and branch order classification are shown.

4.2 L-type VGCC and TRPC3 channels have different effects on spontaneous pericyte calcium signaling.

To study pericyte calcium channel machinery and their contributions to spontaneous calcium events, we evaluated calcium signaling in EP and CP by two-photon microscopy and assessed the resting calcium (baseline fluctuations) and the effect of calcium channel blockers to L-type VGCC and TRPC3 channels in different repeated imaging sessions of the same fields of view. We recorded one minute calcium movies in baseline conditions and after the intraperitoneal injection application of calcium channel blockers that have different mechanism of action, L-type VGCC blocker Nimodipine (1mg/kg) and the specific TRPC3 channel blocker Pyr3 (20mg/kg). The movies were processed in MATLAB with our Cellular and Hemodynamic Two-photon Image Analysis (CHIPS; Section 3.5.1 Materials and Methods) to extract calcium signaling features such as amplitude (d/dF of calcium peaks) and frequency (signals/minute). Additionally, we monitored the calcium signaling of pericyte morphological structures, somata and processes, to detail the calcium mechanisms in each of these compartments (Fig. 2A-B & D-E). We found that calcium amplitude and frequency of signals in EP soma and processes significantly decreased under the presence of nimodipine (Fig. 2B & C; Table 1.1 and 1.2). Furthermore, we saw a decrease with Pyr3 only in the calcium frequency of EP processes.

In contrast with EP calcium signaling, the amplitude of CP processes significantly decreased with Pyr3, and there was a tendency for reduced somata amplitude as well ($P = 0.086$). Similar to EP, nimodipine decreased amplitude and frequency of both soma and processes of CP (Figure 2E & F).

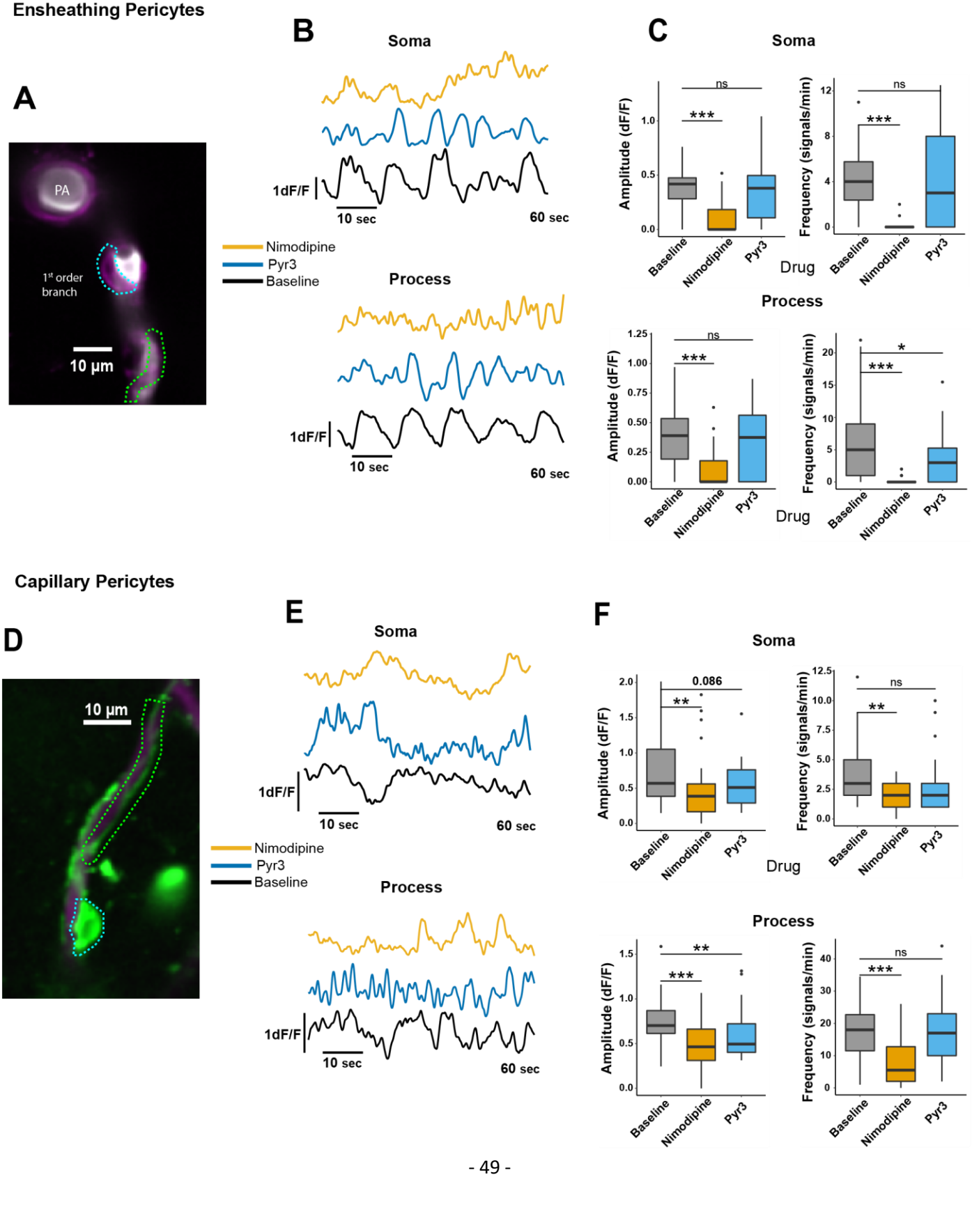
Ensheathing Pericytes
A
PA
1st order branch
10 µm
B
Soma
1dF/F
10 sec
60 sec
Nimodipine
Pyr3
Baseline
Process
1dF/F
10 sec
60 sec
C
Soma
Amplitude (dF/F)
Frequency (signals/min)
ns
***
Baseline
Nimodipine
Pyr3
Drug
Process
Amplitude (dF/F)
Frequency (signals/min)
ns
***
*
Baseline
Nimodipine
Pyr3
Drug
Capillary Pericytes
D
10 µm
E
Soma
1dF/F
10 sec
60 sec
Nimodipine
Pyr3
Baseline
Process
1dF/F
10 sec
60 sec
F
Soma
Amplitude (dF/F)
0.086
**
Frequency (signals/min)
ns
**
Baseline
Nimodipine
Pyr3
Drug
Process
Amplitude (dF/F)
**
***
Frequency (signals/min)
ns
***
Baseline
Nimodipine
Pyr3

Figure 2. L-type VGCC and TRPC3 channels have different effects on spontaneous pericyte calcium signaling. A) Two-photon image of a brain ensheathing pericyte from Acta2-RCaMP1.07 mice line. Soma of pericyte marked with cyan dashed line; Process of the pericyte marked with green dashed line. *Following panels B, C, E and F make a comparison between baseline and calcium channel blockers **Nimodipine** and **Pyr3.*** **B)** Individual calcium signaling traces of pericyte from panel "A" marked areas. **C)** Calcium signaling properties (amplitude and frequency) of ensheathing pericyte morphology structures (soma and process). N=7; n=43 **D)** Two-photon image of brain capillary pericyte from PDGFRβ-CreERT2:GCaMPs$^{fl/fl}$ mice line. Soma of pericyte marked with cyan dashed line; Process of the pericyte marked with green dashed line. **E)** Individual calcium signaling traces of pericyte from panel "D" marked areas. **F)** Calcium signaling properties (amplitude and frequency) of capillary pericyte morphology structures (soma and process). N=7; n=44. N= # of animals, n= # of pericytes P-value<0.05=*; P-value<0.01=**; P-value<0.001=***. For specific p-values and mean ± SD information please refer to table 1.1 and table 1.2 (Section 4.7, P-Values and mean ± SD Results). Linear mixed models for repeated measurements and pairwise comparisons with Holm-sequential Bonferroni correction were used in the statistical tests.

4.3 Blood vessel hemodynamic properties of the transition zone are affected by ensheathing pericyte calcium channel activity.

As mentioned before, EP have been recently classified as mural cells that significantly contribute to the regulation of brain blood flow. Several studies have shown their capacity to constrict and dilate blood vessels [15,97,101,115,127,128,166–168]. L-type VGCC are known to contribute to EP contraction/dilation,[115,169,170] but the role of other calcium channels,[132,133,171] such as TRPC3, are yet to be fully elucidated. To investigate the extent of influence of L-type VGCC and TRPC3 channels of EP in the regulation of CBF, we measured blood vessel hemodynamics, such as diameter (μm), RBC velocity (mm/s) and RBC flux (cells/sec), in vessels covered by EP in baseline and under the effect of nimodipine and Pyr3. The hemodynamic measurements were done in the same two-photon imaging session of the EP calcium signaling recording using the same mice subjects (Acta2-RCaMP1.07 mice line) and applying the calcium channel blockers via intraperitoneal injections. Line scan features from the two-photon microscope were used to measure changes in fluorescence of brain vasculature labeled with fluorescein dextran. The resulting output consists of kymographs, which are graphical representations that visually depict the spatial position of RBC over a period of time (Fig. 3D). The kymographs were processed in CHIPS MATLAB toolbox to obtain mean numeric values for diameter, velocity, and flux. (Section 3.5.2 Materials and Methods).

Figures 3A & B show a representative image and diameter traces from a 1st order branch blood vessel covered by an ensheathing pericyte during baseline and after the calcium

channel blockers. Our results show that both nimodipine and Pyr3 cause a dilatory effect in blood vessels of the transition zone (Fig. 3A-C; Table 2.1 and 2.2). Since the blood vessels of the transition zone have vasomotion[132,172], we also examined attributes like vasomotor index which the diameter amplitude change (ΔD/D) during vasomotor fluctuations and peak frequency that gives the number of diameter oscillations of the vessel wall per minute. We found that these characteristics of vasomotion significantly decreased with nimodipine (Fig. 3C). In contrast, Pyr3 decreased the vasomotor index of the blood vessels covered by EP but did not impact the frequency of vasomotor oscillations (Figure 3C-E).

To evaluate the impact of the changes in diameter and vasomotion in blood flow dynamics caused by the calcium channel blockers, we measured velocity (mm/s) and RBC flux (cells/second) of the blood vessels covered by EP. Figure 3D includes kymographs illustrating a specific example of a 3rd branch order blood vessel in the transition zone in baseline and with calcium channel blockers. In these kymographs, black areas represent RBC, and white areas indicate blood plasma. Figure 3E and G are the representative traces of the velocity and flux measurements from figure 3D showing quantitatively the changes in the three conditions. We found that nimodipine caused a significant decrease in the velocity of blood flow, and in some cases, we noticed rapid and contrasting drops of velocity (Figure 3D, 3E, 3F). Inversely, Pyr3 tended to increase velocity (p-value=0.067), and significantly increased RBC flux (Figure 3G, 3H).

Recent studies have found that the kinetics of dilation/constriction differ in the distinct branches of the brain vasculature in the transition zone[165,167,173]. Furthermore, it has been found that first branch blood vessel plays a crucial role in brain capillary perfusion[173]. Therefore, we evaluated the role of L-type VGCC and TRPC3 channels in hemodynamics in the 1st to 3rd branches of the transition zone. Figure 4A shows a representative example of the branch order classification. Nimodipine caused a significant diameter increase in the 1st and 2nd branches, but had no significant effect in the 3rd branch (Fig. 4B). However, Pyr3 dilated only the 2nd branch (Fig. 4B left). Regarding the vasomotion features, we found that nimodipine significantly decreased the vasomotor index in all the three branches, whereas Pyr3 decreased the vasomotor index of the 2nd and 3rd branches (Fig. 4C). Lastly, peak

frequency was reduced by nimodipine in the 2nd and 3rd branches, but unaffected by Pyr3 (Fig. 4D).

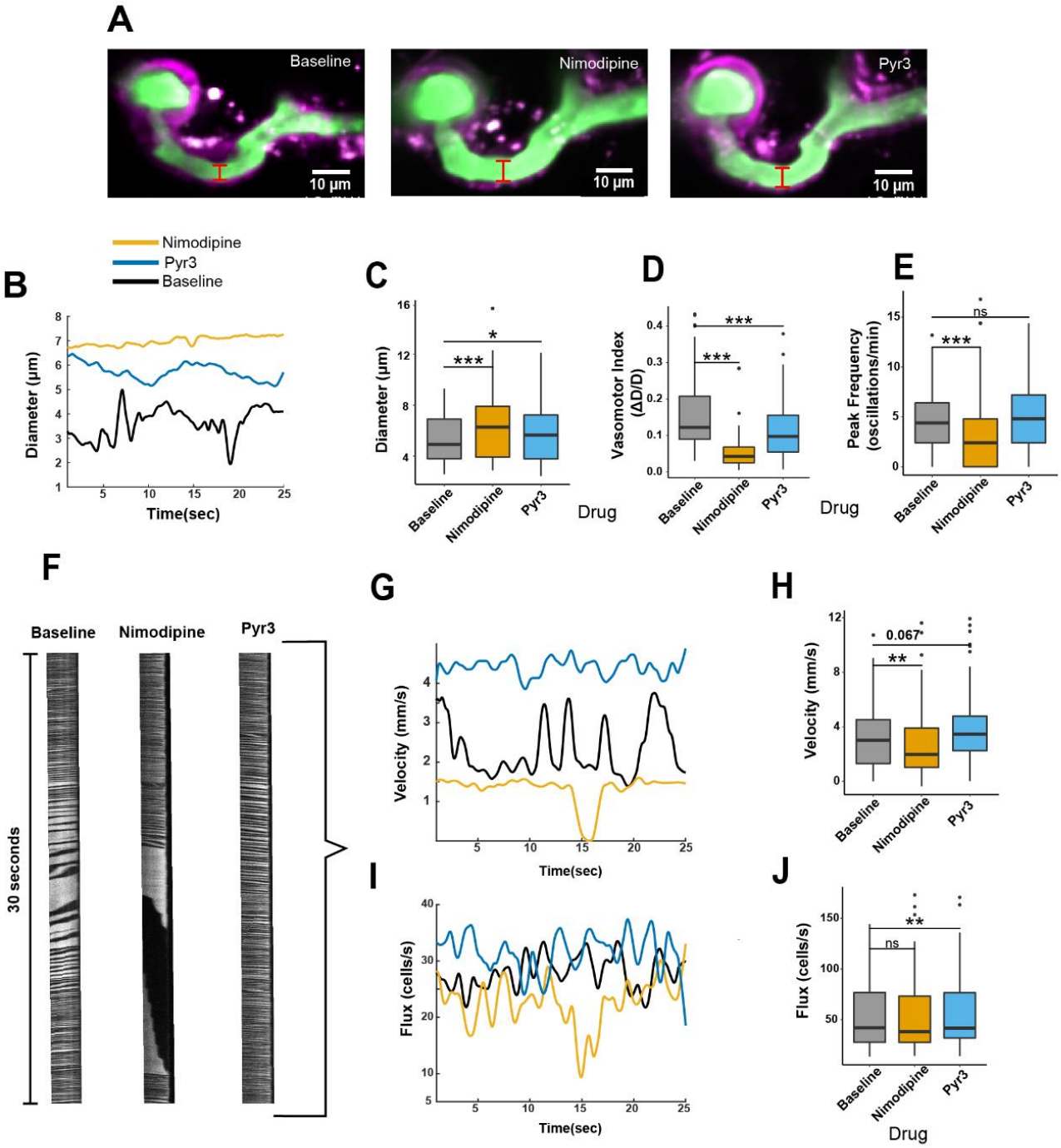

Figure 3. Blood vessel hemodynamic properties of the transition zone are affected by ensheathing pericyte calcium channel activity. *All the following panels make a comparison between baseline and calcium channel blockers* ***nimodipine*** *and* ***Pyr3*****. A)** Two-photon images of a first branch order blood vessel covered by ensheathing pericytes from Acta2-RCaMP1.07 mice line. The vasculature is labeled fluorescein dextran. **B)** Individual traces of diameter from blood vessel of panel "A" area marked with a red line. **C)** Diameter, **D)** vasomotor index and **E)** peak frequency of blood vessels from the transition zone covered by ensheathing pericytes. N=7; n= 101. **F)** Representative kymographs of 3rd branch order blood vessel. The black spaces represent RBC, and the white spaces represent blood plasma. Duration of the kymographs= 30 seconds. Individual traces of velocity (**G)** and flux (**H**) from blood vessel kymographs of panel "D". Box plots of **I)** velocity and **J)** flux of blood vessels from the transition zone covered by ensheathing pericytes. N=7; n= 101. N= # of animals, n= # of blood vessels P-value<0.05=*; P-value<0.01=**; P-value<0.001 For specific p-values and mean ± SD information please refer to table 2.1 and table 2.2 (Section 4.7, P-Values and mean ± SD Results). Linear mixed models for repeated measurements and pairwise comparisons with Holm-sequential Bonferroni correction were used in the statistical tests.

In the evaluation of blood flow dynamics, nimodipine slightly decreased the velocity of the 1st branch (P= 0.062) but did not affect velocity in the2nd and 3rd branches (Fig. 4E), nor the flux in any branch (Fig. 4F). In contrast, Pyr3 increased velocity and flux of 2nd and 3rd branches (Fig. 4E and 4F).

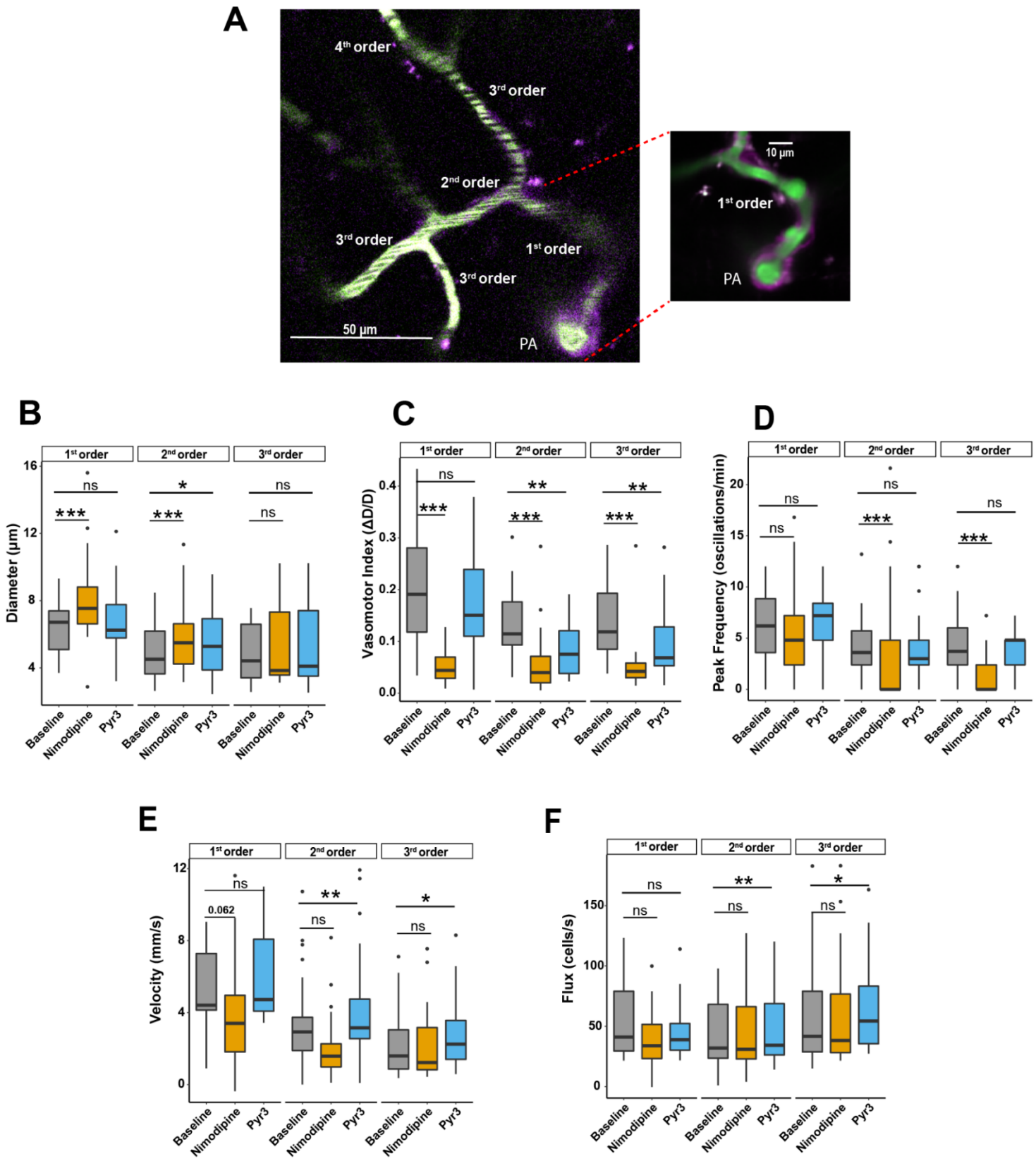
A
4th order
3rd order
2nd order
3rd order
1st order
3rd order
50 µm
PA
10 µm
1st order
PA
B
1st order
2nd order
3rd order
Diameter (µm)
ns
***
*
***
ns
***
Baseline
Nimodipine
Pyr3
C
Vasomotor Index (ΔD/D)
ns
***
**
***
**
***
D
Peak Frequency (oscillations/min)
ns
ns
***
ns
***
E
Velocity (mm/s)
0.062
ns
**
ns
*
ns
F
Flux (cells/s)
ns
ns
**
ns
*
ns

Figure 4: Hemodynamic properties of the blood vessels from the arteriole transition zone vary according to their branching order under the effect of calcium channel blockers. A) Two photon images of brain vasculature from Acta2-RCaMP1.07 mice line showing blood vessels branching. Dashed red lines show the magnification of the selected frame for better visualization. The vasculature is labeled with fluorescein dextran. *All the following panels make a comparison between baseline and calcium channel blockers **Nimodipine** and **Pyr3.*** **B)** Diameter **C)** vasomotor index **D)** peak frequency, **E)** velocity and **F)** flux of 1st, 2nd, and 3rd branch order blood vessels. N=7; b1= 27; b2=32; b3=29. N= # of animals, b(n)= # of blood vessels from a given branch order P-value<0.05=*; P-value<0.01=**; P-value<0.001=***. For specific p-values and mean ± SD information please refer to table 2.1 and table 2.2 (Section 4.7, P-Values and mean ± SD Results). Linear mixed models for repeated measurements and pairwise comparisons with Holm-sequential Bonferroni correction were used in the statistical tests.

4.4 L-type VGCC and TRPC3 channels have differential effects on resting capillary hemodynamics.

To investigate the contributions of L-type VGCC and TRPC3 channels to capillary blood flow, we evaluated capillary hemodynamics in the same two-photon imaging session in which we monitored CP calcium signaling using PDGFRβ-CreERT2:GCaMP6s$^{fl/fl}$ mice, applying the calcium channel blockers via intraperitoneal injections and using Texas red dextran to label the brain vasculature. We followed the same line scan methodology and processing as with the blood vessels of the transition zone (Section 3.4.3 & 3.5.2 Materials and Methods). Blood vessels covered by CP significantly dilated with TRPC3 channel blocker, Pyr3, in comparison with baseline conditions and the L-type VGCC blocker, Nimodipine (Fig. 5A- C; Table 3.1 and 3.2). In terms of blood flow, nimodipine decreased velocity and RBC flux (Fig. 5D-H), but also caused heterogenous fluctuations in velocity (Fig. 5E). In contrast, Pyr3 did not alter these properties compared to baseline (Fig.5D-H).

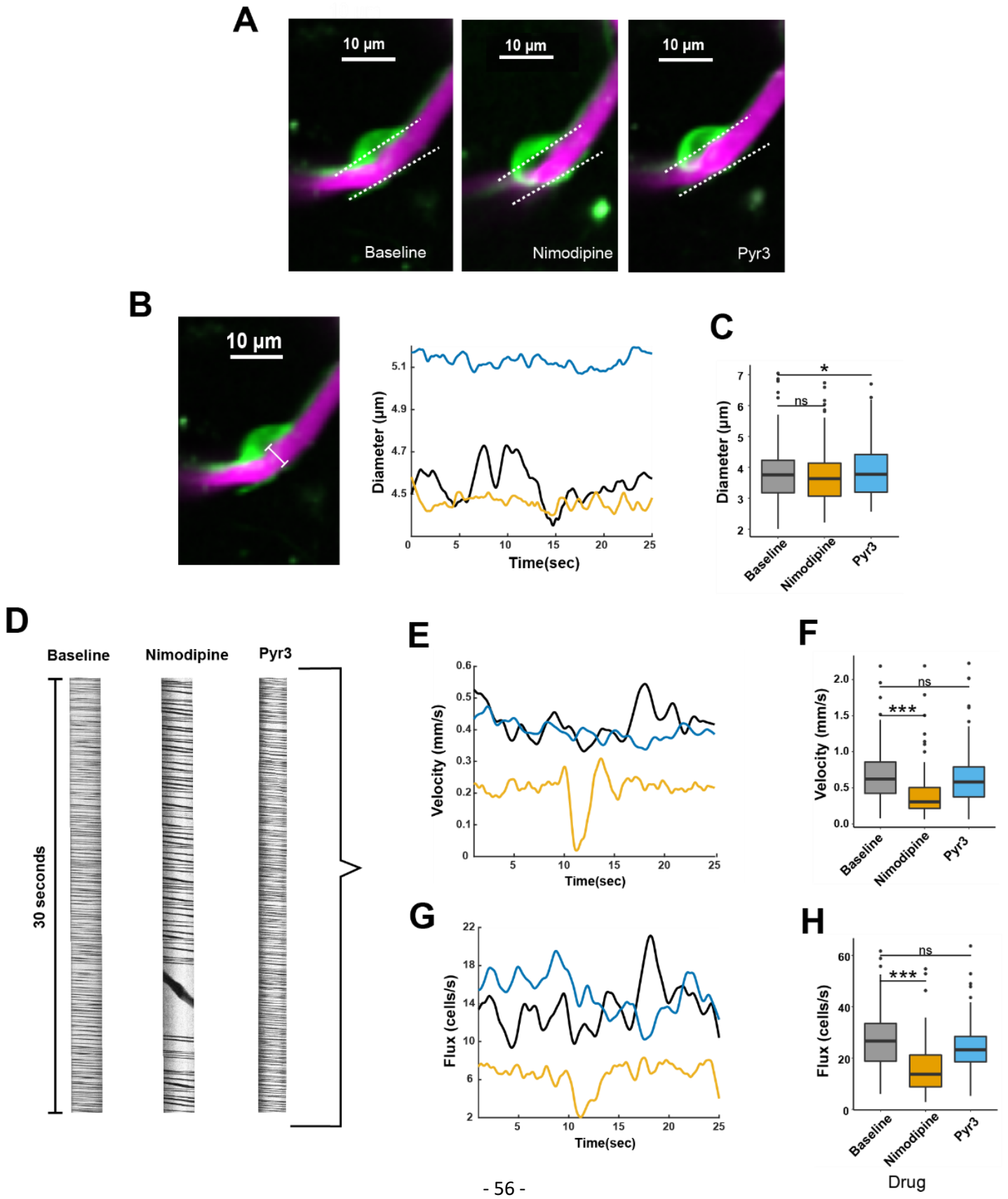
A
10 µm
Baseline
Nimodipine
Pyr3
B
10 µm
Diameter (µm)
Time(sec)
C
Diameter (µm)
ns
*
Baseline
Nimodipine
Pyr3
D
Baseline
Nimodipine
Pyr3
30 seconds
E
Velocity (mm/s)
Time(sec)
F
Velocity (mm/s)
ns
***
Baseline
Nimodipine
Pyr3
G
Flux (cells/s)
Time(sec)
H
Flux (cells/s)
ns
***
Baseline
Nimodipine
Pyr3
Drug

Figure 5: L-type VGCC and TRPC3 channels have differential effects on resting capillary hemodynamics. *All the following panels make a comparison between baseline and calcium channel blockers* ***Nimodipine*** *and* ***Pyr3*****. A)** Two-photon image of a brain capillary covered by a capillary pericyte from PDGFRβ-CreERT2:GCaMPs$^{fl/fl}$ mice line. The vasculature is labeled with Texas red dextran. The white dashed line represents the same magnitude of area encasing tangentially the brain capillary. **B)** Two-photon image and Individual traces of brain capillary diameter from panel "A", the continuous white line represents the area of the diameter measured shown in the traces. **C)** Box plots of diameter of brain capillaries covered by capillary pericytes. N=7 n=109**. D)** Individual representative kymographs of one brain capillary. The black spaces represent RBC, and the white spaces represent blood plasma. Duration of the kymographs= 30 seconds. Individual traces of velocity **(E)** and flux (**G)** from blood vessel kymographs of panel "D". Box plots of velocity **(F)** and flux **(H)** of brain capillaries covered by capillary pericytes. N=7; n= 109. N= # of animals, n= # of blood vessels, P-value<0.05=*; P-value<0.01=**; P-value<0.001=***. For specific p-values and mean ± SD information please refer to table 3.1 and table 3.2 (Section 4.7, P-Values and mean ± SD Results). Linear mixed models for repeated measurements and pairwise comparisons with Holm-sequential Bonferroni correction were used in the statistical tests.

4.5 Brain pericyte calcium response during neurovascular coupling is altered by calcium channel blockers.

To further investigate the influence of L-type VGCC and TRPC3 channels on pericyte calcium signaling during sensory stimulation known to evoke NVC, we monitored calcium signaling from EP and CP located in a highly activated areas of the somatosensory cortex following injection of calcium channel blockers, nimodipine and Pyr3, in our two mice lines. Intrinsic optical imaging (IOI) was used to map activated brain regions corresponding to the whisker area and pericytes in these locations were the focus for the two-photon imaging sessions. To ensure a strong sensory stimulation in anesthetized mice, we used a mild electric shock applied to the whisker area at 500μA at 4Hz for 5 seconds during the two-photon imaging sessions (Fig. 6A). Previous studies have shown that nearby neuronal activity induces a drop in EP and CP calcium signaling[132,174]. Similarly, we found that EP somata and processes experience a drop in calcium signaling during the 5 seconds period of stimulation and a slight rise of calcium after this period (Fig. 6B; baseline). Nimodipine and Pyr3 decreased this EP calcium behaviour during stimuli in both pericyte structures, but nimodipine had a stronger impact on calcium signaling in EP processes (Fig.6B & C; Table 4.1 and 4.2). CP also showed the decrease of calcium during the 5 seconds period of whisker stimulation in both soma and process, but in contrast with EP, the drop of calcium appears to happen slower after the stimulation starts and they do not show the rise in Ca^{2+} in the post-stimulation period (Fig. 6D). Furthermore, nimodipine abolished the calcium decrease in CP,

particularly in the processes; however, we did not find any significant effects of Pyr3 (Fig.6D & E; Table 4.1 and 4.2).

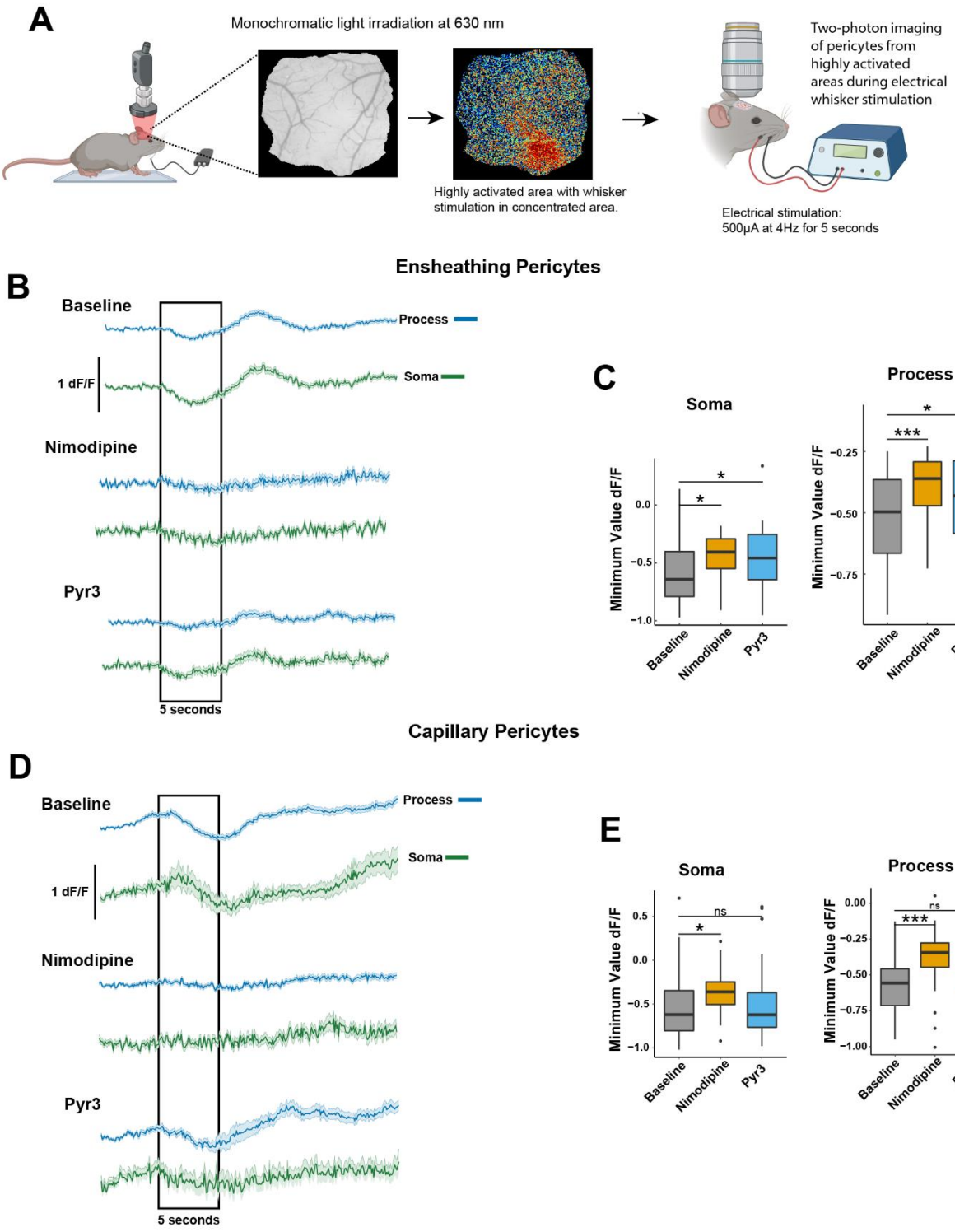

Figure 6. Brain pericyte calcium response during neurovascular coupling is altered by calcium channel blockers. A) Cartoon illustrating the experimental set up of IOI and electrical whisker stimulation. *All the following panels make a comparison between baseline and calcium channel blockers* ***Nimodipine*** *and* ***Pyr3.*** **B)** Calcium signaling traces of EP during NVC. Black box represents the 5 seconds of electrical whisker stimulation (500 μA at 4 Hz). The traces show the mean value + SEM. Total seconds of traces=25; N=5; n=33 **C)** Box plots of the minimum value of calcium peak amplitude of EP morphology structures (soma and process) during the stimulation period. N=5; n=33 **D)** Calcium signaling traces of CP during NVC. Black box represents the stimulation period. The traces show the mean value + SEM. Total seconds of traces=25; N=7; n=42**. E)** Box plots of the minimum value of calcium peak amplitude of CP morphology structures (soma and process) during the stimulation period; N=7; n=42. N= # of animals, n= # of pericytes P-value<0.05=*; P-value<0.01=**; P-value<0.001=***. For specific p-values and mean ± SD information please refer to table 4.1 and table 4.2 (Section 4.7, P-Values and mean ± SD Results). Linear mixed models for repeated measurements and pairwise comparisons with Holm-sequential Bonferroni correction were used in the statistical tests.

4.6 Blood vessel hemodynamic properties are differentially altered by brain pericyte calcium channel activity during neurovascular coupling.

Since brain pericyte calcium signaling is decreased during NVC and it has been shown that this influences CBF[130,167,175,176] we were also interested to evaluate hemodynamics during electrical whisker stimulation and with calcium channel blockers. We measured diameter, velocity, and flux of blood vessels from the transition zone and brain capillaries in the same imaging sessions and in the same mice in which we imaged pericyte calcium signaling. We calculated the percent change in hemodynamics during stimulation relative to the pre-stimulus baseline period. There was a significant increase in diameter during the period of stimulation (5 seconds) and it lasted a few seconds more after the stimulation ceased, followed by a strong decrease of diameter (Fig. 7A). Calcium channel blockers reduced this behavior, with nimodipine having the greatest effect (Fig. 7A & 7B; Table 5.1 and 5.2). We also classified vessels as the 1st to the 3rd branch order based on their position in the transition zone. Nimodipine greatly reduced the dilation caused by whisker stimulation in the 1st and 2nd branches, but only minorly impaired the 3rd branch (P=0.059). Pyr3 caused a significant reduction of the dilation caused by stimulation at the 2nd branch, but had no effect on the 1st and 3rd branch (Fig. 7C). RBC velocity increased during the period of whisker stimulation and, similar to diameter, this increase lasted longer than the stimuli followed by an undershoot after the velocity increase (Fig. 7D).

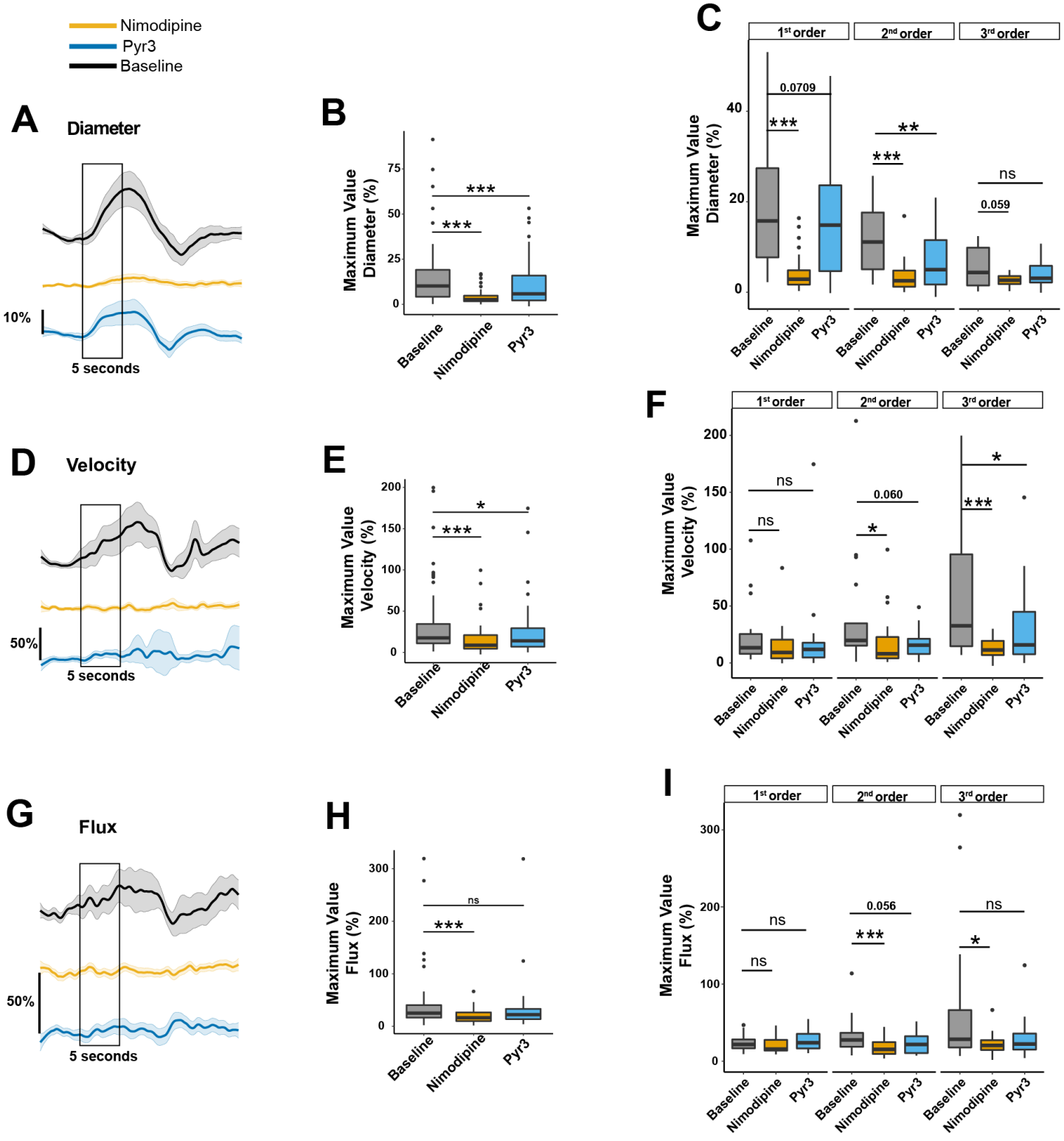
Nimodipine
Pyr3
Baseline
A
Diameter
10%
5 seconds
B
Maximum Value Diameter (%)
***
***
Baseline
Nimodipine
Pyr3
C
1st order
2nd order
3rd order
0.0709
***
**
***
ns
0.059
Maximum Value Diameter (%)
D
Velocity
50%
5 seconds
E
Maximum Value Velocity (%)
*
***
F
ns
ns
0.060
*
*
***
Maximum Value Velocity (%)
G
Flux
50%
5 seconds
H
Maximum Value Flux (%)
ns
***
I
ns
ns
0.056
***
ns
*
Maximum Value Flux (%)

Figure 7: Blood vessel from the arteriole transition zone hemodynamic properties are differentially altered by brain pericyte calcium channel activity during neurovascular coupling. *All the following panels make a comparison between baseline and calcium channel blockers* ***Nimodipine*** *and* ***Pyr3.*** Traces of the percentage change of diameter (**A),** velocity **(D)** and flux **(G)** of blood vessels from transition zone during 5 seconds of whisker electrical stimulation (500 μA at 4 Hz) relative to diameter baseline. The black box represents the start of 5 seconds of stimulation. The traces show the mean value ± SEM. Total seconds of traces=25; N=5; n=65**. Box** plots of maximum value of diameter **(B)**, velocity **(E)** and flux **(H)** percentage change during the 5 seconds of whisker electrical stimulation of blood vessels from the transition zone. N=5; n=65**. Box** plots of maximum value of diameter **(C)**, velocity **(F)** and flux **(I)** percentage change during the 5 seconds of whisker electrical stimulation of 1st, 2nd, and 3rd branch order blood vessels from the transition zone. N=5; b1=16, b2=21, b3=19. N= # of animals, n= #of blood vessels, b(n)= # of blood vessels from a given branch order P-value<0.05=*; P-value<0.01=**; P-value<0.001=***. For specific p-values and mean ± SD information please refer to table 5.1 and table 5.2 (Section 4.7, P-Values and mean ± SD Results). Linear mixed models for repeated measurements and pairwise comparisons with Holm-sequential Bonferroni correction were used in the statistical tests.

Both calcium channel blockers reduced this effect during whisker stimulation, but nimodipine caused a greater reduction in velocity than Pyr3 (Fig. 7D & 7E). The effects of these blockers on velocity were obvious in the 2nd and 3rd branches, but not the 1st branch (Fig. 7F). In the terms of RBC flux during whisker stimulation, there was also an increase during stimulation and then undershoot after. Similar to velocity, nimodipine reduced the flux (Fig. 7G & H), particularly in the 2nd and 3rd branches (Fig. 7I). However, Pyr3 did not significantly reduce the flux elevation, though there was a tendency in the 2nd branch for a reduction (P=0.056; Fig. 7I).

Brain capillaries covered by CP behaved somewhat differently than vessels from the transition zone covered by EP. We detected a subtle but substantial capillary dilation during the whisker stimulation without an undershoot of the diameter following the dilation (Fig. 8A). Nimodipine significantly reduced this dilation during the stimulation period, while Pyr3 had no effect (Fig. 8A & 8B; Table 6.1 and 6.2). Likewise, electrical stimulation increased RBC velocity and flux through capillaries (Fig. 8C & E). Nimodipine significantly abolished this velocity and flux behavior, whereas Pyr3 did not cause any alteration (Fig. 8C-F).

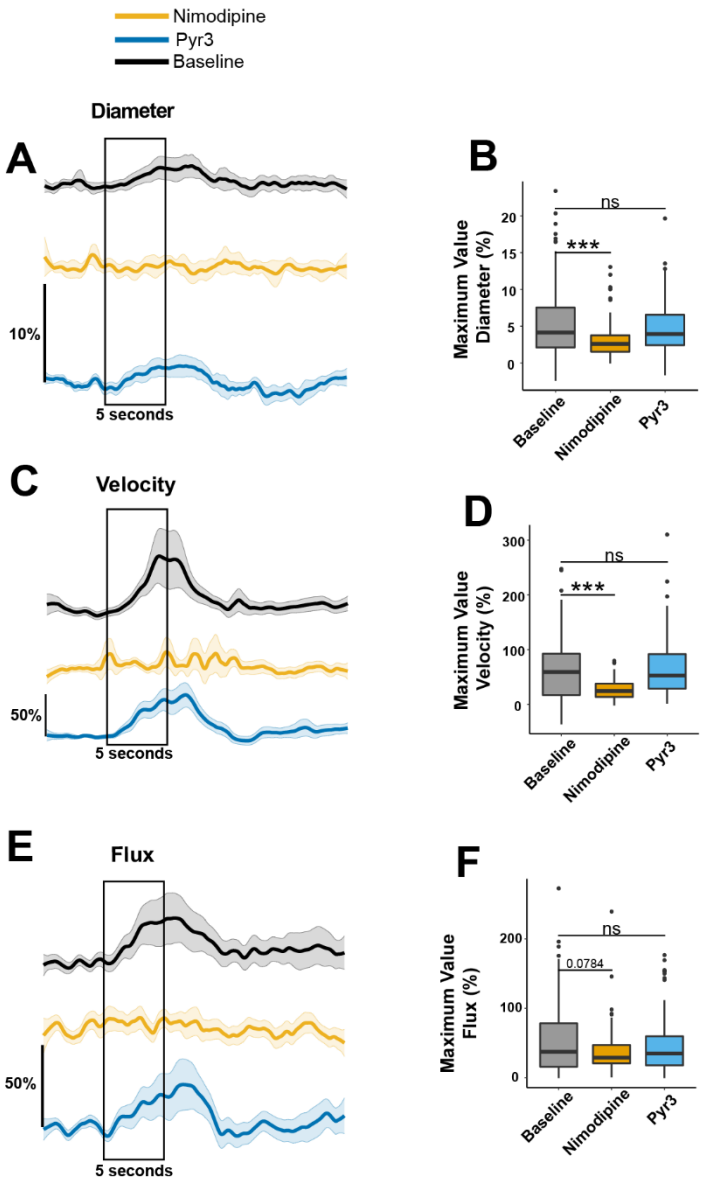

Figure 8: Brain capillaries hemodynamic properties are differentially altered by brain pericyte calcium channel activity during neurovascular coupling. *All the following panels make a comparison between baseline and calcium channel blockers* ***Nimodipine*** *and* ***Pyr3.*** Traces of the percentage change of diameter (**A),** velocity **(C)** and flux **(E)** of brain capillaries during 5 seconds of whisker electrical stimulation (500 µA at 4 Hz) relative to diameter baseline. The black box represents the start of 5 seconds of stimulation. The traces show the mean value ± SEM. Total seconds of traces=25; N=7; n=96**.** Box plots of maximum value of diameter **(B)**, velocity **(D)** and flux **(F)** percentage change during the 5 seconds of whisker electrical stimulation of blood vessels from the transition zone. N=5; n=96**.** N= # of animals, n= #of blood vessels, b(n)= # of blood vessels from a given branch order P-value<0.05=*; P-value<0.01=**; P-value<0.001=***. For specific p-values and mean ± SD information please refer to table 6.1 and table 6.2 (Section 4.7, P-Values and mean ± SD Results). Linear mixed models for repeated measurements and pairwise comparisons with Holm-sequential Bonferroni correction were used in the statistical tests.

4.7 P-values and mean ± SD Results.

Table 1.1 P-values. Brain pericyte calcium signaling analysis.

	Amplitude		**Frequency**	
	Baseline-nimodipine	Baseline-Pyr3	Baseline-nimodipine	Baseline-Pyr3
Acta2-RCaMP1.07				
Soma	8.40e-09***	ns 0.319	1.81e-11***	ns 0.435
Process	6.12e-08***	ns 0.665	6.45e-12 ***	0.0178*
PDGFRβ-CreERT2:GCaMP6s$^{fl/fl}$				
Soma	0.00425**	0.0862c	0.00472**	ns 0.180
Process	2.4e-06***	0.00449**	1.96e-10***	ns 0.947

Table 1.2. Mean ± SD. Brain pericyte calcium signaling analysis.

	Amplitude (dF/F)			**Frequency (signals/min)**		
	Baseline	Nimodipine	Pyr3	Baseline	Nimodipine	Pyr3
Acta2-RCaMP1.07						
Soma	0.374± 0.207	0.093± 0.164	0.336± 0.258	3.964± 2.714	0.103± 0.409	4.25± 4.163
Process	0.382± 0.260	0.0947± 0.167	0.362± 0.282	6.138± 5.899	0.212± 0.545	3.611± 3.781
PDGFRβ-CreERT2:GCaMP6s$^{fl/fl}$						
Soma	0.740± 0.429	0.473± 0.435	0.542± 0.298	3.581± 2.468	1.941± 1.344	2.98± 2.485
Process	0.753± 0.242	0.505± 0.258	0.598±0 .258	17.394± 8.814	8± 7.635	17.405± 9.967

Table 2.1. P-values. Blood vessels of the transition zone covered by EP hemodynamic analysis.

	Diameter		**Vasomotor Index**		**Peak frequency**	
Acta2-RCaMP1.07	Baseline-nimodipine	Baseline-Pyr3	Baseline-nimodipine	Baseline-Pyr3	Baseline-nimodipine	Baseline-Pyr3
All blood vessels	9.96e-10 ***	0.0222*	< 2e-16 ***	2e-04 ***	1.79e-07 ***	ns 0.797
1st Branch	0.000365 ***	ns 0.361	5.99e-08 ***	ns 0.183	ns 0.75	ns 0.75

2nd Branch	1.89e-06 ***	0.0199*	2.95e-09 ***	0.00210**	0.000108 ***	ns 0.940
3rd Branch	ns 0.141	ns 0.571	5.59e-07 ***	0.00861**	0.000317 ***	ns 0.706

	Velocity		**Flux**	
	Baseline-nimodipine	Baseline-Pyr3	Baseline-nimodipine	Baseline-Pyr3
All blood vessels	0.00761**	0.0678c	ns 0.187	0.00458**
1st Branch	0.0626c	ns 0.184	ns 0.585	ns 0.476
2nd Branch	ns 0.113	0.00566**	ns 0.682	ns 0.58
3rd Branch	ns 0.192	0.01958*	ns 0.620	0.04*

Table 2.2. Mean ± SD. Blood vessels of the transition zone covered by EP hemodynamic analysis.

	Diameter (µm)			**Vasomotor Index (ΔD/D)**			**Peak frequency (oscillations/min)**		
Acta2-RCaMP1.07	Baseline	Nimodipine	Pyr3	Baseline	Nimodipine	Pyr3	Baseline	Nimodipine	Pyr3
All blood vessels	5.247± 1.755	6.335± 2.591	5.719± 2.165	0.155± 0.093	0.055± 0.049	0.114± 0.081	4.677± 3.195	3.189± 4.173	4.784± 3.284
1st Branch	6.398± 1.556	8.061± 2.457	6.870± 2.025	0.209± 0.117	0.052± 0.031	0.172± 0.095	6.146± 3.524	5.353± 4.814	6.469± 3.190
2nd Branch	4.837± 1.689	5.741± 2.068	5.379± 1.891	0.136± 0.065	0.060± 0.060	0.084± 0.049	4.245± 2.874	2.488± 3.908	4.427± 3.686
3rd Branch	4.805± 1.676	5.337± 2.504	5.159± 2.338	0.136± 0.067	0.056± 0.058	0.100± 0.077	4.168± 2.864	1.466± 2.348	3.714± 2.209

	Velocity (mm/sec)			**Flux (cells/sec)**		
	Baseline	Nimodipine	Pyr3	Baseline	Nimodipine	Pyr3
All blood vessels	3.376± 2.494	2.715± 2.495	4.069± 2.830	54.183± 32.012	55.493± 38.007	58.554± 37.332
1st Branch	5.192± 2.361	3.915± 2.839	6.033± 2.579	55.739± 31.653	44.459± 22.826	47.483± 25.687
2nd Branch	3.601± 2.437	2.278± 1.843	4.486± 3.213	53.839± 29.948	46.331± 30.872	47.795± 31.127
3rd Branch	2.359± 1.897	2.275± 2.099	2.851± 1.869	61.367± 44.345	61.261± 45.978	66.667± 40.130

Table 3.1. P-values. Blood vessels of the capillary zone covered by CP hemodynamic analysis.

	Diameter		**Velocity**		**Flux**	
PDGFRβ-CreERT2:GCaMP6s$^{fl/fl}$	Baseline-nimodipine	Baseline-Pyr3	Baseline-nimodipine	Baseline-Pyr3	Baseline-nimodipine	Baseline-Pyr3
All blood vessels	ns 0.303	0.0224 *	<2e-16 ***	ns 0.197	< 2e-16 ***	ns 0.321
			Baseline-PEG400		Baseline-PEG400	
All blood vessels			6.29e-13 ***		2.59e-06 ***	

Table 3.2. Mean ± SD. Blood vessels of the capillary zone covered by CP hemodynamic analysis.

	Diameter (µm)			**Velocity (mm/sec)**			**Flux cells/sec)**		
PDGFRβ-CreERT2:GCaMP6s$^{fl/fl}$	Baseline	Nimodipine	Pyr3	Baseline	Nimodipine	Pyr3	Baseline	Nimodipine	Pyr3
All blood vessels	3.838±0.977	3.808±1.028	3.978±0.986	0.676±0.380	0.419±0.356	0.677±0.446	26.826±12.032	16.392±10.014	24.821±10.392
				PEG400			PEG400		
All blood vessels				0.466±0.296			20.402±9.254		

P-values and mean ± SD of experiments during whisker stimulation.

Table 4.1. P-values. Brain pericyte calcium signaling analysis during NVC.

	Minimum Value	
	Baseline-nimodipine	Baseline-Pyr3
Acta2-RCaMP1.07		
Soma	0.0179 *	0.0347 *
Process	0.000919 ***	0.0108 *
PDGFRβ-CreERT2:GCaMP6s$^{fl/fl}$		
Soma	0.0107 *	ns0.344
Process	1.23e-05 ***	ns0.307

Table 4.2. Mean ± SD. Brain pericyte calcium signaling analysis during NVC.

	Minimum Value (dF/F)		
	Baseline	Nimodipine	Pyr3
Acta2-RCaMP1.07			
Soma	-0.583±0.276	-0.433±0.188	-0.445±0.284
Process	-0.527±0.186	-0.40±0.119	-0.433±0.171
PDGFRβ-CreERT2:GCaMP6s$^{fl/fl}$			
Soma	-0.549±0.365	-0.368±0.237	-0.457±0.458
Process	-0.570±0.205	-0.376±0.193	-0.608±0.198

Table 5.1. P-values. Blood vessels of the transition zone covered by EP hemodynamic analysis during NVC.

	Max Value Diameter		**Max Value Velocity**		**Max Value Flux**	
Acta2-RCaMP1.07	Baseline-nimodipine	Baseline-Pyr3	Baseline-nimodipine	Baseline-Pyr3	Baseline-nimodipine	Baseline-Pyr3
All blood vessels	2.35e-10 ***	0.011 *	0.000551***	0.0328 *	5.49e-05 ***	ns 0.10805
1st Branch	6.53e-05 ***	ns 0.411	ns 0.99	ns 0.627	ns 0.443	ns 0.678
2nd Branch	5.2e-06 ***	0.0105 *	0.0174 *	0.0606c	0.000645 ***	0.0567c
3rd Branch	0.0592c	ns 0.258	0.000901 ***	0.0305 *	0.0175 *	ns0.1491

Table 5.2. Mean ± SD.Blood vessels of the transition zone covered by EP hemodynamic analysis during NVC.

	Max Value Diameter (%)			**Max Value Velocity (%)**			**Max Value Flux (%)**		
Acta2-RCaMP1.07	Baseline	Nimodipine	Pyr3	Baseline	Nimodipine	Pyr3	Baseline	Nimodipine	Pyr3
All blood vessels	15.650± 18.032	3.882± 3.771	10.413± 12.494	38.144± 46.944	16.018± 19.109	24.515± 32.379	41.254± 56.268	19.348± 12.205	31.018± 42.948
1st Branch	23.238± 20.734	4.693± 4.616	16.691± 14.760	25.620± 29.947	16.1±20 .920	24.096± 44.764	24.596± 11.906	21.266± 11.501	26.771± 12.546
2nd Branch	15±18.0 64	3.619± 3.678	9.191±1 1.696	77.929± 101.661	19.87± 24.912	17.521± 12.614	33.431± 23.891	17.610± 9.814	23.568± 13.212
3rd Branch	5.492± 4.4790	2.637± 1.426	3.766±2 .888	80.616± 82.611	13.351± 9.599	33.078± 36.763	71.567± 93.544	22.355± 15.146	29.747± 26.822

Table 6.1. Blood vessels of the capillary zone covered by CP hemodynamic analysis during NVC.

	Max Value Diameter		**Max Value Velocity**		**Max Value Flux**	
PDGFRβ-CreERT2:GCaMP6s$^{fl/fl}$	Baseline-nimodipine	Baseline-Pyr3	Baseline-nimodipine	Baseline-Pyr3	Baseline-nimodipine	Baseline-Pyr3
All blood vessels	0.00248 **	ns0.33083	3.85e-09 ***	ns0.819	ns 0.102	ns0.909

Table 6.2 Blood vessels of the capillary zone covered by CP hemodynamic analysis during NVC.

	Max Value Diameter (%)			**Max Value Velocity (%)**			**Max Value Flux (%)**		
PDGFRβ-CreERT2:GCaMP6s$^{fl/fl}$	Baseline	Nimodipine	Pyr3	Baseline	Nimodipine	Pyr3	Baseline	Nimodipine	Pyr3
All blood vessels	5.677± 5.030	3.368± 2.774	4.727± 3.594	67.729± 57.556	27.378± 18.563	69.306± 58.596	52.477± 49.349	37.953± 33.898	49.551± 45.553

ns = no significant difference

P-value<0.05=*; P-value<0.01=**; P-value<0.001=***.

A letter “c” besides the numerical value indicates that the p-value is close to a significant difference.

Chapter V. Discussion

Although brain pericytes were first described more than a century ago, many of their characteristics, mechanisms, and functions have only recently been characterized. In this research the utilization of two mice lines that expressed genetically encoded calcium indicators (GECI) under promoters differentially expressed by the distinct pericytes sub-populations was helpful to make a clear definition of features like their morphology and calcium signaling (Figure 1 A). Additionally, we used an advanced surgical procedure to access the same pericytes in the somatosensory cortex repeatedly[177]. By implanting a chronic cranial window, we were able to observe the calcium signaling behavior of pericytes and its effect on CBF using two-photon imaging under various pharmacological conditions and at various levels of the brain vascular bed, all within the same mouse subjects (Figure 1A-C). Furthermore, we used the recently developed classification of the brain vasculature (Figure 1D), which is becoming the standard in the field[15,146,178,179] and is an important factor to precisely define pericyte subtypes to avoid the disparities and misunderstanding that has previously happened in the pericyte field. Lastly, we optimized and developed algorithms in programming platforms to analyze the calcium movies and kymographs obtained from two-photon microscopy. This standardization of our results allowed for consistent measurements that can be compared with other research studies in the field (Section 3.5 Materials and Methods).

5.1 L-type VGCC and TRPC3 channel blockade impact brain pericyte calcium signaling.

Recent studies have identified different calcium signaling properties in EP and CP [15,132,135]. Glück et al. have shown that EP have synchronous calcium signaling that correlates with nearby blood vessel oscillations, whereas CP calcium signaling was more irregular and spontaneous fluctuations in calcium did not relate to the diameter of brain capillaries[132]. Consistent with this study, our results demonstrate that the calcium signaling of EP has a pattern of synchronous waves with similar amplitude and frequency in the EP morphological compartments, soma and process (Fig. 2B; black traces). We also confirmed that CP calcium

signaling was more asynchronous and irregular in both morphological compartments compared to EP (Figure 2E).

Moreover, existing literature has demonstrated that EP calcium signaling is influenced by L-type VGCCs[59,98,180] and that inhibiting these channels with drugs like dihydropyridines, leads to a reduction in this signaling [132,148,181,182]. We found similar results where the L-type VGCC blocker, nimodipine, reduced EP calcium signaling amplitude and frequency in both soma and processes, showing that L-type VGCC plays a major role in EP calcium signaling behavior (Figure 2C).

We found that CP calcium signaling was also significantly affected by nimodipine with a decrease in amplitude and frequency in both soma and processes (Figure 2F). This partially agrees with a study that showed a mild decrease in calcium signals frequency with nimodipine just in CP soma[132]. Still, another study reported no alterations at all in CP calcium signaling when using VGCC blockers[135]. The fact that we saw a strong decrease in CP calcium signaling and this has not been reported in the mentioned studies could be due to the discrepancies in the methodology. The mentioned studies have evaluated CP calcium signaling in *ex-vivo* brain slices preparations, which could potentially impact physiological processes like NVU responses to changes in the blood flow and cellular communication, thus, influencing in CP channels gating properties. For instance, in research conducted by Klug et al., it was observed that calcium signaling in CP can exhibit variations under different cell membrane conditions. This study revealed that VGCC blockers did not impact calcium signaling CP at a baseline membrane potential of -40 mV. However, when the CP membrane was depolarized, VGCC blockers led to a notable decrease in calcium signaling[15]. An explanation worth considering is that within our live mice model, CP depolarization may occur due to a natural physiological response, as part of the intrinsic signaling mechanisms of the brain, hence increasing CP sensitivity to VGCC blockers.

Likewise, we demonstrated that TRPC3 channels influence in a different way EP and CP calcium signaling. In recent studies, the influence of TRPC channels on pericyte calcium signaling has been explored through their inhibition, showing a reduction in calcium

signaling features under these circumstances [132,135]. However, these studies have overlooked the specific subfamilies of TRPC channels utilizing blockers that impact multiple subfamilies which also have been reported to be expressed by other cells in the neurovascular unit (NVU), such as neurons[183,184]. Specifically, it has been reported that in Purkinje cells, TRPC3 channels can regulate calcium entry in response to GPCRs such as mGluR1, and that this signaling process influences important physiological functions such as synaptic transmission[185,186]. Furthermore, there is evidence demonstrating a relationship between the modulation of vascular tone and the activation of TRPC3 channels in vascular smooth muscle cells in response to molecules such as endothelin-1 (ET-1) and angiotensin II (ANG II). These studies suggest that TRPC3 channels operate through a receptor-operated channels (ROCs) mechanism, leading to a calcium entry when stimulated by these GPCRs agonists[187,188].

In brain pericytes, TRPC3 channels have been recently found to be present with transcriptomes studies[72]; nevertheless, their confirmed protein expression in pericytes and how these channels influence pericyte subtypes have never been shown. To test the influence of TRPC3 channels in brain pericytes we used Pyr3, a highly specific blocker of the TRPC3 channels. Pyr3 has been shown to successfully block TRPC3 channels in endothelial[189] and SMC[190] disturbing their calcium signaling.

Our findings in brain pericytes revealed that the presence of Pyr3 had an effect on EP calcium signaling by decreasing its frequency, which was observed exclusively in EP processes (Figure 2C). Additionally, Pyr3 decreased the calcium amplitude within the processes of CP. While there was a noticeable trend towards reducing calcium amplitude in the soma, this trend did not reach statistical significance. Notably, Pyr3 did not influence calcium frequency in either compartment of CP morphology (Figure 2F). It is interesting to note the fact that Pyr3 affects different features of the calcium signaling of EP and CP and in different morphology compartments. One potential explanation for the observed variations is that TRPC3 channels contribute to the amplification of calcium responses in CP processes, potentially through ROCs signaling following the activation of GPCRs. Upon GPCR activation, there is a release of calcium from intracellular stores, specifically the endoplasmic

reticulum (ER). This calcium release subsequently activates TRPC3 channels, enabling the passage of calcium ions. Consequently, in the event that TRPC3 channels are inhibited in the CP, the activation of GPCRs would still trigger calcium events originating from the ER stores. This would lead to no alteration in the frequency of calcium events. However, due to the reduced calcium influx resulting from the blockade of TRPC3 channels, the amplitude of these events would decrease.

Conversely, the fact that we saw a decrease of calcium frequency in EP processes could suggest that TRPC3 channels have the capacity to produce calcium events on their own, via other mechanisms that differ from ROCs calcium signaling enhancement. Further studies to disentangle these possible signaling differences between EP and CP should be considered to corroborate the above hypothesis.

5.2 Brain pericyte L-type VGCCs strongly influence hemodynamics and vasomotion of blood vessels from the arteriole transition zone.

In accordance with alterations of ensheathing and capillary pericytes calcium signaling with nimodipine and Pyr3, we also saw changes in the nearby blood vessel hemodynamics under the effect of these calcium channel blockers. Nimodipine is a drug currently used to improve neurological deficits and controlling the vasospasms following a subarachnoid hemorrhage[191,192]. In contrast with other types of dihydropyridines, nimodipine acts primarily on the smooth muscle of blood vessels[193]. In SMC of the brain vasculature, the blocking of calcium signaling by nimodipine has been associated with the suppression of the constriction effect due to the disruption of (myosin light chain kinase) MLCK pathway activated with the formation of calcium-calmodulin complex[194,195]. Moreover, studies in the brain pericyte field have shown that nimodipine was able to induce dilation of blood vessels covered by them[148], and to slow pericyte-evoked constriction in ischemia conditions[196]. Similar to the above, we saw that nimodipine caused a dilatory effect in blood vessels of the arteriole transition zone covered by EP (Figure 3A-C). Furthermore, nimodipine abolished the oscillation features of vasomotion in amplitude and frequency (Figure 3D & 3E). This indicates that L-type VGCC

signaling influences not just the diameter of the blood vessels of the transition zone, but also, they are involved in the constriction-dilation process of vasomotion.

In the evaluation of cerebral blood flow (CBF) with nimodipine, we noticed that nimodipine caused a reduction of velocity (Figure 3F-H). This decrease could be likely due to 1) the increase of blood vessel diameter impacting CBF velocity, 2) a decrease of blood pressure coming from bigger arteries resulting in a reduction of CBF velocity since it has been reported that nimodipine affects both, systolic and diastolic pressure[197,198]. Despite this decrease in velocity, we did not find a significant difference in red blood cells (RBC) flux. The above could be explained by the velocity-flow relationship that occurs in vessels assuming a laminar flow. This relationship states that in a constant diameter, the changes in flow are proportional to changes in velocity and vice versa, nevertheless, if the diameter changes unevenly, this relationship can be affected. For instance, if the diameter of a blood vessel increases the blood velocity and flux would decrease, but if there are blood vessels dilating downstream, even though the velocity of the evaluated blood vessel decreases the flux would stay unchanged[199]. As a result, the vasodilatory effect of nimodipine causes a decrease in blood flow velocity, but the fact that nimodipine also dilates downstream vessels results in unchanged RBC flux.

The novel classification of the brain vasculature by branch order based on their bifurcation pattern has helped the understanding of temporal and regional mechanisms of blood flow distribution within the brain. For example, Zambach et al. showed that the 1st branch order had the strongest response when different vasoconstrictor and vasodilatory stimuli were applied[98]. To thoroughly evaluate the dilatory effect of nimodipine in blood vessels of the arteriole transition zone, we assessed the previously obtained hemodynamic measurements (from Figure 3) according to their branching pattern. We found that 1st and 2nd branches dilate with nimodipine, whereas the 3rd branch order did not show any significant alteration (Figure 4B). This could be a consequence of the gradual decrease of αSMA expressed by pericytes as they go deeper in the brain vasculature, which has been well established in the field[73,98,146,147,178,200], resulting in a reduced capacity of the 3rd branch to dilate/constrict comparing to the 1st and 2nd branches[4].

Regarding the vasomotion features, we noticed a decrease in the frequency of blood vessel wall oscillations in the 2nd and 3rd branch with nimodipine (Figure 4D). This implies that vasomotion in the 2nd and 3rd branches could be more sensitive to a lack of calcium influx. Furthermore, nimodipine showed a decrease in the amplitude of vasomotion oscillations in all the branch orders (Figure 4 C), which indicates that L-type VGCC strongly participate in the magnitude of oscillations during vasomotion in all branch orders.

In the terms of velocity and flux, it was observed that nimodipine had a notable reduction in the velocity of the 1st branch, although it did not reach statistical significance. Despite a clear trend of reduced blood flow velocity in both the 1st and 2nd branches (Figure 4E), the lack of a significant difference may be attributed to the division of the number of samples. The sample size might not have been sufficient to achieve the significant difference necessary to demonstrate a clear reduction in blood flow velocity per branch order, as it was seen when all the blood vessels of the arteriole transition zone were evaluated together under the effect of nimodipine.

The contraction/dilation property of brain capillaries has been a subject of debate in recent years. Due to the lack of αSMA expression in capillary pericytes it has been argued that they do not possess the contractile machinery to significantly modulate brain capillary diameter or influence the regulation of CBF[131]. Nevertheless, recent work has shown that CP may have the capacity to constrict brain capillaries with slower kinetics compared to EP, possibly using a rapid actin polymerization mechanism and Rho kinase activity[165,201]. Likewise, studies have also shown that CP constrict brain capillaries in aging[202] and Alzheimer's Disease[113]. Although the constriction effect of CP is starting to be more established in the field, the mechanism in which they constrict and dilate are yet to be elucidated. Besides, new data about CP calcium signaling indicates that they could work differently than EP to evoke this constriction, for example, the same study conducted by Klug et al., showed that L-type VGCC can affect CP calcium signaling without causing an alteration in the brain capillary tone[15]. Consistent with this, we found that regardless of the decrease of calcium that CP showed with nimodipine, it did not affect the brain capillary diameter (Figure 5B & 5C), suggesting that L-type VGCC may not influence changes in brain capillary diameter.

Similar to the blood vessels of the arteriole transition zone, we saw a decrease in blood flow velocity with nimodipine in brain capillaries (Figure 5D-F). Since there was no dilation, this effect was likely due to the decrease of these hemodynamic properties in the upstream vessels, or as mentioned before, due to a systemic decrease of blood pressure leading to a decrease in CBF velocity. In contrast, differing with the results of blood vessels from the arteriole transition zone, we saw that brain capillaries RBC flux was decreased with nimodipine (Figure 5G).

This could potentially be attributed to the elevated cerebrovascular resistance exerted by the brain capillaries, which is a result of their small diameter. Besides, the lack of dilation of brain capillaries makes the relationship velocity-flow mentioned above comply with these measurements being proportionally changed, since there are not changes in diameter in the measured vessel or downstream vessels when the velocity decreases then the flux decreases as well.

5.3 TRPC3 channels cause vasodilation of blood vessels from the arteriole transition zone and brain capillaries affecting the blood flow dynamics.

In the evaluation of the effect of TRPC3 channels on hemodynamic properties of blood vessels covered by pericytes, we noticed that their blockade caused vasodilation in both arteriole transition zone blood vessels and brain capillaries. In contrast with nimodipine, Pyr3 had a milder effect in the vasodilation of blood vessels covered by ensheathing pericytes (Figure 3A-C). Furthermore, we showed for the first time that brain capillaries dilate in physiological conditions after the blockade of TRPC3 channels (Figure 5A-C). The observed dilation effect can be attributed to the inhibition of calcium influx resulting from the blockade of TRPC3 channels in pericytes. The fact that in EP, the decrease of calcium released by TRPC3 channels signaling caused a milder dilation as the one seen with nimodipine could be because L-type VGCC still provide calcium influx, and since these channels have shown to be primarily involved in their contractile capacity[135,168,203], they would still provide enough calcium influx participating in blood vessels vasomotion. Conversely, TRPC3 channels in

CP could be a significant provider of calcium influx related with the maintenance of the myogenic tone, thus, its decrease would lead to dilation as observed with our results.

Interestingly, we saw an increase in CBF flux and velocity of blood vessels arteriole transition zone when Pyr3 was applied (Figure 3F-J). This could mean that Pyr3 has a more localized and specific vasodilatory effect in EP in comparison with nimodipine. It could be that, while in the EP processes there is a decrease of calcium frequency with TRPC3, resulting in vasodilation, EP somata could exert a higher contraction effect, possibly creating heterogeneous oscillations of the vessel wall increasing CBF velocity and flux. The above could be an explanation of why we found vasomotor index changes with Pyr3 (Figure 3D). It is worth mentioning that the 2nd and 3rd branches showed the major changes in vasomotor index (Figure 4C) and the increase of CBF velocity and flux with Pyr3 (Figure 4E & 4F), this could be a result of TRPC3 channel calcium decrease inducing a local effect on specific blood vessels hemodynamics in the arteriole transition zone. Precise evaluation of calcium signaling behavior in each branch order with Pyr3 would be needed to further evaluate this hypothesis. In addition, the fact that velocity increased specifically in the 2nd and 3rd branches could be a reflection of the vascular resistance of the 3rd branch due to its lower capacity to constrict/dilate as dynamically as the 1st and 2nd branch, resulting in CBF velocity and flux increase.

In contrast, the velocity and flux of brain capillaries remained unchanged from baseline conditions when exposed to Pyr3 (Figure 5D-H). This observation suggests that the observed dilation could be an example of cerebral autoregulation mechanisms to maintain capillary perfusion in the wake of upstream changes. The dilatory effect could potentially decrease vascular resistance and uphold blood flow homeostasis within the brain. Furthermore, the dilation of brain capillaries in response to Pyr3, could indicate that the regulation of blood vessel tone is primarily driven by ROCs mechanisms in CP, since TRPC3 channels have shown to follow this pathway[144,204]. Some studies have provided support for this by demonstrating the significant impact of ROCs mechanisms on the elevation in calcium signaling during vasoconstriction in CP [15,135]

It is important to note that we cannot disregard the potential involvement of endothelial cells in the aforementioned mechanism, as they also possess TRPC3 channels. Suppression of these channels has been demonstrated to cause endothelium-dependent hyperpolarization (EDH) induced dilation effect in heart[205], mesenteric[205] and cerebral[206] arteries.

Altogether, our results suggest that brain pericytes L-type VGCC and TRPC3 channels calcium signaling play a significant role in the regulation of brain blood vessels hemodynamics, however, their influence differ according to the pericyte type and the location in the brain vasculature. While L-type VGCC strongly impact hemodynamic features of the EP and blood vessels from the arteriole transition zone like diameter and vasomotion, they do not have a significant impact in the regulation of brain capillary tone. In contrast, TRPC3 channels were found to have an impact on the tone of brain capillaries, indicating their ability to induce dilation. Additionally, TRPC3 channels exert an influence on the velocity and flux of blood in the upstream blood vessels of the arteriole transition zone, potentially contributing to the signaling mechanism for blood supply in the downstream brain capillaries.

5.4 Brain pericyte calcium signaling during neurovascular coupling.

Situated at the core of the neurovascular unit (NVU), brain pericytes benefit from their central location, enabling effective communication with neurons, astrocytes, and endothelial cells[130]. Recent studies have shown that pericytes play a crucial role during neurovascular coupling, receiving signals from the neighboring cells and redirecting cerebral blood flow during functional hyperemia. For instance, Cai et al showed that the optimal functionality of ensheathing pericytes is crucial for maintaining neurovascular coupling, as the integrity of these pericytes decreases in aged mice[207]. Similarly, Kisler et al. demonstrated that the loss pericytes in a transgenic mouse model diminishes blood vessel responsiveness to neuronal stimuli, ultimately resulting in a state of neurovascular uncoupling[208]. In addition, Nikolakopoulou et al., revealed that the loss of pericytes in this model can contribute to neuronal death that was associated with the absence of pericyte-derived pleiotrophin, which is a neurotrophic growth factor[209]. In order to advance research in this area, we investigated the calcium signaling mechanisms of brain pericytes that could influence neurovascular

coupling by evaluating the activity of ensheathing and capillary pericytes L-type VGCC and TRPC3 channels. Through the use of whisker pad stimulation to identify the highly active regions in the mouse somatosensory cortex (Figure 6A), we found that calcium signaling of EP and CP decreases when whisker stimulation is performed.

Under baseline conditions, there is an initial decrease in calcium signaling observed in both the soma and processes of EP as soon as the stimulation commences (Figure 6B). This decrease is followed by a subsequent rise in calcium levels that appears to be more pronounced than calcium levels previous to stimulation. The drop in pericyte calcium during NVC has been shown in previous studies using ex-vivo retina and cerebellar preparations[96,210]. However, it is possible that in our *in-vivo* model this post-stimulus calcium rise is a myogenic response that would help EP to recover their basal calcium state after stimulus is induced.

In addition, we found that the decrease in calcium during sensory stimulation occurs with slower kinetics in CP. These slower response of calcium signaling from CP have been reported by other studies[146,210], and although one would expect that the calcium signaling in the mural cells of the capillary bed would be faster due to neuronal and glial communication, there is not a clear explanation yet of why CP calcium signaling behaves in a lower time scale compared with EP. Rungta et al., speculate that this could be due to different gap-junction coupling with the endothelium between the two pericytes types.

Moreover, the administration of nimodipine had a notable effect on the behavior of NVC calcium in both the soma and processes of EP and CP, with a greater impact observed in the disruption of the NVC-related calcium decrease in the processes (Figure 6C & 6E). The above indicates that brain pericyte processes L-type VGCC could be the primary structure responding to stimulus during NVC. In EP processes, this goes in accordance with their capacity to change the blood vessels vasomotion according to functional hyperemia and the surface area they cover in the brain vasculature, making them more susceptible to signals from the neighboring cells while NVC occurs. Conversely, in CP elongated processes are vastly found across brain capillaries and in close contact with brain endothelial cells[211], which

could make them accessible to NVC signals during whisker stimulation activating their L-type VGCC. It is worth noting that EP were the sole participants to exhibit a decrease in their NVC calcium behavior when exposed to Pyr3 (Figure 6C). This observation suggests that EP may possess an extensive calcium regulatory mechanism involving both VGCC and TRPC3 in NVC, which potentially enables them to promptly respond and facilitate functional hyperemia.

5.5 Brain pericyte calcium signaling influence brain blood vessels hemodynamics during neurovascular coupling.

Recent literature has revealed that molecules released during neuronal activity lead to a decrease in pericyte calcium levels, triggering subsequent dilation of blood vessels. Furthermore, it has been reported that this dilation primarily manifests in the blood vessels covered by brain pericytes before affecting arterioles [175,176,212]. In our study, we also explored the effect of EP and CP calcium decrease originated by NVC in brain vasculature hemodynamics and the involvement of L-type VGCC and TRPC3 channels in this process. According to our results, whisker pad stimulation in baseline condition induced dilation of the blood vessels from the arteriole transition zone (Figure 7A). This NVC-induced dilation reached its peak near the end of the stimulation period, and it was followed by a constriction effect. The above observation goes in accordance with EP calcium dynamics shown in Figure 6B. It is worth to mention that this dilation-constriction effects originated by stimulus have also been reported in a study conducted by Cai et al[176]., in which they applied the gliotransmitter ATP with a puffing pipette on EP from *in-vivo* mice models. As part of their supplementary material in this publication, they make the relationship of the dilation-constriction mechanism with EP calcium dynamics, which is consistent with our observations. Interestingly, our study also shows the same dynamics of an increase-reduction behavior in velocity and flux of the blood vessels from the arteriole transition zone (Figure 7D and 7G), which indicates that EP response to NVC with dilation is related with their ability to supply CBF to brain activated areas.

In addition, we showed for the first time that brain capillaries have the ability to dilate during NVC in physiological conditions (Figure 8A), and that this is goes in accordance with CP calcium behavior to whisker stimulation. Furthermore, we observed a notable rise in brain capillary blood flow velocity and flux during NVC (Figure 8C & 8E). This observation suggests that while the dilation of brain capillaries may be smaller in scale compared to upstream blood vessels, it has a substantial effect on blood flow dynamics. This finding aligns with Hagen-Poiseuille's law and demonstrates that even slight alterations in diameter can influence brain vascular resistance, thereby modifying CBF.

It is important to note that in contrast to EP, capillary pericytes do not have a post-stimulation compensation effect. We did not observe any increase in calcium or brain capillary constriction following whisker stimulation. The above implies that CP could contribute to the regulation of vascular resistance and blood flow supply, but brain autoregulation mechanisms could be primarily driven by EP to maintain the equilibrium in CBF direction to downstream capillaries.

5.6 L-type VGCC are the primary contributors to the calcium response in brain pericytes that influence the hemodynamics of blood vessels during neurovascular coupling.

Regarding the involvement of brain pericyte calcium channels during NVC, we observed that the stimulation-induced dilation, and the increase of CBF velocity and RBC flux was suppressed with the application of nimodipine in blood vessels of the arteriole transition zone and brain capillaries (Figure 7 & Figure 8). In past studies, the expression of L-type VGCC in capillary pericytes has been debatable[15,135,213], our findings demonstrate that L-type VGCC play a crucial role in the NVC responses originating from both EP and CP, which have an impact on functional hyperemia. Besides, we raise the possibility that brain capillaries dilation during NVC is not necessarily a response to the upstream dilation of the blood vessels. Since we did not see a resting dilation with nimodipine in brain capillaries and the dilation during stimulus is blocked, this could mean that brain capillaries have a limited capacity for diameter expansion, making it not possible for them to dilate further.

Similarly, we observed a notable decrease in NVC-induced vasodilation and increase in CBF velocity when Pyr3 was applied specifically to the blood vessels in the arteriole transition zone. However, the extent of its suppression on dilation/constriction behavior was not as pronounced as nimodipine. This suggests that while blocking TRPC3 channels can influence NVC, it may primarily be attributed to a decrease in calcium levels rather than directly affecting pericytes' response to NVC and functional hyperemia. This could also indicate that L-type VGCC signaling is the more prevalent mechanism from EP to regulate vasomotion of the blood vessels in the arteriole transition zone when NVC occurs.

Furthermore, we examined the impact of nimodipine and Pyr3 on the hemodynamic responses during NVC, specifically focusing on the blood vessels of the 1st, 2nd, and 3rd branch order. Our results indicate that the inhibition of vasodilation during NVC, caused by both calcium channel blockers, predominantly affects the first and second branches (Figure 7C). Moreover, both nimodipine and Pyr3 suppressed the increase in velocity and flux observed in the 2nd and 3rd branches during NVC (Figure 7F & 7I). This is consistent with a study made by Rungta et al. which showed that blood vessels of 1st branch order will have the greatest dilation during functional hyperemia, thus, the blocking with calcium channel blockers affected in a greater scale the NVC-induced dilation. Furthermore, this study also shows that during stimulation, the brain capillaries will have the major increase in velocity, followed by the blood vessels from the arteriole transition zone. Our results agree with this since the major suppression in velocity and blood flux occurred in the 2nd and 3rd branches with both calcium channel blockers. This effect also goes in accordance with our previous results showing that resting velocity and flux are affected from the calcium decrease and subsequent vasodilation primarily in the 2nd and 3rd branch when Pyr3 is applied.

Collectively, these findings indicate that both L-type VGCC and TRPC3 channels in brain pericytes play a role in influencing the hemodynamic response of blood vessels during NVC. L-type VGCC exhibit a stronger influence in attenuating the hemodynamic responses in blood vessels within the arteriole transition zone and brain capillaries, likely due to their significant calcium influx during brain activity. In contrast, TRPC3 channels only partially affect the hemodynamic responses in blood vessels within the arteriole transition zone during

NVC, suggesting that the calcium influx through these channels is not primarily associated with NVC-induced hemodynamic changes.

5.7. Study Limitations.

One limitation of this research project is that nimodipine, while having a preferential affinity for L-type VGCC in vascular smooth muscle, has been shown to also affect L-type VGCC in smooth muscle of other organs, such as those in the heart, potentially influencing blood flow changes [198,214]. Due to these effects, we decided to measure the blood pressure of the mice during the repeated pharmacology sessions when administering systemically nimodipine and Pyr3, while also monitoring pericyte calcium signaling and blood vessel hemodynamics (Supplementary Figure 1A). Our results demonstrate that there is no difference in mean blood pressure when Pyr3 is applied, suggesting that the hemodynamic effects seeing in the brain caused by Pyr3 could be caused by a local effect in the brain. However, we were unable to obtain any blood pressure measurements when nimodipine was administered (Supplementary Figure 1B). This could be attributed to a considerable decrease in blood pressure that could hinder the accurate measurements with the non-invasive blood pressure CODA system. Since this system relies on the volume of the tail, a substantial change in blood pressure could potentially affect the readings. It should be noted that in all sessions involving nimodipine, the readings consistently indicated "low tail-volume." Similar mishaps when measuring arterial blood pressure in mice with hypotension using the tail-cuff system were discussed by Zhao et al. They also mention that vasoactive substances could lead to vasoconstriction of the tail artery affecting the accuracy of the measurements[215]. The above could be a possible explanation of why we were unable to obtain blood pressure readings when nimodipine was applied.

Due to the inability to obtain blood pressure measurements, we opted to perform acute *in-vivo* experiments as an alternative approach. In these experiments, rather than administering nimodipine systemically, we applied it topically to investigate whether the observed effects on blood vessels were due to a local effect from brain pericytes, rather than a reduction in mean blood pressure (Supplementary Figure 1C, Section 3.6 Materials and methods). In the

acute experiments, we also measured blood pressure in two groups: one group receiving topical application of the vehicle (sham group) and another group receiving topical application of nimodipine. The absence of any significant difference in mean blood pressure between these two groups (Supplementary Figure 1D) further suggests that when nimodipine is systemically applied it reduces in the mean blood pressure.

In the evaluation of the effect of nimodipine topically applied in brain pericyte calcium signaling and the blood vessels hemodynamics covered by them, we found that topically applied nimodipine also influenced the calcium signaling of EP and CP, exhibiting a similar decrease as observed in the repeated *in-vivo* experiments when nimodipine was systemically applied. This indicates that nimodipine has a direct effect blocking the L-type VGCC of brain pericytes regardless of the administration route (Supplementary Figure 2A, 2B, 3A & 3B). However, we encountered inconsistencies in the hemodynamic measurements. The sham hemodynamic results displayed altered values due to difficulties arising from bone growth underneath the cranial window. This made the subsequent removal of the window more challenging on certain occasions, leading to vessel damage. We speculated that the increased diameter and reduced vasomotion observed in the sham samples were caused by vessel damage compared to the nimodipine group (Supplementary Figure 2C-E). However, despite the vessel damage, we observed a decrease in CBF velocity with the topical application of nimodipine compared to the sham group (Supplementary Figure 2F). This suggests that, in addition to vessel damage, CBF velocity is still affected when nimodipine is applied topically. The above could be attributed to the combined effects of decreased calcium levels and dilation, which, (although not directly comparable in terms of vessel diameter between sham and nimodipine groups due to the aforementioned vessel damage) were still evident in the dynamics of CBF. Further acute experiments with nimodipine vs. sham are required in order to draw a conclusion about hemodynamics.

With regards to brain capillaries, we did not observe any differences in their hemodynamics (Supplementary Figure 3C-E). This lack of significant findings could potentially be attributed to the reduction in velocity and flux observed in brain capillaries when nimodipine was

administered systemically, which may be a consequence of the overall decrease in systemic blood pressure.

Furthermore, it is worth noting that in only these two measurements of our repeated pharmacology study (brain capillaries velocity and flux), we identified a difference between the baseline and the vehicle (PEG400) (Supplementary Figure 3F and 3G, table 3.1 and 3.2 Results section). Several studies have utilized polyethylene glycols (PEGs) to explore their interactions with endothelial cells and SMC and how they can impact in their normal functioning[216–220]. It has been reported that PEGs with high molecular weights (1.5-3.5 kDa) can interact with surface proteins and organelles, leading to beneficial effects such as plasma membrane repair[221–223]. The effects of PEGs can vary significantly due to their amphiphilic nature and the diverse range of interactions they can induce depending on their molecule size. However, low molecular weight PEGs, such as PEG400, have been considered inert and have been commonly employed as drug carriers without any reported alterations[224]. In our study, the difference in brain capillaries CBF velocity and flux when comparing PEG400 systemically applied to the baseline could be attributed to PEG400 being evaluated as a vehicle for the first time in thin brain capillaries. It is possible that PEG400 systemically applied binds to plasma proteins in the blood, which may have more pronounced effects in the brain capillaries due to their small diameter, causing a decrease in CBF flow. However, further research is required to elucidate the precise mechanisms underlying this observation. The above interaction could be the reason why we did not find a significant difference in CBF velocity and flux between sham and nimodipine groups in the acute experiments.

Another limitation of our study is the utilization of the anesthetics ketamine/xylazine during in-vivo two-photon imaging. Several studies have shown the effect of general anesthesia using ketamine/xylazine on calcium transients in glial cells, and sensory response in murine models[132,225–229]. Thrane et al. reported that under the effect of ketamine/xylazine calcium signaling in neocortical astrocytes was markedly suppressed, as well as their calcium responses evoked by whisker stimulation[227]. Zandieh et al. studied sensory and motor evoked potentials under the effect of ketamine/xylazine anesthesia, reporting that the somatosensory evoked signals have a dependency on the level of anesthesia[228]. Taking the above literature

in consideration and due to cells in neurovascular unit have a cross-talked communication[48], one cannot discard the possibility that the effect of ketamine/xylazine anesthetics in glial cells calcium signaling likewise affect calcium signaling in mural cells, as well as their calcium responses evoked by whisker stimulation. In addition, a study conducted by Glück et al. compared the reduction effect in calcium signals on distinct type of pericytes under isoflurane, finding that, although calcium signaling was decreased, pericytes still maintained the same calcium dynamics among their different types, as seen in awake conditions[132], nevertheless, no study making comparison in pericyte calcium signaling between anesthetized and awake animals using ketamine/xylazine has been performed.

5.8 Conclusions and significance.

In this research project, we demonstrated distinct calcium signaling dynamics between ensheathing pericytes (EP) and capillary pericytes (CP), which align with their roles in vasomotion and maintaining the myogenic tone of blood vessels. Our study revealed that EP's L-type voltage-gated calcium channels (VGCC) play a primary role in the contraction/dilation process of arteriole transition zone blood vessels. Additionally, we found that TRPC3 channels can contribute to calcium influx in EP, exerting a more localized effect that influences the hemodynamic properties of the covered blood vessels. Conversely, CP also possesses L-type VGCC and TRPC3 channels; however, their functionality differs from EP. Specifically, we observed that TRPC3 channels in CP are the major contributors to calcium influx, impacting the myogenic tone of brain capillaries. Furthermore, we demonstrated the significant participation of L-type VGCC in both pericyte types during neurovascular coupling, influencing their ability to dilate during functional hyperemia. These findings partially agree with this project’s hypothesis, since we showed that L-type VGCC and TRPC3 channels regulate calcium signaling in both types of pericytes, following different pathways that work synergically to maintain cerebral autoregulation. Notably, we provided the first evidence of brain capillaries' dilation capacity, which is associated with the functioning of L-type VGCC during neurovascular coupling. Our findings establish a clear distinction between brain pericyte types and their respective functions, paving the way for

novel strategies to selectively target their calcium dynamics in controlling cerebral blood flow (CBF).

Chapter VI. Supplementary material.

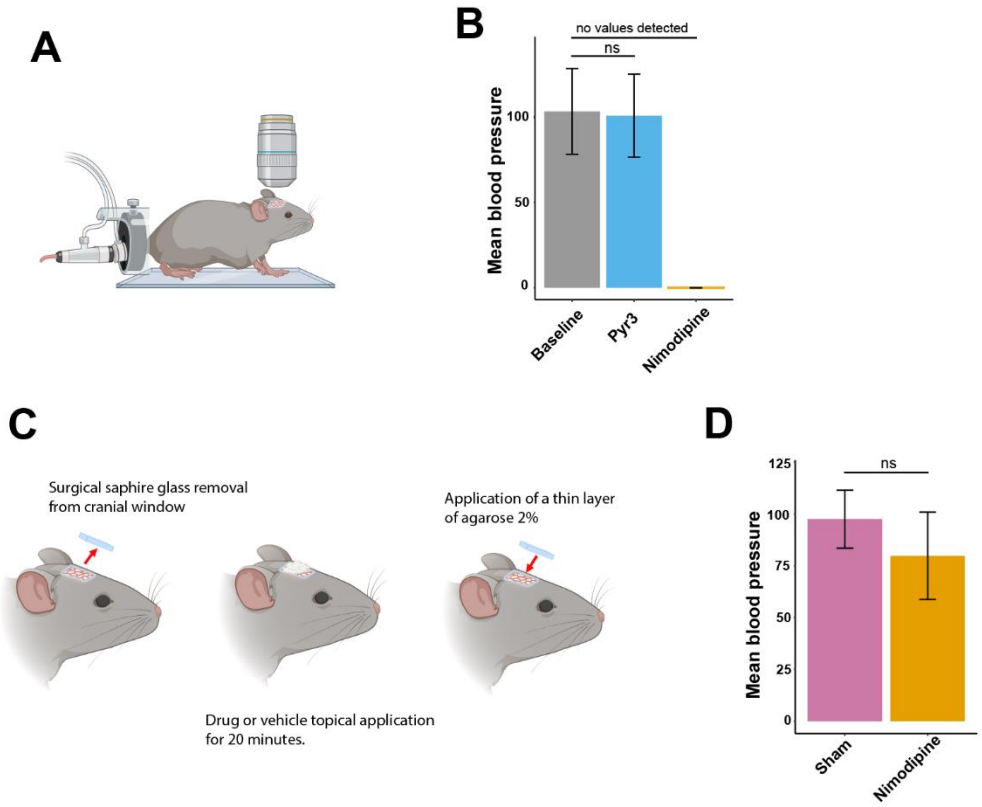

Supplementary Figure 1. Blood pressure and acute experiments. **A)** Cartoon exemplifying the experimental set up of CODA monitor non-invasive blood pressure system. **B)** Mean blood pressure measured in repeated pharmacology experiments of mice in baseline conditions and under the effect of nimodipine and pyr3 applied via i.p. No values of blood pressure were detected with CODA system when nimodipine was applied. N=11. **C)** Acute pharmacology experiments drug application scheme. **D)** Mean blood pressure of mice in sham and nimodipine acute pharmacology experiments. NSh=6; N-nim=9. N= #animals used in repeated pharmacology experiments; NSh= # of animals used in sham acute experiments; N-nim= # of animals used in nimodipine acute experiments. P-value<0.05=*; P-value<0.01=**; P-value<0.001=***. For specific p-values and mean ± SD information please refer to table 7 (Section 6.1, P-Values and mean ± SD Results). Independent samples t-test was used for comparisons.

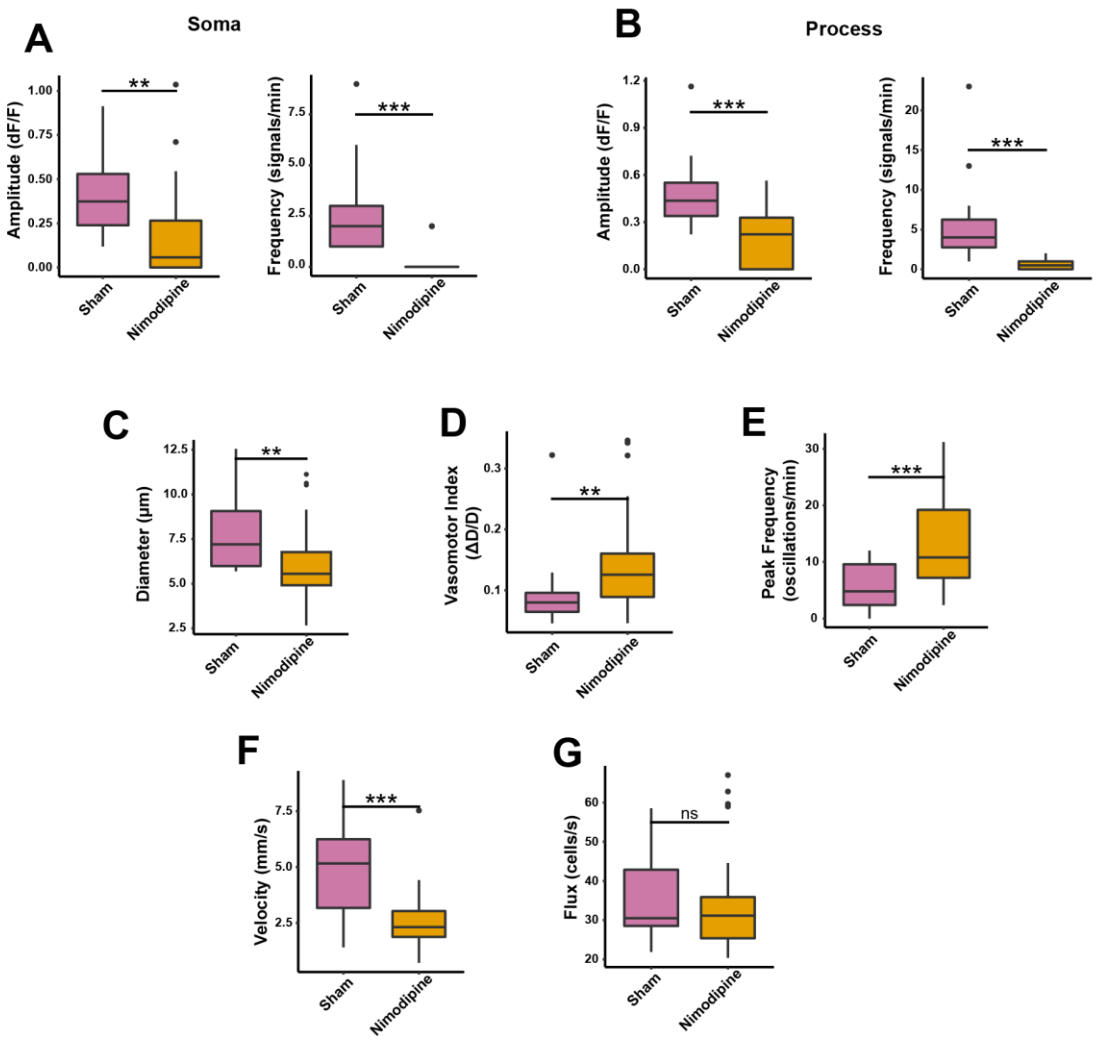

Supplementary Figure 2. **EP calcium signaling and blood vessels from the arteriole transition zone hemodynamic results from acute *in-vivo* pharmacology experiments** *All the panels make a comparison between sham and the calcium channel blocker* ***Nimodipine*****.** Calcium signaling properties (amplitude and frequency) of ensheathing pericyte morphology structures **A)** soma and **B)** process. NSh=3; nSh=28; N-nim=4; n-nim=34. **C)** Diameter **D)** vasomotor index and **E)** Peak frequency **F)** velocity and **G)** flux of blood vessels from the transition zone covered by ensheathing pericytes. NSh=3; nShV=22; N-nim=4; n-nimV=38 NSh= # of animals used in sham acute experiments, nSh= # of pericytes in sham acute experiments; N-nim= # of animals used in nimodipine acute experiments, n-nim= # of pericytes in nimodipine acute experiments. nShV= # blood vessels in sham acute experiments; n-nimV= # blood vessels in nimodipine acute experiments. P-value<0.05=*; P-value<0.01=**; P-value<0.001=***. For specific p-values and mean ± SD information please refer to tables 8 and tables 9 (Section 6.1, P-Values and mean ± SD Results). Independent samples t-test and Mann-Whitney U test were used for comparisons.

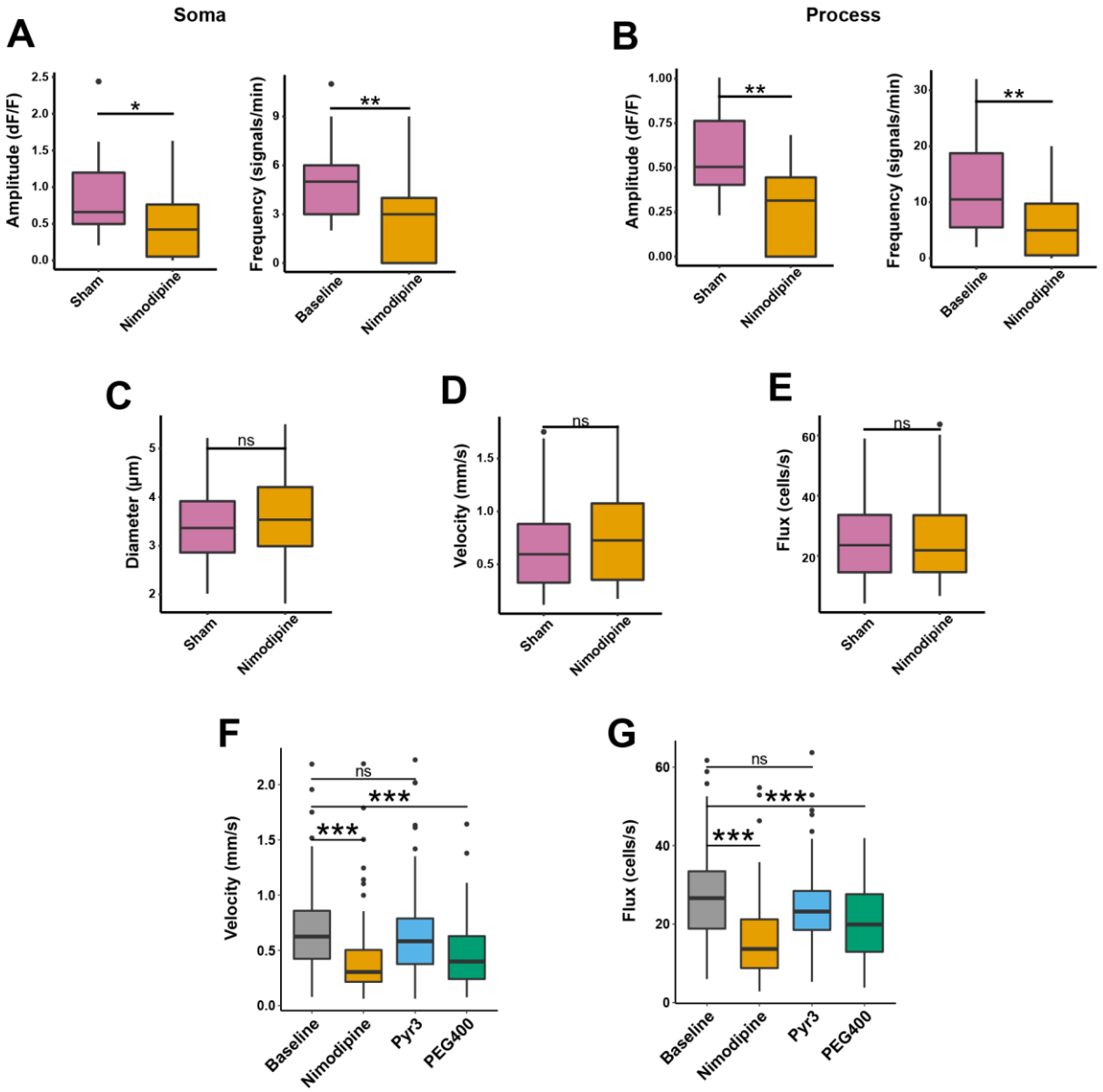

Supplementary Figure 3. **CP calcium signaling and brain capillaries hemodynamic results from acute *in vivo* pharmacology experiments** Panels A,B,C,D and E make a comparison between sham and the calcium channel blocker **Nimodipine.** Calcium signaling properties (amplitude and frequency) of capillary pericyte morphology structures **A)** soma and **B)** process. NSh=3; nSh=21; N-nim=3; n-nim=26. **C)** Diameter **D)** velocity and **E)** flux of brain capillaries covered by capillary pericytes. NSh=3; nShV=48; N-nim=4; n-nimV=34. NSh= # of animals used in sham acute experiments, nSh= # of pericytes in sham acute experiments; N-nim= # of animals used in nimodipine acute experiments, n-nim= # of pericytes in nimodipine acute experiments. nShV= # blood vessels in sham acute experiments; n-nimV= = # blood vessels in nimodipine acute experiments. P-value<0.05=*; P-value<0.01=**; P-value<0.001=***. For specific p-values and mean ± SD information please refer to tables 8 and tables 10 (Section 6.1, P-Values and mean ± SD Results). Independent samples t-test and Mann-Whitney U test were used for comparisons. **F)** Box plots of velocity **(F)** and flux **(G)** in baseline conditions and under the effect of the calcium channel blockers **nimodipine**, **pyr3** and their vehicle PEG400 applied separately via i.p. . N=7; n= 109. . N= # of animals, b(n)= # of blood vessels, P-value<0.05=*; P-

value<0.01=**; P-value<0.001=***. For specific p-values and mean ± SD information please refer to table 3.1 and table 3.2 (Section 6.1, P-Values and mean ± SD Results). Linear mixed models for repeated measurements and pairwise comparisons with Holm-sequential Bonferroni correction were used in the statistical tests.

6.1 P-values and mean ± SD Results.

Table 7. Supplementary material. P-values and mean ± SD of the mean blood pressure in repeated and acute pharmacology experiments.

	P-Value	**P-Value**	**Mean ±SD**		
Repeated pharmacology experiments	**Baseline-nimodipine**	**Baseline-pyr3**	Baseline	Nimodipine	Pyr3
	NO VALUES DETECTED	ns 0.751	106.932±25.028	NA	101.642±24.927
	P-Value	**Mean ±SD**			
Acute pharmacology experiments	**Sham-Nimodipine**	**Sham**	**Nimodipine**		
	ns0.103	78.84±12.595	97.619±23.938		

Table 8.1. Supplementary material. P-values. Brain pericyte calcium signaling analysis.

	Amplitude	**Frequency**
	Sham-nimodipine	Sham-nimodipine
Acta2-RCaMP1.07		
Soma	0.00262**	0.000367 ***
Process	0.0002 ***	2.831e-05 ***
PDGFRβ-CreERT2:GCaMP6s$^{fl/fl}$		
Soma	0.01181*	0.00166 **
Process	0.00158**	0.00939 **

Table 8.2. Supplementary material. Mean ± SD. Brain pericyte calcium signaling analysis.

	Amplitude (dF/F)		**Frequency (signals/min)**	
	Sham	Nimodipine	Sham	Nimodipine
Acta2-RCaMP1.07				
Soma	0.390±0.215	0.195±0.283	2.8±2.210	0.444±0.881
Process	0.471±0.209	0.190±0.193	5.687±5.582	0.6±0.699

PDGFRβ-CreERT2:GCaMP6s$^{fl/fl}$				
Soma	0.936±0.659	0.472±0.439	5±2.380	2.666±2.566
Process	0.573±0.242	0.296±0.226	12.444±8.276	5.954±5.802

Table 9.1. Supplementary material. P-values. Blood vessels of the transition zone covered by EP hemodynamic analysis.

	Diameter	**Vasomotor Index**	**Peak Frequency**
Acta2-RCaMP1.07	Sham-nimodipine	Sham-nimodipine	Sham-nimodipine
All blood vessels	0.00212 **	0.00102 **	6.887e-05 ***
	Velocity	**Flux**	
	Sham-nimodipine	Sham-nimodipine	
All blood vessels	1.639e-06***	ns 0.497	

Table 9.2. Supplementary material. Mean ± SD. Blood vessels of the transition zone covered by EP hemodynamic analysis.

	Diameter (µm)		**Vasomotor Index (ΔD/D)**		**Peak frequency**	
Acta2-RCaMP1.07	Sham	Nimodipine	Sham	Nimodipine	Sham	Nimodipine
All blood vessels	7.794±2.081	6.017±2.187	0.0915±0.058	0.145±0.078	6.057±3.528	13.341±7.192
	Velocity (mm/sec)		**Flux (cells/sec)**			
	Sham	Nimodipine	Sham	Nimodipine		
All blood vessels	4.903±2.066	2.572±1.219	35.278±10.314	33.886±12.054		

Table 10.1. Supplementary material. P-values. Blood vessels of the capillary zone covered by CP hemodynamic analysis.

	Diameter	**Velocity**	**Flux**
PDGFRβ-CreERT2:GCaMP6s$^{fl/fl}$	Sham-nimodipine	Sham-nimodipine	Sham-nimodipine
All blood vessels	ns 0.4091	ns 0.4617	ns 0.8023

Table 10.2. Supplementary material. Mean ± SD. Blood vessels of the capillary zone covered by CP hemodynamic analysis.

	Diameter (µm)		**Velocity (mm/sec)**		**Flux cells/sec)**	
PDGFRβ-CreERT2:GCaMP6s$^{fl/fl}$	Sham	Nimodipine	Sham	Nimodipine	Sham	Nimodipine
All blood vessels	3.431±0.740	3.579±0.833	0.694±0.421	0.773±0.455	26.126±15.190	26.751±15.640

ns = no significant difference

P-value<0.05=*; P-value<0.01=**; P-value<0.001=***.

A letter “c” besides the numerical value indicates that the p-value is close to a significant difference.

NA= No Applicable

References.

1. Leonard WR, Snodgrass JJ, Robertson ML. Effects of Brain Evolution on Human Nutrition and Metabolism. *https://doi-org.uml.idm.oclc.org/101146/annurev.nutr27061406093659*. 2007;27:311-327. doi:10.1146/ANNUREV.NUTR.27.061406.093659

2. Gofur EM, Bordoni B. Anatomy, Head and Neck: Cerebral Blood Flow. *StatPearls*. Published online July 25, 2022.

3. Muoio V, Persson PB, Sendeski MM. The neurovascular unit – concept review. *Acta Physiologica*. 2014;210(4):790-798. doi:10.1111/APHA.12250

4. Iadecola C. The Neurovascular Unit Coming of Age: A Journey through Neurovascular Coupling in Health and Disease. *Neuron*. 2017;96(1):17-42. doi:10.1016/j.neuron.2017.07.030

5. Iadecola C. The Neurovascular Unit Coming of Age: A Journey through Neurovascular Coupling in Health and Disease. *Neuron*. 2017;96(1):17-42. doi:10.1016/j.neuron.2017.07.030

6. Attwell D, Mishra A, Hall CN, O'Farrell FM, Dalkara T. What is a pericyte? *Journal of Cerebral Blood Flow and Metabolism*. 2016;36(2):451-455. doi:10.1177/0271678X15610340

7. Handbuch der Lehre von den Geweben des Menschen und der Thiere - Stricker - Google Livres. Accessed March 22, 2021. https://books.google.bf/books/about/Handbuch_der_Lehre_von_den_Geweben_des_M.html?hl=fr&id=PXq9fGM8k1IC

8. Rouget C. Développement, la structure et les propriétés physiologiques des capillaires sanguins et lymphatiques. *Archives de Physiologie normal et pathologique*. Published online 1883:604-674.

9. Zimmermann KW. Der Ieinere Bau der Bluteapillaren. 1922;9.

10. Uemura MT, Maki T, Ihara M, Lee VMY, Trojanowski JQ. Brain Microvascular Pericytes in Vascular Cognitive Impairment and Dementia. *Front Aging Neurosci*. 2020;12(April):1-22. doi:10.3389/fnagi.2020.00080

11. Grubb S, Lauritzen M, Aalkjær C. Brain capillary pericytes and neurovascular coupling. *Comp Biochem Physiol A Mol Integr Physiol*. 2021;254(January):110893. doi:10.1016/j.cbpa.2020.110893

12. Cipolla MJ. Control of Cerebral Blood Flow. Published online 2009. Accessed May 29, 2023. https://www-ncbi-nlm-nih-gov.uml.idm.oclc.org/books/NBK53082/

13. Mandeville JB, Rosen BR. Functional MRI. *Brain Mapping: The Methods*. Published online 2002:315-349. doi:10.1016/B978-012693019-1/50015-0

14. Purves D, Augustine GJ, Fitzpatrick D, et al. The Blood Supply of the Brain and Spinal Cord. Published online 2001.

15. Klug NR. Intraluminal pressure elevates intracellular calcium and contracts CNS pericytes : Role of voltage-dependent calcium channels. Published online 2023:1-12. doi:10.1073/pnas.

16. Agarwal N, Carare RO. Cerebral Vessels: An Overview of Anatomy, Physiology, and Role in the Drainage of Fluids and Solutes. *Front Neurol*. 2021;11:1748. doi:10.3389/FNEUR.2020.611485/BIBTEX

17. Cipolla MJ. Anatomy and Ultrastructure. Published online 2009. Accessed August 18, 2023. https://www-ncbi-nlm-nih-gov.uml.idm.oclc.org/books/NBK53086/

18. Taylor AM, Bordoni B. Histology, Blood Vascular System. *StatPearls*. Published online May 1, 2023. Accessed August 18, 2023. https://www-ncbi-nlm-nih-gov.uml.idm.oclc.org/books/NBK553217/

19. Leopold JA. The Endothelium. *Vascular Medicine: A Companion to Braunwald's Heart Disease: Second Edition*. Published online 2013:14-24. doi:10.1016/B978-1-4377-2930-6.00002-1

20. Agarwal N, Carare RO. Cerebral Vessels: An Overview of Anatomy, Physiology, and Role in the Drainage of Fluids and Solutes. *Front Neurol*. 2021;11:611485. doi:10.3389/FNEUR.2020.611485/BIBTEX

21. Grant RI, Hartmann DA, Underly RG, Berthiaume AA, Bhat NR, Shih AY. Organizational hierarchy and structural diversity of microvascular pericytes in adult mouse cortex. *Journal of Cerebral Blood Flow and Metabolism*. 2019;39(3):411-425. doi:10.1177/0271678X17732229

22. Wilson D. Vascular Smooth Muscle Structure and Function. *Mechanisms of Vascular Disease: A Reference Book for Vascular Specialists*. Published online January 1, 2011:13-24. doi:10.1017/UPO9781922064004.003

23. Grant RI, Hartmann DA, Underly RG, Berthiaume AA, Bhat NR, Shih AY. Organizational hierarchy and structural diversity of microvascular pericytes in adult mouse cortex. *Journal*

of Cerebral Blood Flow and Metabolism. 2019;39(3):411-425. doi:10.1177/0271678X17732229

24. Tykocki NR, Boerman EM, Jackson WF. Smooth Muscle Ion Channels and Regulation of Vascular Tone in Resistance Arteries and Arterioles. 2018;7(2):485-581. doi:10.1002/cphy.c160011.Smooth

25. Hall CN, Reynell C, Gesslein B, et al. Capillary pericytes regulate cerebral blood flow in health and disease. *Nature*. 2014;508(1):55-60. doi:10.1038/nature13165

26. Hartmann DA, Berthiaume AAA, Grant RI, et al. Brain capillary pericytes exert a substantial but slow influence on blood flow. *Nat Neurosci*. 2021;24(5):633-645. doi:10.1101/2020.03.26.008763

27. Riera JJ, Parthasarathy AB, Zheng Y, et al. Cerebrovascular Resistance: The Basis of Cerebrovascular Reactivity. Published online 2018. doi:10.3389/fnins.2018.00409

28. Wahl M, Schilling L. Regulation of cerebral blood flow--a brief review. *Acta Neurochir Suppl (Wien)*. 1993;59:3-10. doi:10.1007/978-3-7091-9302-0_1/COVER

29. Trammel JE, Sapra A. Physiology, Systemic Vascular Resistance. *StatPearls*. Published online July 18, 2022. Accessed May 28, 2023. https://www-ncbi-nlm-nih-gov.uml.idm.oclc.org/books/NBK556075/

30. Nilsson H, Aalkjaer C. Vasomotion: mechanisms and physiological importance. *Mol Interv*. 2003;3(2):79-89. doi:10.1124/mi.3.2.79

31. McKetton L, Cohn M, Tang-Wai DF, et al. Cerebrovascular resistance in healthy aging and mild cognitive impairment. *Front Aging Neurosci*. 2019;11(APR):79. doi:10.3389/FNAGI.2019.00079/BIBTEX

32. Heistad DD, Marcus ML, Abboud FM. Role of Large Arteries in Regulation of Cerebral Blood Flow in Dogs.

33. Faraci FM, Heistad DD. Regulation of large cerebral arteries and cerebral microsvascular pressure. *Circ Res*. 1990;66(1):8-17. doi:10.1161/01.RES.66.1.8

34. Aalkjær C, Boedtkjer D, Matchkov V. Vasomotion – what is currently thought? *Acta Physiologica*. 2011;202(3):253-269. doi:10.1111/j.1748-1716.2011.02320.x

35. Gustafsson H. Vasomotion and underling mechanisms in small arteries. An in vitro study of rat blood vessels. *Acta Physiologica Scandinavica, Supplement*. 1993;149(614):1-44.

36. Fujii K, Heistad DD, Faraci FM. Ionic mechanisms in spontaneous vasomotion of the rat basilar artery in vivo. *J Physiol*. 1990;430(1):389-398. doi:10.1113/jphysiol.1990.sp018297

37. Stergiopulos N, Porret CA, De Brouwer S, Meister JJ. Arterial vasomotion: Effect of flow and evidence of nonlinear dynamics. *Am J Physiol Heart Circ Physiol*. 1998;274(6 43-6). doi:10.1152/AJPHEART.1998.274.6.H1858/ASSET/IMAGES/LARGE/AHEA40606006X.JPEG

38. Das A, Murphy K, Drew PJ. Rude mechanicals in brain haemodynamics: non-neural actors that influence blood flow. *Philosophical Transactions of the Royal Society B*. 2021;376(1815). doi:10.1098/RSTB.2019.0635

39. Lacza Z, Hermán P, Görlach C, et al. NO Synthase Blockade Induces Chaotic Cerebral Vasomotion via Activation of Thromboxane Receptors. *Stroke*. 2001;32(11):2609-2614. doi:10.1161/HS1101.098526

40. Di Marco LY, Farkas E, Martin C, Venneri A, Frangi AF. Is Vasomotion in Cerebral Arteries Impaired in Alzheimer's Disease? *Journal of Alzheimer's Disease*. 2015;46(1):35. doi:10.3233/JAD-142976

41. Peng H, Matchkov V, Ivarsen A, Aalkjær C, Nilsson H. Hypothesis for the initiation of vasomotion. *Circ Res*. 2001;88(8):810-815. doi:10.1161/hh0801.089603

42. Amberg GC, Navedo MF. Calcium Dynamics in Vascular Smooth Muscle. *Microcirculation*. 2013;20(4):281-289. doi:10.1111/micc.12046

43. Intaglietta M. Arteriolar Vasomotion: Implications for Tissue Ischemia. *J Vasc Res*. 1991;28(1):1-7. doi:10.1159/000158912

44. van Veluw SJ, Hou SS, Calvo-Rodriguez M, et al. Vasomotion as a Driving Force for Paravascular Clearance in the Awake Mouse Brain. *Neuron*. 2020;105(3):549-561.e5. doi:10.1016/J.NEURON.2019.10.033

45. Galiano A, Mengual E, Eulate RG De, et al. Coupling of cerebral blood flow and functional connectivity is decreased in healthy aging. *Brain Imaging Behav*. 2020;14(2):436-450. doi:10.1007/s11682-019-00157-w

46. Girouard H, Iadecola C. Neurovascular coupling in the normal brain and in hypertension, stroke, and Alzheimer disease. *J Appl Physiol*. 2006;100(1):328-335. doi:10.1152/japplphysiol.00966.2005

47. Rungta RL, Chaigneau E, Osmanski BF, Charpak S. Vascular Compartmentalization of Functional Hyperemia from the Synapse to the Pia. *Neuron*. 2018;99(2):362-375.e4. doi:10.1016/j.neuron.2018.06.012

48. Banks WA, Kovac A, Morofuji Y. Neurovascular unit crosstalk : Pericytes and astrocytes modify cytokine secretion patterns of brain endothelial cells. Published online 2018. doi:10.1177/0271678X17740793

49. Meng W, Tobin JR, Busija DW. Glutamate-Induced Cerebral Vasodilation Is Mediated by Nitric Oxide Through N-Methyl-d-Aspartate Receptors. *Stroke*. 1995;26(5):857-863. doi:10.1161/01.STR.26.5.857

50. Freed JK, Gutterman DD. Communication is Key: Mechanisms of Intercellular Signaling in Vasodilation. *J Cardiovasc Pharmacol*. 2017;69(5):264. doi:10.1097/FJC.0000000000000463

51. Sweeney MD, Ayyadurai S, Zlokovic B V. Pericytes of the neurovascular unit: Key functions and signaling pathways. *Nat Neurosci*. 2016;19(6):771-783. doi:10.1038/nn.4288

52. Phillips AA, Chan FH, Mu M, Zheng Z, Krassioukov A V, Ainslie PN. Neurovascular coupling in humans: Physiology, methodological advances and clinical implications. doi:10.1177/0271678X15617954

53. Stackhouse TL, Mishra A. Neurovascular Coupling in Development and Disease: Focus on Astrocytes. *Front Cell Dev Biol*. 2021;9:1745. doi:10.3389/FCELL.2021.702832/BIBTEX

54. Gonzales AL, Klug NR, Moshkforoush A, et al. Contractile pericytes determine the direction of blood flow at capillary junctions. *Proc Natl Acad Sci U S A*. 2020;117(43):27022-27033. doi:10.1073/pnas.1922755117

55. Beishon LC, Minhas JS. Cerebral Autoregulation and Neurovascular Coupling in Acute and Chronic Stroke. *Front Neurol*. 2021;12:1565. doi:10.3389/FNEUR.2021.720770/BIBTEX

56. Tarantini S, Tran CHT, Gordon GR, Ungvari Z, Csiszar A. Impaired neurovascular coupling in aging and Alzheimer's disease: Contribution of astrocyte dysfunction and endothelial impairment to cognitive decline. *Exp Gerontol*. 2017;94:52-58. doi:10.1016/J.EXGER.2016.11.004

57. Hartmann DA, Underly RG, Grant RI, Watson AN, Lindner V, Shih AY. Pericyte structure and distribution in the cerebral cortex revealed by high-resolution imaging of transgenic mice. *Neurophotonics*. 2015;2(4):041402. doi:10.1117/1.nph.2.4.041402

58. Berthiaume AA, Grant RI, McDowell KP, et al. Dynamic Remodeling of Pericytes In Vivo Maintains Capillary Coverage in the Adult Mouse Brain. *Cell Rep*. 2018;22(1):8-16. doi:10.1016/j.celrep.2017.12.016

59. Burdyga T, Borysova L. Calcium signalling in pericytes. *J Vasc Res*. 2014;51(3):190-199. doi:10.1159/000362687

60. Smyth LCD, Rustenhoven J, Scotter EL, et al. Markers for human brain pericytes and smooth muscle cells. *J Chem Neuroanat*. 2018;92(June):48-60. doi:10.1016/j.jchemneu.2018.06.001

61. Bondjers C, He L, Takemoto M, et al. Microarray analysis of blood microvessels from PDGF-B and PDGF-Rβ mutant mice identifies novel markers for brain pericytes. *The FASEB Journal*. 2006;20(10):1703-1705. doi:10.1096/fj.05-4944fje

62. Watson AN, Berthiaume A anne A, Faino A V., et al. Mild pericyte deficiency is associated with aberrant brain microvascular flow in aged PDGFRβ+/− mice. *Journal of Cerebral Blood Flow and Metabolism*. 2020;40(12):2387-2400. doi:10.1177/0271678X19900543

63. Song S, Ewald AJ, Stallcup W, Werb Z, Bergers G. PDGFRβ+ perivascular progenitor cells in tumours regulate pericyte differentiation and vascular survival. *Nat Cell Biol*. 2005;7(9):870-879. doi:10.1038/ncb1288

64. Elena Ivanova , Carlo Corona , Cyril G. Eleftheriou PB and BTS. Retina-specific targeting of pericytes reveals structural diversity and enables control of capillary blood flow. Published online 2020. doi: https://doi.org/10.1101/2020.05.29.124586

65. Bhowmick S, D'Mello V, Caruso D, Wallerstein A, Abdul-Muneer PM. Impairment of pericyte-endothelium crosstalk leads to blood-brain barrier dysfunction following traumatic brain injury. *Exp Neurol*. 2019;317:260-270. doi:10.1016/J.EXPNEUROL.2019.03.014

66. Itoh Y, Suzuki N. Control of brain capillary blood flow. *Journal of Cerebral Blood Flow and Metabolism*. 2012;32(7):1167-1176. doi:10.1038/jcbfm.2012.5

67. Nelson AR, Sagare MA, Wang Y, Kisler K, Zhao Z, Zlokovic B V. Channelrhodopsin Excitation Contracts Brain Pericytes and Reduces Blood Flow in the Aging Mouse Brain in vivo. *Front Aging Neurosci*. 2020;12(April):1-11. doi:10.3389/fnagi.2020.00108

68. Yang S, Jin H, Zhu Y, et al. Diverse Functions and Mechanisms of Pericytes in Ischemic Stroke. *Curr Neuropharmacol*. 2017;15(6). doi:10.2174/1570159x15666170112170226

69. Chen Q, Zhang H, Liu Y, et al. Endothelial cells are progenitors of cardiac pericytes and vascular smooth muscle cells. *Nat Commun*. 2016;7(1):1-13. doi:10.1038/ncomms12422

70. Damisah EC, Hill RA, Tong L, Murray KN, Grutzendler J. A fluoro-Nissl dye identifies pericytes as distinct vascular mural cells during in vivo brain imaging. *Nat Neurosci*. 2017;20(7):1023-1032. doi:10.1038/nn.4564

71. Berthiaume AA, Hartmann DA, Majesky MW, Bhat NR, Shih AY. Pericyte structural remodeling in cerebrovascular health and homeostasis. *Front Aging Neurosci*. 2018;10(JUL):1-12. doi:10.3389/fnagi.2018.00210

72. Vanlandewijck M, He L, Mäe MA, et al. A molecular atlas of cell types and zonation in the brain vasculature. *Nature*. 2018;554(7693):475-480. doi:10.1038/nature25739

73. Alarcon-Martinez L, Yilmaz-Ozcan S, Yemisci M, et al. Capillary pericytes express α-smooth muscle actin, which requires prevention of filamentous-actin depolymerization for detection. *Elife*. 2018;7:1-17. doi:10.7554/eLife.34861

74. Hartmann DA, Berthiaume AAA, Grant RI, et al. Brain capillary pericytes exert a substantial but slow influence on blood flow. *Nat Neurosci*. 2021;24(5):633-645. doi:10.1101/2020.03.26.008763

75. Kisler K, Nelson AR, Rege S V., et al. Pericyte degeneration leads to neurovascular uncoupling and limits oxygen supply to brain. *Nat Neurosci*. 2017;20(3):406-416. doi:10.1038/nn.4489

76. Dalkara T, Alarcon-Martinez L. Cerebral microvascular pericytes and neurogliovascular signaling in health and disease. *Brain Res*. 2015;1623:3-17. doi:10.1016/j.brainres.2015.03.047

77. Hill RA, Tong L, Yuan P, Murikinati S, Gupta S, Grutzendler J. Regional Blood Flow in the Normal and Ischemic Brain Is Controlled by Arteriolar Smooth Muscle Cell Contractility and Not by Capillary Pericytes. *Neuron*. 2015;87(1):95-110. doi:10.1016/j.neuron.2015.06.001

78. Kisler K, Nikolakopoulou AM, Sweeney MD, Lazic D, Zhao Z, Zlokovic B V. Acute Ablation of Cortical Pericytes Leads to Rapid Neurovascular Uncoupling. *Front Cell Neurosci*. 2020;14(February):1-8. doi:10.3389/fncel.2020.00027

79. Hamilton NB. Pericyte-mediated regulation of capillary diameter: a component of neurovascular coupling in health and disease. *Front Neuroenergetics*. 2010;2(May):1-14. doi:10.3389/fnene.2010.00005

80. Daneman R, Zhou L, Kebede AA, Barres BA. Pericytes are required for blood brain barrier integrity during embryogenesis. *Nature*. 2010;468(7323):562-566. doi:10.1038/nature09513

81. Lopes Pinheiro MA, Kooij G, Mizee MR, et al. Immune cell trafficking across the barriers of the central nervous system in multiple sclerosis and stroke. *Biochim Biophys Acta Mol Basis Dis*. 2016;1862(3):461-471. doi:10.1016/j.bbadis.2015.10.018

82. Eilken HM, Diéguez-Hurtado R, Schmidt I, et al. Pericytes regulate VEGF-induced endothelial sprouting through VEGFR1. *Nat Commun*. 2017;8(1). doi:10.1038/s41467-017-01738-3

83. Birbrair A, Zhang T, Wang ZM, Messi ML, Mintz A, Delbono O. Pericytes at the intersection between tissue regeneration and pathology. *Clin Sci*. 2015;128(2):81-93. doi:10.1042/CS20140278

84. *Starting the Scar: A Primary Role for Pericytes?*; 2011. doi:10.1038/nm0911-1052

85. Ma Q, Zhao Z, Sagare AP, et al. Blood-brain barrier-associated pericytes internalize and clear aggregated amyloid-β42 by LRP1-dependent apolipoprotein e isoform-specific mechanism. *Mol Neurodegener*. 2018;13(1):57. doi:10.1186/s13024-018-0286-0

86. Teichert M, Milde L, Holm A, et al. Pericyte-expressed Tie2 controls angiogenesis and vessel maturation. *Nat Commun*. 2017;8(May):1-12. doi:10.1038/ncomms16106

87. Rustenhoven J, Jansson D, Smyth LC, Dragunow M. Brain Pericytes As Mediators of Neuroinflammation. *Trends Pharmacol Sci*. 2017;38(3):291-304. doi:10.1016/j.tips.2016.12.001

88. Gunst SJ, Tang DD. The contractile apparatus and mechanical properties of airway smooth muscle. Published online 2000:600-616.

89. Flavahan NA, Bailey SR, Flavahan WA, et al. Imaging remodeling of the actin cytoskeleton in vascular smooth muscle cells after mechanosensitive arteriolar constriction. 2023;43210:660-669. doi:10.1152/ajpheart.00608.2004.

90. Phwmocol C. Modulation of the calcium sensitivity of the smooth muscle contractile apparatus: molecular mechanisms, pharmacological and pathophysiological implications. Published online 1997.

91. Lehman W, Morgan KG, Ba M. Structure and dynamics of the actin-based smooth muscle contractile and cytoskeletal apparatus. Published online 2012:461-469. doi:10.1007/s10974-012-9283-z

92. Paulin D, Li Z. Desmin: a major intermediate filament protein essential for the structural integrity and function of muscle. *Exp Cell Res*. 2004;301(1):1-7. doi:10.1016/J.YEXCR.2004.08.004

93. Agnetti G, Herrmann H, Cohen S. New roles for desmin in the maintenance of muscle homeostasis. *FEBS J*. 2022;289(10):2755-2770. doi:10.1111/FEBS.15864

94. Hartmann DA, Underly RG, Grant RI, Watson AN, Lindner V, Shih AY. Pericyte structure and distribution in the cerebral cortex revealed by high-resolution imaging of transgenic mice. *Neurophotonics*. 2015;2(4):041402. doi:10.1117/1.nph.2.4.041402

95. Grant RI, Hartmann DA, Underly RG, Berthiaume AA, Bhat NR, Shih AY. Organizational hierarchy and structural diversity of microvascular pericytes in adult mouse cortex. *Journal of Cerebral Blood Flow and Metabolism*. 2019;39(3):411-425. doi:10.1177/0271678X17732229

96. Peppiatt CM, Howarth C, Mobbs P, Attwell D. Bidirectional control of CNS capillary diameter by pericytes. *Nature*. 2006;443(7112):700-704. doi:10.1038/nature05193

97. Kovacs-Oller T, Ivanova E, Bianchimano P, Sagdullaev B. Dynamic connectivity maps of pericytes and endothelial cells mediate neurovascular coupling in health and disease. Published online 2019. doi:10.1101/830398

98. Zambach SA, Cai C, Helms HCC, et al. Precapillary sphincters and pericytes at first-order capillaries as key regulators for brain capillary perfusion. *Proc Natl Acad Sci U S A*. 2021;118(26). doi:10.1073/pnas.2023749118

99. Armulik A, Genové G, Mäe M, et al. Pericytes regulate the blood-brain barrier. *Nature*. 2010;468(7323):557-561. doi:10.1038/nature09522

100. Mihajlica N, Betsholtz C, Hammarlund-Udenaes M. Pharmacokinetics of pericyte involvement in small-molecular drug transport across the blood-brain barrier. Published online 2018. doi:10.1016/j.ejps.2018.06.018

101. Fernández-klett F, Offenhauser N, Dirnagl U, Priller J, Lindauer U. Pericytes in capillaries are contractile in vivo , but arterioles mediate functional hyperemia in the mouse brain. Published online 2010. doi:10.1073/pnas.1011321108/-/DCSupplemental.www.pnas.org/cgi/doi/10.1073/pnas.1011321108

102. Wei HS, Kang H, Rasheed IYD, et al. Erythrocytes Are Oxygen-Sensing Regulators of the Cerebral Microcirculation. *Neuron*. 2016;91(4):851-862. doi:10.1016/j.neuron.2016.07.016

103. Gu Y, Rampin A, Alvino V V., Spinetti G, Madeddu P. Cell Therapy for Critical Limb Ischemia: Advantages, Limitations, and New Perspectives for Treatment of Patients with Critical Diabetic Vasculopathy. *Curr Diab Rep*. 2021;21(3):1-13. doi:10.1007/S11892-021-01378-4/TABLES/2

104. Rom S, Gajghate S, Winfield M, Reichenbach NL, Persidsky Y. Combination of HIV-1 and Diabetes Enhances Blood Brain Barrier Injury via Effects on Brain Endothelium and Pericytes. *International Journal of Molecular Sciences 2020, Vol 21, Page 4663*. 2020;21(13):4663. doi:10.3390/IJMS21134663

105. Yamanaka G, Takata F, Kataoka Y, et al. The neuroinflammatory role of pericytes in epilepsy. *Biomedicines*. 2021;9(7). doi:10.3390/biomedicines9070759

106. Sweeney MD, Kisler K, Montagne A, Toga AW, Zlokovic B V. The role of brain vasculature in neurodegenerative disorders. *Nat Neurosci*. 2018;21(October):1318-1331. doi:10.1038/s41593-018-0234-x

107. Lopes Ribeiro A, Keith Okamoto O. Combined Effects of Pericytes in the Tumor Microenvironment. Published online 2015. doi:10.1155/2015/868475

108. Sengillo JD, Winkler EA, Walker CT, Sullivan JS, Johnson M, Zlokovic B V. Deficiency in mural vascular cells coincides with blood-brain barrier disruption in alzheimer's disease. *Brain Pathology*. 2013;23(3):303-310. doi:10.1111/bpa.12004

109. Bohannon DG, Okhravi HR, Kim J, Kuroda MJ, Didier ES, Kim W ki. Neurobiology of Aging A subtype of cerebrovascular pericytes is associated with blood-brain barrier disruption that develops during normal aging and simian immunode fi ciency virus infection. *Neurobiol Aging*. 2020;96:128-136. doi:10.1016/j.neurobiolaging.2020.08.006

110. Ueno M, Tomimoto H, Akiguchi I, Wakita H, Sakamoto H. *Blood-Brain Barrier Disruption in White Matter Lesions in a Rat Model of Chronic Cerebral Hypoperfusion*.; 2002.

111. Nortley R. The role of capillary pericytes in regulating cerebral blood flow in health, ischaemia and Alzheimer's disease. *Acta Physiologica*. 2019;227(Supplement 721):45.

112. Sagare AP, Bell RD, Zhao Z, et al. Pericyte loss influences Alzheimer-like neurodegeneration in mice. *Nat Commun*. 2013;4. doi:10.1038/ncomms3932

113. Nortley R, Korte N, Izquierdo P, et al. Amyloid b oligomers constrict human capillaries in Alzheimer's disease via signaling to pericytes. *Science (1979)*. 2019;365(6450):1-19. doi:10.1126/science.aav9518

114. Stamatovic SM, Keep RF, Andjelkovic A V. Brain Endothelial Cell-Cell Junctions: How to "Open" the Blood Brain Barrier.

115. Kamouchi M, Kitazono T, Ago T, et al. Calcium influx pathways in rat CNS pericytes. *Molecular Brain Research*. 2004;126(2):114-120. doi:10.1016/j.molbrainres.2004.03.008

116. Shen J, Xu G, Zhu R, et al. PDGFR-β restores blood-brain barrier functions in a mouse model of focal cerebral ischemia. *Journal of Cerebral Blood Flow and Metabolism*. 2019;39(8):1501-1515. doi:10.1177/0271678X18769515

117. Tallquist MD, French WJ, Soriano P. Additive Effects of PDGF Receptor b Signaling Pathways in Vascular Smooth Muscle Cell Development. 1(2):288-299. doi:10.1371/journal.pbio.0000052

118. Schumacher L, Slimani R, Zizmare L, et al. TGF-Beta Modulates the Integrity of the Blood Brain Barrier In Vitro, and Is Associated with Metabolic Alterations in Pericytes. *Biomedicines*. 2023;11(1):214. doi:10.3390/BIOMEDICINES11010214/S1

119. Nadeem T, Bogue W, Bigit B, Cuervo H. Deficiency of Notch signaling in pericytes results in arteriovenous malformations. *JCI Insight*. 2020;5(21). doi:10.1172/JCI.INSIGHT.125940

120. Von Tell D, Armulik A, Betsholtz C. Pericytes and vascular stability. *Exp Cell Res*. 2006;312(5):623-629. doi:10.1016/J.YEXCR.2005.10.019

121. Annika Armulik, Alexandra Abramsson CB, Abstract—Interactions. Endothelial/Pericyte Interactions. Published online 2005. doi:DOI: 10.1161/01.RES.0000182903.16652.d7

122. Bai Y, Zhu X, Chao J, et al. Pericytes Contribute to the Disruption of the Cerebral Endothelial Barrier via Increasing VEGF Expression: Implications for Stroke. Germain S, ed. *PLoS One*. 2015;10(4):e0124362. doi:10.1371/journal.pone.0124362

123. Geevarghese A, Herman IM. Pericyte-endothelial crosstalk: Implications and opportunities for advanced cellular therapies. *Translational Research*. 2014;163(4):296-306. doi:10.1016/j.trsl.2014.01.011

124. Longden TA, Dabertrand F, Koide M, et al. Capillary K+-sensing initiates retrograde hyperpolarization to increase local cerebral blood flow. *Nat Neurosci*. 2017;20(5):717-726. doi:10.1038/nn.4533

125. Borysova L, Wray S, Eisner DA, Burdyga T. How calcium signals in myocytes and pericytes are integrated across in situ microvascular networks and control microvascular tone. *Cell Calcium*. 2013;54(3):163-174. doi:10.1016/j.ceca.2013.06.001

126. Petersen OH, Michalak M, Verkhratsky A. Calcium signalling: Past, present and future. *Cell Calcium*. 2005;38(3-4 SPEC. ISS.):161-169. doi:10.1016/j.ceca.2005.06.023

127. Gonzales AL, Klug NR, Moshkforoush A, et al. Contractile pericytes determine the direction of blood flow at capillary junctions. *Proc Natl Acad Sci U S A*. 2020;117(43):27022-27033. doi:10.1073/pnas.1922755117

128. Grubb S, Cai C, Hald BO, et al. Precapillary sphincters maintain perfusion in the cerebral cortex. *Nat Commun*. 2020;11(1). doi:10.1038/s41467-020-14330-z

129. Sweeney MD, Ayyadurai S, Zlokovic B V. Pericytes of the neurovascular unit: Key functions and signaling pathways. *Nat Neurosci*. 2016;19(6):771-783. doi:10.1038/nn.4288

130. Grubb S, Lauritzen M, Aalkjær C. Brain capillary pericytes and neurovascular coupling. *Comp Biochem Physiol A Mol Integr Physiol*. 2021;254(November 2020). doi:10.1016/j.cbpa.2020.110893

131. Hill RA, Tong L, Yuan P, Murikinati S, Gupta S, Grutzendler J. Regional Blood Flow in the Normal and Ischemic Brain Is Controlled by Arteriolar Smooth Muscle Cell Contractility and Not by Capillary Pericytes. *Neuron*. 2015;87(1):95-110. doi:10.1016/j.neuron.2015.06.001

132. Glück C, Ferrari KD, Binini N, et al. Distinct signatures of calcium activity in brain mural cells. *Elife*. Published online 2021:1-27. doi:https:// doi. org/ 10. 7554/ eLife. 70591

133. Phillips B, Clark J, Martineau E, Rungta R. Store-Operated Ca2+ Channels Mediate Microdomain Ca2+ Signals and Amplify Gq- 2 Coupled Ca2+ Elevations in Capillary Pericytes. Published online 2022. doi:https://doi.org/10.1101/2022.05.25.493438

134. Helbig H, Kornacker S, Berweck S, Stahl F, Lepple-Wienhues A, Wiederholt M. Membrane potentials in retinal capillary pericytes: Excitability and effect of vasoactive substances. *Invest Ophthalmol Vis Sci*. 1992;33(7):2105-2112.

135. Phillips B, Clark J, Martineau É, Rungta RL, Martineau E, Rungta RL. Store-Operated Ca2+ Channels Mediate Microdomain Ca2+ Signals and Amplify Gq- 2 Coupled Ca2+ Elevations in Capillary Pericytes. Published online 2022. doi:https://doi.org/10.1101/2022.05.25.493438

136. Feng T, Kalyaanamoorthy S, Barakat K. L-Type Calcium Channels: Structure and Functions. In: *Ion Channels in Health and Sickness*. InTech; 2018. doi:10.5772/intechopen.77305

137. Grubb S, Cai C, Hald BO, et al. Precapillary sphincters maintain perfusion in the cerebral cortex. *Nat Commun*. 2020;11(1). doi:10.1038/s41467-020-14330-z

138. Matsushita K, Fukumoto M, Kobayashi T, et al. Diabetes-induced inhibition of voltage-dependent calcium channels in the retinal microvasculature: Role of spermine. *Invest Ophthalmol Vis Sci*. 2010;51(11):5979-5990. doi:10.1167/iovs.10-5377

139. Alonso-Carbajo L, Kecskes M, Jacobs G, et al. Muscling in on TRP channels in vascular smooth muscle cells and cardiomyocytes. *Cell Calcium*. 2017;66:48-61. doi:10.1016/j.ceca.2017.06.004

140. Sabourin J, Robin E, Raddatz E. A key role of TRPC channels in the regulation of electromechanical activity of the developing heart. *Cardiovasc Res*. 2011;92(2):226-236. doi:10.1093/cvr/cvr167

141. Sabourin J, Antigny F, Robin E, Frieden M, Raddatz E. Activation of transient receptor potential canonical 3 (TRPC3)-mediated Ca2+ entry by A1 adenosine receptor in

cardiomyocytes disturbs atrioventricular conduction. *Journal of Biological Chemistry*. 2012;287(32):26688-26701. doi:10.1074/jbc.M112.378588

142. He L, Vanlandewijck M, Mäe MA, et al. Data descriptor: Single-cell RNA sequencing of mouse brain and lung vascular and vessel-associated cell types. *Sci Data*. 2018;5(1):1-11. doi:10.1038/sdata.2018.160

143. Inoue R, Jensen LJ, Shi J, et al. Transient receptor potential channels in cardiovascular function and disease. *Circ Res*. 2006;99(2):119-131. doi:10.1161/01.RES.0000233356.10630.8a

144. Philipp S, Strauss B, Hirnet D, et al. TRPC3 mediates T-cell receptor-dependent calcium entry in human T-lymphocytes. *Journal of Biological Chemistry*. 2003;278(29):26629-26638. doi:10.1074/jbc.M304044200

145. Moran MM, McAlexander MA, Bíró T, Szallasi A. Transient receptor potential channels as therapeutic targets. *Nat Rev Drug Discov*. 2011;10(8):601-620. doi:10.1038/nrd3456

146. Hartmann DA, Berthiaume AAA, Grant RI, et al. Brain capillary pericytes exert a substantial but slow influence on blood flow. *Nat Neurosci*. 2021;24(5):633-645. doi:10.1101/2020.03.26.008763

147. Kureli G, Yilmaz-Ozcan S, Erdener SE, et al. F-actin polymerization contributes to pericyte contractility in retinal capillaries. *Exp Neurol*. 2020;332. doi:10.1016/j.expneurol.2020.113392

148. Gonzales AL, Klug NR, Moshkforoush A, et al. Contractile pericytes determine the direction of blood flow at capillary junctions. *Proc Natl Acad Sci U S A*. 2020;117(43):27022-27033. doi:10.1073/pnas.1922755117

149. Erdener ŞE, Küreli G, Dalkara T. Contractile apparatus in CNS capillary pericytes. *Neurophotonics*. 2022;9(02):1-15. doi:10.1117/1.nph.9.2.021904

150. Oh J, Lee C, Kaang BK. Imaging and analysis of genetically encoded calcium indicators linking neural circuits and behaviors. *Korean J Physiol Pharmacol*. 2019;23(4):237. doi:10.4196/KJPP.2019.23.4.237

151. Stobart JL, Ferrari KD, Barrett MJPP, et al. Long-term in vivo calcium imaging of astrocytes reveals distinct cellular compartment responses to sensory stimulation. *Cerebral Cortex*. 2018;28(1):184-198. doi:10.1093/cercor/bhw366

152. Kalganova T, Maslennikova A, Orlova A, Laufer J, Delpy D, Elwell C. Physical model for the spectroscopic analysis of cortical intrinsic optical signals spectroscopy haemoglobin concentration intrinsic optical signals. Published online 2000.

153. Petersen CCH. Sensorimotor processing in the rodent barrel cortex. *Nat Rev Neurosci*. 2019;20(September). doi:10.1038/s41583-019-0200-y

154. Meza-Resillas J, Ahmadpour N, Stobart M, Stobart J. Brain mural cell calcium and hemodynamic imaging in transgenic mice in vivo. *JoVE*. Published online 2021.

155. Fluorescent and Biotinylated Dextrans—Section 14.5 - AU. Accessed June 24, 2023. https://www.thermofisher.com/au/en/home/references/molecular-probes-the-handbook/fluorescent-tracers-of-cell-morphology-and-fluid-flow/fluorescent-and-biotinylated-dextrans.html

156. Meza-Resillas J, Ahmadpour N, Stobart M, Stobart J. Brain Pericyte Calcium and Hemodynamic Imaging in Transgenic Mice In Vivo. *Journal of Visualized Experiments*. 2021;2021(177):1-17. doi:10.3791/62725

157. Ellefsen KL, Settle B, Parker I, Smith IF. An algorithm for automated detection, localization and measurement of local calcium signals from camera-based imaging. *Cell Calcium*. 2014;56(3):147-156. doi:10.1016/j.ceca.2014.06.003

158. Barrett MJP, Ferrari KD, Stobart JL, Holub M, Weber B. CHIPS: an Extensible Toolbox for Cellular and Hemodynamic Two-Photon Image Analysis. *Neuroinformatics*. 2018;16(1):145-147. doi:10.1007/s12021-017-9344-y

159. Daugherty A, Rateri D, Hong L, Balakrishnan A. Measuring Blood Pressure in Mice using Volume Pressure Recording, a Tail-cuff Method. Published online 2009:27. doi:10.3791/1291

160. CODA Surgical Monitor | NIBP Monitor from Kent Scientific. Accessed June 25, 2023. https://www.kentscientific.com/products/coda-monitor/

161. Stobart JL, Ferrari KD, Barrett MJP, et al. Cortical Circuit Activity Evokes Rapid Astrocyte Calcium Signals on a Similar Timescale to Neurons. *Neuron*. 2018;98(4):726-735.e4. doi:10.1016/j.neuron.2018.03.050

162. Wu DM, Kawamura H, Sakagami K, et al. Cholinergic regulation of pericyte-containing retinal microvessels. Published online 2023:2083-2090.

163. Attwell D, Mishra A, Hall CN, O'Farrell FM, Dalkara T. What is a pericyte? *Journal of Cerebral Blood Flow and Metabolism*. 2016;36(2):451-455. doi:10.1177/0271678X15610340

164. Grant RI, Hartmann DA, Underly RG, Berthiaume AA, Bhat NR, Shih AY. Organizational hierarchy and structural diversity of microvascular pericytes in adult mouse cortex. *Journal of Cerebral Blood Flow and Metabolism*. 2019;39(3):411-425. doi:10.1177/0271678X17732229

165. Hartmann DA, Berthiaume AA, Grant RI, et al. Brain capillary pericytes exert a substantial but slow influence on blood flow. *Nat Neurosci*. 2021;24(5):633-645. doi:10.1038/s41593-020-00793-2

166. Nortley R. The role of capillary pericytes in regulating cerebral blood flow in health, ischaemia and Alzheimer's disease. *Acta Physiologica*. 2019;227(Supplement 721):45.

167. Hall CN, Reynell C, Gesslein B, et al. Capillary pericytes regulate cerebral blood flow in health and disease. *Nature*. 2014;508(1):55-60. doi:10.1038/nature13165

168. Kisler K, Nelson AR, Montagne A, Zlokovic B V. Cerebral blood flow regulation and neurovascular dysfunction in Alzheimer disease. *Nature Publishing Group*. 2017;18(7):419-434. doi:10.1038/nrn.2017.48

169. Attwell D, Mishra A, Hall CN, O'Farrell FM, Dalkara T. What is a pericyte? *Journal of Cerebral Blood Flow and Metabolism*. 2016;36(2):451-455. doi:10.1177/0271678X15610340

170. Burdyga T, Borysova L. Calcium signalling in pericytes. *J Vasc Res*. 2014;51(3):190-199. doi:10.1159/000362687

171. Vanlandewijck M, He L, Mäe MA, et al. A molecular atlas of cell types and zonation in the brain vasculature. *Nature*. 2018;554(7693):475-480. doi:10.1038/nature25739

172. Hartmann DA, Coelho-Santos V, Shih AY. Pericyte Control of Blood Flow Across Microvascular Zones in the Central Nervous System. *Annu Rev Physiol*. 2022;84(1):1-24. doi:10.1146/annurev-physiol-061121-040127

173. Andreas Zambach S, Cai C, Christian Cederberg Helms H, et al. Precapillary sphincters and pericytes at first-order capillaries as key regulators for brain capillary perfusion. doi:10.1073/pnas.2023749118/-/DCSupplemental

174. Rungta RL, Chaigneau E, Osmanski BF, Charpak S. Vascular Compartmentalization of Functional Hyperemia from the Synapse to the Pia. *Neuron*. 2018;99(2):362-375.e4. doi:10.1016/j.neuron.2018.06.012

175. Rungta RL, Chaigneau E, Osmanski BF, Charpak S. Vascular Compartmentalization of Functional Hyperemia from the Synapse to the Pia. *Neuron*. 2018;99(2):362-375.e4. doi:10.1016/j.neuron.2018.06.012

176. Cai C, Fordsmann JC, Jensen SH, et al. Stimulation-induced increases in cerebral blood flow and local capillary vasoconstriction depend on conducted vascular responses. *Proc Natl Acad Sci U S A*. 2018;115(25):E5796-E5804. doi:10.1073/pnas.1707702115

177. Stobart JL, Ferrari KD, Barrett MJPP, et al. Long-term in vivo calcium imaging of astrocytes reveals distinct cellular compartment responses to sensory stimulation. *Cerebral Cortex*. 2018;28(1):184-198. doi:10.1093/cercor/bhw366

178. Grant RI, Hartmann DA, Underly RG, Berthiaume AA, Bhat NR, Shih AY. Organizational hierarchy and structural diversity of microvascular pericytes in adult mouse cortex. *Journal of Cerebral Blood Flow and Metabolism*. 2019;39(3):411-425. doi:10.1177/0271678X17732229

179. Hariharan A, Robertson CD, Garcia DCG, et al. Brain capillary pericytes are metabolic sentinels that control blood flow through a K ATP channel- dependent energy switch. *CellReports*. 2022;41(13):111872. doi:10.1016/j.celrep.2022.111872

180. Sweeney MD, Ayyadurai S, Zlokovic B V. Pericytes of the neurovascular unit: Key functions and signaling pathways. *Nat Neurosci*. 2016;19(6):771-783. doi:10.1038/nn.4288

181. Prakriya M. *Store-Operated Orai Channels: Structure and Function*. Vol 71. 1st ed. Elsevier Inc.; 2013. doi:10.1016/B978-0-12-407870-3.00001-9

182. Korte N, Ilkan Z, Pearson CL, et al. The Ca2+-gated channel TMEM16A amplifies capillary pericyte contraction and reduces cerebral blood flow after ischemia. *Journal of Clinical Investigation*. 2022;132(9):1-17. doi:10.1172/JCI154118

183. Storch U, Forst AL, Philipp M, Gudermann T, Mederos Y Schnitzler M. Transient receptor potential channel 1 (TRPC1) reduces calcium permeability in heteromeric channel complexes. *Journal of Biological Chemistry*. 2012;287(5):3530-3540. doi:10.1074/jbc.M111.283218

184. Qiu J, Fang Y, Rønnekleiv OK, Kelly MJ. Leptin Excites Proopiomelanocortin Neurons via Activation of TRPC Channels. *Journal of Neuroscience*. 2010;30(4):1560-1565. doi:10.1523/JNEUROSCI.4816-09.2010

185. Prestori F, Moccia F, D'angelo E. Disrupted Calcium Signaling in Animal Models of Human Spinocerebellar Ataxia (SCA). *International Journal of Molecular Sciences 2020, Vol 21, Page 216*. 2019;21(1):216. doi:10.3390/IJMS21010216

186. Aslam N, Alvi F. TRPC3 Channel Activity and Viability of Purkinje Neurons can be Regulated by a Local Signalosome. *Front Mol Biosci*. 2022;9:818682. doi:10.3389/FMOLB.2022.818682/BIBTEX

187. Earley S, Brayden JE. Transient receptor potential channels in the vasculature. *Physiol Rev*. 2015;95(2):645-690. doi:10.1152/PHYSREV.00026.2014

188. Ghosh D, Syed AU, Prada MP, et al. Calcium Channels in Vascular Smooth Muscle. *Adv Pharmacol*. 2017;78:49-87. doi:10.1016/BS.APHA.2016.08.002

189. Jackson-Weaver O, Friedman JK, Rodriguez LA, et al. Hypoxia/reoxygenation decreases endothelial glycocalyx via reactive oxygen species and calcium signaling in a cellular model for shock. *Journal of Trauma and Acute Care Surgery*. 2019;87(5):1070-1076. doi:10.1097/TA.0000000000002427

190. Koenig S, Schernthaner M, Maechler H, et al. A TRPC3 Blocker, Ethyl-1-(4-(2,3,3-Trichloroacrylamide)Phenyl)-5-(Trifluoromethyl)-1H-Pyrazole-4-Carboxylate (Pyr3), Prevents Stent-Induced Arterial Remodeling. *Journal of Pharmacology and Experimental Therapeutics*. 2013;344(1):33-40. doi:10.1124/JPET.112.196832

191. Nimodipine - StatPearls - NCBI Bookshelf. Accessed June 6, 2023. https://www-ncbi-nlm-nih-gov.uml.idm.oclc.org/books/NBK534870/

192. Kim SS, Park DH, Lim DJ, Kang SH, Cho TH, Chung YG. Angiographic Features and Clinical Outcomes of Intra-Arterial Nimodipine Injection in Patients with Subarachnoid Hemorrhage-Induced Vasospasm. *J Korean Neurosurg Soc*. 2012;52(3):172-178. doi:10.3340/JKNS.2012.52.3.172

193. Kazda S, Towart R. Nimodipine: a new calcium antagonistic drug with a preferential cerebrovascular action. *Acta Neurochir (Wien)*. 1982;63(1-4):259-265. doi:10.1007/BF01728880/METRICS

194. Haven W. Pharmacological basis for the use of nimodipine in central nervous system disorders. *The FASEB Journal*. 1989;3:1799-1806.

195. Kazda S, Garthoff B, Krause HP, Schlossmann K. Cerebrovascular effects of the calcium antagonistic dihydropyridine derivative nimodipine in animal experiments. *Arzneimittelforschung*. 1982;32(4):331-338. Accessed June 6, 2023. https://europepmc-org.uml.idm.oclc.org/article/med/7201801

196. Nortley R. The role of capillary pericytes in regulating cerebral blood flow in health, ischaemia and Alzheimer's disease. *Acta Physiologica*. 2019;227(Supplement 721):45. http://ovidsp.ovid.com/ovidweb.cgi?T=JS&PAGE=reference&D=emedx&NEWS=N&AN=631641646

197. Helbok R, Kathirvelu B, Alex Choi H, et al. Nimodipine-Induced Blood Pressure Changes Can Predict Delayed Cerebral Ischemia. *Frontiers in Neurology | www.frontiersin.org*. 2019;10:1161. doi:10.3389/fneur.2019.01161

198. Tettenborn D, Dycka J, Volberg E, Dudden P. Blood pressure and heart rate during treatment with nimodipine in patients with subarachnoid hemorrhage. *Neurochirurgia (Stuttg)*. 1985;28(SUPPL. 1):84-86. doi:10.1055/S-2008-1054109/BIB

199. CV Physiology | Velocity versus Flow of Moving Blood. Accessed June 17, 2023. https://cvphysiology.com/hemodynamics/h013

200. Skalli, Omar Pelte, Marie-Francoise Peclet, Marie-Claire Gabbiani, Giulio Gugliotta, Patrizia Bussolati, Gianni Ravazzola M, Orci L. α-Smooth Muscle Actin, a Differentiation Marker of Smooth Muscle Cells, Is Present in Microfilamentous Bundles of Pericytes. Published online 1989:315-321.

201. Kureli G, Yilmaz-Ozcan S, Erdener SE, et al. F-actin polymerization contributes to pericyte contractility in retinal capillaries. *Exp Neurol*. 2020;332. doi:10.1016/j.expneurol.2020.113392

202. Nelson AR, Sagare MA, Wang Y, Kisler K, Zhao Z, Zlokovic B V. Channelrhodopsin Excitation Contracts Brain Pericytes and Reduces Blood Flow in the Aging Mouse Brain in vivo. *Front Aging Neurosci*. 2020;12(April):1-11. doi:10.3389/fnagi.2020.00108

203. Hartmann DA, Coelho-Santos V, Shih AY. Pericyte Control of Blood Flow Across Microvascular Zones in the Central Nervous System. *Annu Rev Physiol*. 2022;84(1):1-24. doi:10.1146/annurev-physiol-061121-040127

204. Vazquez G, Lievremont JP, Bird GSJ, Putney JW. Human Trp3 forms both inositol trisphosphate receptor-dependent and receptor-independent store-operated cation channels in DT40 avian B lymphocytes. *Proc Natl Acad Sci U S A*. 2001;98(20):11777-11782. doi:10.1073/pnas.201238198

205. Kochukov MY, Balasubramanian A, Noel RC, Marrelli SP. Role of TRPC1 and TRPC3 Channels in Contraction and Relaxation of Mouse Thoracic Aorta. *J Vasc Res*. 2012;50(1):11-20. doi:10.1159/000342461

206. Kochukov MY, Balasubramanian A, Abramowitz J, Birnbaumer L, Marrelli SP. Activation of endothelial transient receptor potential C3 channel is required for small conductance calcium-activated potassium channel activation and sustained endothelial hyperpolarization and vasodilation of cerebral artery. *J Am Heart Assoc*. 2014;3(4). doi:10.1161/JAHA.114.000913

207. Cai C, Zambach SA, Grubb S, et al. Impaired dynamics of brain precapillary sphincters and pericytes at first order capillaries explains reduced neurovascular functions in aging. *bioRxiv*. Published online August 6, 2021:2021.08.05.455300. doi:10.1101/2021.08.05.455300

208. Kisler K, Nelson AR, Rege S V., et al. Pericyte degeneration leads to neurovascular uncoupling and limits oxygen supply to brain. *Nat Neurosci*. 2017;20(3):406-416. doi:10.1038/nn.4489

209. Nikolakopoulou AM, Montagne A, Kisler K, et al. Pericyte loss leads to circulatory failure and pleiotrophin depletion causing neuron loss. *Nat Neurosci*. 2019;22(7):1089-1098. doi:10.1038/s41593-019-0434-z

210. Rungta RL, Chaigneau E, Osmanski BF, Charpak S. Vascular Compartmentalization of Functional Hyperemia from the Synapse to the Pia. *Neuron*. 2018;99(2):362-375.e4. doi:10.1016/j.neuron.2018.06.012

211. Ornelas S, Berthiaume AA, Bonney SK, et al. Three-dimensional ultrastructure of the brain pericyte-endothelial interface. *Journal of Cerebral Blood Flow and Metabolism*. 2021;41(9):2185-2200. doi:10.1177/0271678X211012836

212. Hall CN, Reynell C, Gesslein B, et al. Capillary pericytes regulate cerebral blood flow in health and disease. *Nature*. 2014;508(1):55-60. doi:10.1038/nature13165

213. Glück C, Ferrari KD, Keller A. Distinct signatures of calcium activity in brain pericytes. Published online 2020.

214. SCRIABINE A, van den KERCKHOFF W. Pharmacology of Nimodipine: A Review. *Ann N Y Acad Sci*. 1988;522(1):698-706. doi:10.1111/j.1749-6632.1988.tb33415.x

215. Zhao X, Ho D, Gao S, Hong C, Vatner DE, Vatner SF. Arterial Pressure Monitoring in Mice. *Curr Protoc Mouse Biol*. 2011;1. doi:10.1002/9780470942390.MO100149

216. Eddie T. Chiang, Sara M. Camp, Steven M. Dudek, Mary E. Brown, Peter V. Usatyuk, Olga Zaborina, John C. Alverdy and JGNG. Protective Effects of High-Molecular Weight Polyethylene Glycol (PEG) in Human Lung Endothelial Cell Barrier Regulation: Role of Actin Cytoskeletal Rearrangement. *National Institutes of Health*. Published online 2013. doi:10.1016/j.mvr.2008.11.007.Protective

217. Aghaie T, Jazayeri MH, Manian M, et al. Gold nanoparticle and polyethylene glycol in neural regeneration in the treatment of neurodegenerative diseases. *J Cell Biochem*. 2019;120(3):2749-2755. doi:10.1002/jcb.27415

218. Hofherr SE, Mok H, Gushiken FC, Lopez JA, Barry MA. Polyethylene glycol modification of adenovirus reduces platelet activation, endothelial cell activation, and thrombocytopenia. *Hum Gene Ther*. 2007;18(9):837-848. doi:10.1089/hum.2007.0051

219. Watson CJ, Rowland M, Warhurst G. Functional modeling of tight junctions in intestinal cell monolayers using polyethylene glycol oligomers. *Am J Physiol Cell Physiol*. 2001;281(2 50-2):388-397. doi:10.1152/ajpcell.2001.281.2.c388

220. Peyton SR, Raub CB, Keschrumrus VP, Putnam AJ. The use of poly(ethylene glycol) hydrogels to investigate the impact of ECM chemistry and mechanics on smooth muscle cells. *Biomaterials*. 2006;27(28):4881-4893. doi:10.1016/j.biomaterials.2006.05.012

221. Shi R. Polyethylene glycol repairs membrane damage and enhances functional recovery: A tissue engineering approach to spinal cord injury. *Neurosci Bull*. 2013;29(4):460-466. doi:10.1007/s12264-013-1364-5

222. Bittner GD, Ballinger ML, Raymond MA. Reconnection of severed nerve axons with polyethylene glycol. *Brain Res*. 1986;367(1-2):351-355. doi:10.1016/0006-8993(86)91617-3

223. Shi R, Borgens RB. Anatomical repair of nerve membranes in crushed mammalian spinal cord with polyethylene glycol. 2000;643:633-643.

224. Zalipsky S. Chemistry of polyethylene glycol conjugates with biologically active molecules. *Adv Drug Deliv Rev*. 1995;16(2-3):157-182. doi:10.1016/0169-409X(95)00023-Z

225. Bimpisidis Z, Öberg CM, Maslava N, Cenci MA, Lundblad C. Differential effects of gaseous versus injectable anesthetics on changes in regional cerebral blood flow and metabolism induced by L-DOPA in a rat model of Parkinson's disease. *Exp Neurol*. 2017;292:113-124. doi:10.1016/j.expneurol.2017.03.006

226. Lei H, Grinberg O, Nwaigwe CI, et al. The effects of ketamine-xylazine anesthesia on cerebral blood flow and oxygenation observed using nuclear magnetic resonance perfusion imaging and electron paramagnetic resonance oximetry. *Brain Res*. 2001;913(2):174-179. doi:10.1016/S0006-8993(01)02786-X

227. Thrane AS, Thrane VR, Zeppenfeld D, et al. General anesthesia selectively disrupts astrocyte calcium signaling in the awake mouse cortex. *Proc Natl Acad Sci U S A*. 2012;109(46):18974-18979. doi:10.1073/pnas.1209448109

228. Zandieh S, Hopf R, Redl H, Schlag MG. The effect of ketamine/xylazine anesthesia on sensory and motor evoked potentials in the rat. *Spinal Cord*. 2003;41(1):16-22. doi:10.1038/sj.sc.3101400

229. Hristovska I, Verdonk F, Comte JC, et al. Ketamine/xylazine and barbiturates modulate microglial morphology and motility differently in a mouse model. *PLoS One*. 2020;15(8 August):1-16. doi:10.1371/journal.pone.0236594